Title
Development and Characterization of Sustainable Self-Consolidating Concrete Containing High Volume of Limestone Powder and Natural or Calcined Pozzolanic Materials

Author
Celik, Kemal

Publication Date
2015

Peer reviewed|Thesis/dissertation

Development and Characterization of Sustainable Self-Consolidating Concrete Containing High Volume of Limestone Powder and Natural or Calcined Pozzolanic Materials

By

Kemal Celik

A dissertation submitted in partial satisfaction of the

requirements for the degree of

Doctor of Philosophy

in

Engineering–Civil and Environmental Engineering

in the

Graduate Division

of the

University of California, Berkeley

Committee in charge

Professor Paulo J.M. Monteiro, Chair
Professor Claudia P. Ostertag
Professor Hans-Rudolf Wenk

Fall 2015

Abstract

Development and Characterization of Sustainable Self-Consolidating Concrete Containing High Volume of Limestone Powder and Natural or Calcined Pozzolanic Materials

by

Kemal Celik

Doctor of Philosophy in Civil and Environmental Engineering

University of California, Berkeley

Professor Paulo J.M. Monteiro, Chair

Carbon dioxide emission from ordinary Portland cement manufacturing is one of the major sustainability issues facing the concrete industry. In fact, the annual worldwide CO_2 emission from cement manufacturing is nearly 7% of the global emissions. Roughly 60% of these emissions come from the calcination of limestone, the main raw material for making Portland-cement clinker. The remaining CO2 emission is as a result of fuel combustion required to generate the heat necessary for the reactions forming clinker. Although considerable gains in energy efficiency have been achieved during the production of cement for the last two decades, calcination of limestone is the major concern as a source of CO2 emissions. Utilization of high-volume of by-products or natural pozzolanic material, such as basaltic ash pozzolan or fly ash as a replacement of Portland cement clinker, is a possible approach to reduce the clinker factor of Portland cement. In addition, self-consolidating concrete mixtures are being increasingly used for the construction of highly reinforced complex concrete elements and for massive concrete structures such as thick foundation due to its technical advantages such as shortened placement time, labor savings, improved compaction, and better encapsulation of rebar. Self-consolidating concrete requires utilization of high dosage of a plasticizing agent or viscosity-modifying chemical admixtures. The purpose of this study is to develop highly flowable self-consolidating concrete mixtures made of high proportions of cement replacement materials such as basaltic ash pozzolan, fly ash and pulverized limestone instead of high dosage of a plasticizer or viscosity-modifying admixtures, and characterize the effects of Portland cement replacement on the strength and durability. The two replacement materials used are high-volume finely-ground basaltic ash, a Saudi Arabian aluminum-silica rich basaltic glass and high-volume Class-F fly ash, from Jim Bridger Power Plant, Wyoming US. As an extension of the study, limestone powder was also used to replace Portland cement, alongside finely-ground basaltic ash and Class-F fly ash, forming ternary blends. Along with compressive strength tests, non-steady state chloride migration, water absorption and gas permeability tests were performed, as durability indicators, on self-consolidating concrete (SCC) specimens. The results were compared to two reference concretes; 100% ordinary Portland cement and 85% ordinary Portland cement – 15% limestone powder by weight. The high-volume of basaltic pozzolan and fly ash concrete mixtures showed strength and durability results comparable to those of the reference concretes at

later ages; identifying that both can effectively be used to produce low-cost and environment–friendly self-consolidating concrete without utilizing viscosity-modifying admixture.

Even though the slump flow diameter of SCC specimens was held in the similar range by utilizing varied amount of water reducer admixture, they were not identical. To enable a precise comparison among the specimens, the mortar specimens were produced that had same cement–replacement ratios with the ones in SCC specimens utilizing basaltic ash pozzolan (NP), Class-F fly ash (FA) and limestone powder without using water reducer admixture. Overall the binary and ternary FA samples had higher strength than NP mortar samples up to 1 year. This can be attributed to the higher pozzolanic reactivity of FA compared to NP which is supported by X-ray diffraction, isothermal calorimetry and thermogravimetric analysis. The normal consistency and setting time of the mixtures were determined. It showed that cement replacement with limestone powder in the ternary blended cements containing either basaltic ash pozzolan or Class-F fly ash along with ordinary Portland cement lowered the initial and final time of setting relative to the binary blended cements containing similar ratio of cement replacement. Also, the water demand of mixtures incorporate with basaltic ash pozzolan was greater than the one with Class-F fly ash.

The influence of the basaltic ash pozzolan, Class-F fly ash and limestone powder in the binary and ternary Portland cement blends is discussed, while following the physicochemical changes such as crystalline transition, hydration kinetics, and mechanical property that are a direct result of the addition of supplementary cementitious material or filler. Selected cement pastes were characterized by X-ray diffraction (XRD), petrographic microscopy and scanning electron microscopy with energy dispersive spectroscopy, isothermal calorimetry and thermogravimetric analysis (TGA). Integrating these techniques helps to understand the fresh and hardened properties of concretes and brings new insight into the effect of basaltic ash pozzolan, Class-F fly ash and limestone powder on the hydration of Portland cement. Isothermal calorimetry analysis presents that the addition of limestone powder, for instance, increased the rate of hydration reaction relative to the control specimen. This suggests that as a result of the further participation of aluminate phases in hydration reaction, the hydration products were improved. This outcome was confirmed with the analysis of XRD results by the finding carboaluminates in the limestone powder containing blended cements. It is important to note that the enhancement of hydration reaction was not adequate to compensate for the dilution effect due to addition of limestone powder. While the replacement of ordinary Portland cement with Class-F fly ash retarded the rate of hydration reaction relative to the one with basaltic ash pozzolan at first, the reactivity of Class-F fly ash improved after 2 days of hydration and surpassed the cumulative heat of hydration of basaltic ash pozzolan. This result is supported by TGA analysis demonstrating that the mixtures containing Class-F fly ash had more hydrate water with respect to the one of with basaltic ash pozzolan. XRD analysis showed that the addition of limestone powder in the ternary cement containing either basaltic ash pozzolan or fly ash led to stabilize the transformation of ettringite to monosulfate and introduce the carboaluminates in the hydration products. TGA analysis indicated that the degree of pozzolanic reaction of fly ash was higher than the one with basaltic ash in the binary and ternary blended mixtures.

For a comprehensive analysis and quantification of emissions and global warming potential (GWP) from concrete production, life-cycle assessment was used on the concrete mixture containing Class-F fly ash. It is found that high volume, up to 55% by weight replacement of

ordinary Portland cement with Class-F fly ash, or Class-F fly ash and limestone powder produces highly workable concrete that has high 28-day and 365-day strength, and extremely high to very high resistance to chloride penetration along with low GWP for concrete production.

To my caring and loving parents, ***Şerife*** *and* ***Cemal***

and siblings, ***Rahime*** *and* ***Metin***

&

To my beloved wife, ***Züleyha*** *and my little angel,* ***Meva***

Acknowledgements

All praises to Allah for the strengths, His bounty and blessings.

Many people deserve recognition and gratitude for their support and contribution to the research. First and foremost, my deepest gratitude and warmest appreciation is due to my research advisor and dissertation committee chair, Professor Paulo J.M. Monteiro. He has contributed an unspeakable amount not only to my dissertation but to my academic, professional and personal enhancement with his continuous guidance, invaluable support and encouragement throughout my doctoral journey. He is an inspiring role model to be a respectable scholar. His personal care and enlightening advises relieved the hard times of stress. I will ever be grateful for him.

I also owe greatly to Prof. Claudia P. Ostertag and Prof. Hans-Rudolf (Rudy) Wenk for serving on my dissertation committee, Prof. Khalid M. Mosalam for chairing my qualifying examination committee, and Prof. Raymond B. Seed, my GeoSystems (geoengineering) minor advisor. I am highly thankful to Prof. P. Kumar Mehta and Prof. Arpad Horvath. Their technical advices and insightful comments helped me to shape and develop my research into a concrete outcome.

I would like to express my special appreciation and thanks to Prof. Kumar Mehta and Mrs. Shanti Mehta for their friendship and caring me as my parents over the last years.

Also, I am thankful to Dr. Rae Taylor who provided me extreme technical input, careful reviews, productive discussions and great inspiration. I am indebted to my many colleagues and friends, including but not limited to Dr. Mohamad A. Moustafa, Dr. Mauricio Mancio, Dr. Marie Jackson, Dr. Cagla Meral, Dr. Juhyuk Moon, Dr. Craig Hargis, Dr. Pierre-Adrien Itty, Dr. A. Petek Gursel, Alexander J. Stack, Dr. Cruz Carlos, Dr. Rotana Hay, Dr. Se Yoon Yoon, Dr. Sungchul Bae, Dr. Wael Hassan, Guoqing Geng, Timothy T. Teague, Lev Stepanov, Turker Beyazoglu and A. Yusuf Mercan. I wish to thank many undergraduate students for help in performing the experimental measurements.

The financial supports from the Ministry of National Education of Turkey, KAUST and SinBerBEST and the technical support from Calera are gratefully acknowledged.

I cannot find words to state my gratitude to my parents and siblings for their unconditional support and love. Without their sacrifices, I would not make my dream come true. I thank my mother, Şerife for her unending prayers that reach me all the times. I thank my father, Cemal for his selfless dedication himself to his family. Rahime has always been a very loving and caring sister. The tremendous support from Rahime and brother, Metin, cannot be underestimated in helping me achieve this work.

Above all, I am especially grateful to my most precious and my beloved wife, Züleyha for her endless love and prayer, exceptional support and patience throughout the years of demanding studies. Dear Züleyha – My life has been gifted with you and our little angel, Meva. I am very fortunate to have you both!

Table of Contents

List of Figures

List of Tables

List of Abbreviations

Cement chemical notation		
A	Al_2O_3	
C	CaO	
$\underline{C}$	CO_3	
F	Fe_2O_3	
H	H_2O	
S	SiO_2	
$\bar{S}$	SO_3	
C_3S	$3CaO.\ SiO_2$	Tricalcium silicate
C_2S	$2CaO.\ SiO_2$	Dicalcium silicate
C_3A	$3CaO.\ Al_2O_3$	Tricalcium aluminate
C_4AF:	$4CaO.\ Al_2O_3.Fe_2O_3$	Ferrite
$C\bar{S}H_2$	$CaSO_4.2H_2O$	Gypsum
$C\underline{C}$	$CaCO_3$	Calcium carbonate
CH	$Ca(OH)_2$	Calcium hydroxide
C–S–H:	$CaO.SiO_2.H_2O$	Calcium silicate hydrate
C–A–S–H	$CaO.\ Al_2O_3.SiO_2.H_2O$	Calcium silicate aluminate-hydrate
AFt phase		
$3C_3A.\ 3C\bar{S}.H_{32}$	$3CaO.Al_2O_3.3CaSO_4.32H_2O$	Ettringite
AFm phases		
$3C_3A.\ C\bar{S}.H_{12}$	$3CaO.\ Al_2O_3.CaSO_4.12H_2O$	Tricalcium monosulfo-aluminate
$3C_3A.\ \underline{C}_{0.5}C_{0.5}.H_{11}$	$3CaO.Al_2O_3.0.5Ca(OH)_2.0.5CaCO_3.11.5H_2O$	Calcium hemicarboaluminate
$3C_3A.\ \underline{C}.H_{11}$	$3CaO.\ Al_2O_3.\ CaCO_3.11H_2O$	Calcium monocarboaluminate

Common abbreviations

BSE	Backscattered
CO_2-eq	CO_2-equivalent
CR	cement replacement
d_s	slump flow diameter
EDS	Energy dispersive spectroscopy
EIO-LCA	Economic input-output analysis-based life-cycle assessment
FA	Class-F fly ash
GWP	Global warming potential
H	Bound water
HVFA	High-volume fly ash
IC	Isothermal calorimetry
LCA	Life-cycle Assessment
LCI	Life-cycle inventory
LCIA	life-cycle impact assessment
LP	Limestone powder in mortar and cement paste
LPC	Limestone powder in concrete
NP	Basaltic ash pozzolan or natural pozzolan
OPC	Ordinary Portland cement
PSD	Particle Size Distribution
SCC	Self-consolidating concrete
SCMs	Supplementary cementitious materials
SEM	Scanning electron microscopy
SEM- EDS	SEM with energy dispersive X-ray analysis
SP	Superplasticizer
SSD	Saturated-surface dry
T_{50} times	Flow time until a diameter of 50 mm (sec)
TEM	Transmission Electron Microscopy
TG	Thermogravimetric
TGA	Thermogravimetric analysis
VMA	Viscosity modifying admixture
VSI	Visual stability index
w/b	Water to binder ratio
w/cm	Water-cementitious materials ratio
wt.%	Weight percent

XRD	X-ray diffraction
XRF	X-Ray Fluorescence

Non-steady state chloride migration test	
D_{nssm}	the non-steady state chloride migration coefficient
z	the absolute value of ion valence for chloride, $z = 1$;
F	Faraday constant, $F = 9.648 \times 10^4$ J/(V·mol);
U	absolute value of the applied voltage, V;
R	Gas constant, $R = 8.314$ J/(K·mol);
T	*Average value of the initial and final temperatures in the anolyte solution, K;*
L	Thickness of the specimen
x_d	Average value of the penetration depths, m;
t	Test duration in seconds
erf^{-1}	Inverse of the error function
c_d	Chloride concentration at which the color of the concrete changes, and c_d generally equals 0.07 N
N	Molar concentration divided by an equivalence factor
Water absorption test	
B	Last weight obtained of specimen
C	Weight of the specimen in room temperature
Gas permeability test	
K_g	gas permeability coefficient (m^2)
Q	Volume flow rate of the fluid ($m^3\ s^{-1}$)
A	Cross-sectional area of the specimen (m^2)
L	Thickness of the specimen in the direction of flow (m)
μ	Dynamic viscosity of the nitrogen at test temperature ($N.s.m^{-2}$)
P	Inlet (applied) pressure (absolute) ($N\ m^{-2}$)
P_a	Outlet pressure assumed in this test to be equal to atmospheric pressure ($N\ m^{-2}$)
P_0	Pressure at which the volume flow rate is determined, assumed in this test to be atmospheric pressure ($N\ m^{-2}$).

Mineral names	
SiO_2	Quartz
Fe_2O_3	Hematite
Fe_3O_4	Magnetite
$3Al_2O_3 \cdot SiO_2$	Mullite
$CaSO_4$	Anhydrite
$CaMg(CO_3)_2$	Dolomite
$CaCO_3$	Calcite
$CaAl_2Si_2O_8$	Plagioclase with an anorthitic composition
Mg_2SiO_4	Olivine with a forsteritic composition
$MgCaSi_2O_6$	Clinopyroxene with a diopsidic composition
$Ca_5(PO_4)_3F$	Fluoroapatite
P_2O_5	Phosphorous
F^-	Fluorine
SF	Silica fume
$Ca(OH)_2$	Portlandite
$3CaO.\ SiO_2$	Alite
$2CaO.\ SiO_2$	Belite or Larnite

1 Introduction

1.1 Background

To meet our society's growing demand for housing, transportation, water and electricity supply, civil infrastructure will continue to be the backbone of our society. However, increasing concerns about sustainable development and resilient communities leads to reconsider current practices and properties of infrastructure, especially in the context of low carbon dioxide (CO_2) footprints, energy efficient and long-lasting materials.

Portland cement concrete is the most widely used human-made commodity on the planet; about 25 billion tons are produced globally each year [1]. According to data compiled by the U.S. Geological Survey (USGS) in 2011 [2], the yearly global production of Portland cement was about 3.3 billion metric tons (mt). Considering typical concrete mixture proportions for ordinary concrete [3], this amount of cement is incorporated into approximately 27 billion mt of concrete, which requires 22 billion mt of aggregates and 2.2 billion mt of fresh water, leading to an annual global average consumption rate of about 4 mt of concrete per person. Concrete domination in construction environments results from its proven flexibility and adaptability, low maintenance requirements during the service life of most structures, and widespread availability of its raw constituents [3]. However, the massive production and consumption cycle of concrete has significant environmental impact [4].

Carbon dioxide (CO_2) emission from Portland cement manufacturing is one of the major environmental issues facing the concrete industry. Although considerable gains in energy efficiency during cement production manufacturing have been realized over the last two decades, according to industry data [5], about 866 kg of CO_2 are being generated for every 1000 kg of clinker made. Roughly 60% of these emissions come from the calcination of limestone, which is the main raw material for making Portland-cement clinker. For every tonne of calcium carbonate calcined in the kiln to form calcium oxide, 440 kg of CO_2 are released into the atmosphere as the chemical reaction progresses. The combustion of fuel required to generate the heat necessary for the clinker minerals forming reactions to take place accounts for the remaining CO_2 emissions.

As a result, considering an average clinker factor (kg of clinker per kg of cement) of 0.78 [6], annual worldwide CO_2 emissions from cement manufacturing add up to about 2.3 billion mt, which is nearly 7% of the global emissions from fossil-fuel [3]. For an average of 866 kg of CO_2 per mt of cement [7], the U.S. cement industry generated about 56 million mt of CO_2 based on the 2010 Portland cement production rate, 61 million mt [2]. These numbers correspond to direct emissions only, i.e., those generated in the cement factory. Based on economic input-output analysis-based life-cycle assessment (EIO-LCA) using U.S. data [8], supply-chain inclusive, life-cycle greenhouse gas emissions associated with cement manufacturing are expected to be 13% higher than direct emissions.

While the current environmental impact of the concrete industry is indeed considerable, the increased use of supplementary cementitious materials (SCMs) offers a possible reduction in global CO_2 emissions. A study involving business leaders and academics [9] singled out construction materials as one of the seven most promising technologies for investment (together

with wind, biofuels, photovoltaics, and concentrating solar power, nuclear, and building efficiency). The report concluded that within the construction materials sector, "the biggest single opportunity for CO_2 reduction is a low-carbon cement," and that annual savings of 1 billion mt of CO_2 could be reached if 50% of Portland cement were replaced by a low-carbon alternative.

In order to achieve such a level of CO_2 reductions, the industry must embrace a comprehensive, integrated approach that necessarily involves the use of less concrete for new structures, consumption of less cement in concrete mixtures, and use of less clinker for making cements [10].

Replacing half of Portland cement would require about 1.7 billion mt of alternative materials, according to USGS data [1]. Yet the global availability of fly ash and ground-granulated-blast furnace slag is roughly 800 million mt [11] and 300 million mt [12], which is a little more than half of the overall amount of materials needed. Thus, other materials, such as natural pozzolan and limestone powder, must be increasingly brought into the mixture.

Fly-ash is a waste product generated from the burning of pulverized coal. The finely divided residue that results from the combustion of ground or powdered coal and that is transported by flue gases from the combustion zone to the particle removal system [13]. Class F-Fly-ash is a fine powder of mainly spherical glass particles having pozzolanic properties which consists mostly of reactive silicon dioxide (SiO_2) and aluminum oxide (Al_2O_3). Class F fly-ash is produced from burning anthracite and bituminous coals [14]. There is also Class C-Fly ash that has calcareous fly-ash which consists of reactive calcium oxide (CaO), reactive silica (SiO_2) and alumina (Al_2O_3). This kind of fly ash, in addition to having pozzolanic properties, also has some cementitious properties. Class C fly-ash is produced from lignite and sub-bituminous coals [14]. Fly-ash is formed when the minerals in the coal melts and then solidifies as glassy droplets. For this reason the fly ash has a high variability and so problems with predicting its behavior when mixed with ordinary Portland cement (OPC) have been common though the years [15].

The majority of the particles in fly-ash are spheres and <1 to 200µm with a maximum distribution of 10-20µm and a density of 0.3 to 0.6 g/cm^3, however this is dependent on the size of the ground coal used and the conditions in which it is produced. There are two types of spheres found in fly-ash [16], cenospheres shown in Figure 1.1a, which are hollow spheres, and plerospheres, shown in Figure 1.1b, which are hollow spheres with smaller spheres inside them. Cenospheres make up a large proportion but the relative amounts of each are dependent on carbon and iron content of the fly-ash [17].

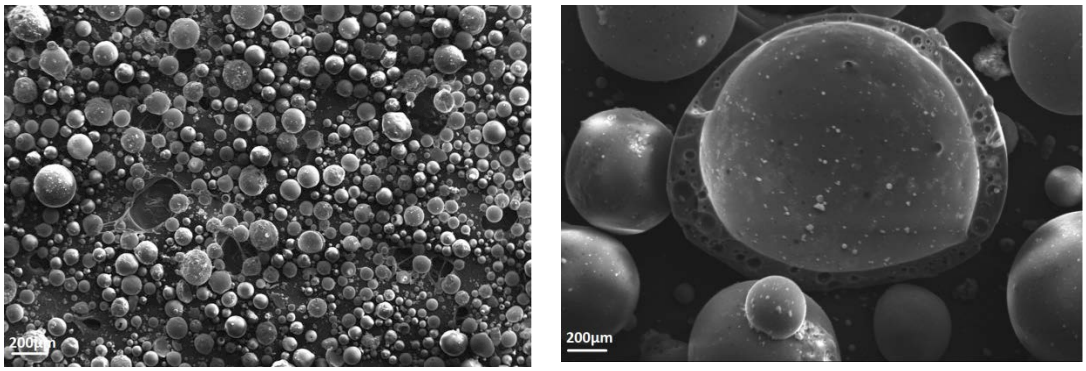

a b

Figure 1.1 Secondary electron image of (a) anhydrous cenospheres and (b) of a broken anhydrous plerosphere [18]

Chemical constituents of fly-ash mainly depend on the chemical composition of the coal; it can also be determined by the production and the coal combustion technology used [15]. Because of this, the ash hydration properties can vary significantly between generating facilities. In 1983 Mehta [19], produced scanning electron microscope (SEM) results indicated the glassy structure, contained mullite and small crystals of quartz, along with hematite, magnetite, sillimanite, and maghemite, but in smaller amounts [20]. When considering the techniques used in analyzing cement blends the presence of the above materials could have a detrimental effect on the results chemical constituents. Work carried out by Hower *et al.* [21] on a Class F fly-ash showed magnetite was the main iron oxide phase, with hematite next. More importantly this work also showed that the majority of the iron oxides were above 100µm on particle size along with most of the mixed phase particles. Gomes *et al.* [22] with the aid of SEM and TEM, observed magnetite on the surface of the cenospheres as broad flat (platy) particles.

When blends of fly ash and cement are mixed with water, cement clinker hydrates first [23] releasing calcium hydroxide (CH) crystals. The CH produces the high pH levels necessary for fly ash to react [24]. Afterwards, the noncrystalline silica and alumina of fly ash reacts with CH producing calcium silicate hydrate (C-S-H) and calcium aluminate hydrate (C-A-S-H). This also results in a decrease in the content of CH and thus the hydration of cement is accelerated [25]. This in turn produces additional C-S-H binder being formed than would be in a neat OPC past [26]. In the presence of gypsum, the calcium aluminate hydrate reacts to produce AFt or AFm [27]. Therefore the main hydration phases formed when fly-ash is hydrated with CH or with OPC are: C-S-H, C-A-S-H; AFm; and calcium aluminate hydrates such as C_4AH_{13} and hydrogarnet [28].

Except for diatomaceous earth, all natural pozzolans are derived from volcanic rocks and minerals [3]. Volcanic ash pozzolans fall into two major categories: cinder cone eruptions produce scoriae, frothy droplets of molten rock with mainly basaltic compositions, where amorphous glass is usually the predominant reactive component, while more explosive pyroclastic flow eruptions of molten and solid rock fragments produce complex deposits that commonly develop secondary pozzolanic clay and zeolitic surface coatings through interactions with interstitial ground and surface waters [29-32]. The binding pozzolanic mortars of 2000-year-old concretes in the monuments of imperial age Rome, for example, contained 40–50

volume% scoriaceous volcanic ash from a specific pyroclastic flow with reactive zeolitic and clay mineral surface coatings [32]. Recently, basaltic ash erupted from cinder cones in Saudi Arabia has been used successfully as SCM that complies with the requirements of ASTM C618 for Class N natural pozzolan [33-35]. Moufti et al. [35] found that the pozzolanic reactivity of lime with finely-ground cinders from Harrat Khaybar, passing the #200 sieve, satisfies the Italian standard. Khan and Alhozaimy [36] found good effectiveness for up to 25% OPC replacement [35]. The effectiveness of the ash as a larger volume 30–50 wt.% OPC replacement has not been evaluated, however, and the reactive components of the ash and associated cementitious products in the resulting concretes have not been described in detail.

During the last decade, limestone powder as calcite, or crystalline $CaCO_3$, has proven to be an effective partial replacement for OPC [37]. The added limestone acts as a limited participant in the hydration process at early ages and/or as a relatively inert calcareous filler depending on levels of calcite and replacement ratio [38-40]. During cement hydration, finely ground $CaCO_3$ reacts with C_3A and C_4AF to form high and low forms of carboaluminates [41]. Calcium hemicarboaluminate forms as an early hydration product in calcite-containing OPC, and then converts nearly completely to calcium monocarboaluminate, a stable AFm phase, after about 28 days [42]. Thermodynamic calculations and experimental observations showed that monocarboaluminate formation is favored instead of monosulfoaluminate [43]. The available sulfate reacts with water and calcium aluminates, crystalizing as ettringite [43, 44]. Due to additional ettringite formation, the total volume of the hydrated phase increases, and the overall porosity decreases [44].

The particle size of limestone powder must be considered in the mixture proportions because the early strength of the concrete depends on blended cement composition and limestone powder fineness, since interaction between gypsum and limestone during early C_3A hydration interferes with setting time [45]. An acceleration of C_3S hydration may occur at early ages when LS is interground with clinker [46]. The catalytic effect results from the high specific surface area of limestone powder, which produces nucleation sites for cement hydration products such as calcium carbosilicate hydrate [47], thus reducing the size of C-S-H agglomerations. In blended cements with up to 5% calcite, for example, almost all of the added calcite reacts with cement [38]. The resulting concretes show compressive strength [48], flexural strength, and drying shrinkage [49] similar to control concretes without limestone powder. Limestone powder has been added to cement and concrete in small volumes for many years, particularly in Europe. Recent research has shown that larger amounts can be successfully used in low water-cementitious materials ratio (w/cm) mixtures to reduce the consumption of Portland cement [40, 50]. At 25% sand mass replacement with limestone powder in mortar specimens, the fine $CaCO_3$ particles produce denser packing of the cement paste and better dispersion of cement grains [51]. When limestone powder replacement of ordinary Portland cement exceeds 15% by weight, however, the less reactive calcite has a dilution effect on the more reactive cement; the amount of cement paste is considerably reduced, resulting in lower compressive strengths and freeze-thaw and abrasion resistance [47, 52]. Durability decreases as water absorption and chloride diffusion coefficients increase [52].

High-volume fly ash (HVFA) concrete has been used successfully for many years in numerous applications with technical and environmental advantages as compared to conventional Portland cement concrete, and its use is expected to keep increasing over time [10, 53, 54]. The term high-

volume fly ash (HVFA) concrete refers to concrete mixtures containing at least 50% Portland cement replacement by weight with ASTM Standard Class F or Class C coal fly ash [55]. Compared to Portland-cement concrete, HVFA concrete shows lower strength at 3 and 7-day, similar strength at 56-day, and almost twice the 28-day strength at 1-year. Due to homogeneous microstructure, and stronger interfacial bond between the cement paste and the aggregate/steel, HVFA concrete undergoes considerably less tensile stress and cracking from drying shrinkage and thermal contraction, and consequently greatly enhanced durability to weather extremes and chemical attacks [56-59].

Recently, natural zeolite and volcanic tuff pozzolan replacement of OPC at 50 wt.%, from Turkey, and a higher w/c ratio than the present study led to a slow strength gain, but relatively good compressive strength and durability characteristics [60]. Studies of Portland cement-based ternary and quaternary blends containing combinations of fly ash, silica fume, blast furnace slag, limestone filler and natural volcanic pozzolans show that blended cements can be optimized to minimize the shortcomings of each component, resulting in synergistic cementitious systems [61, 62].

Self-consolidating concrete (SCC) is a high-performance concrete that can spread readily into place under its own weight and fill restricted sections as well as congested reinforcement structures without the need of mechanical consolidation and without undergoing any significant separation of material constituents [63, 64]. It was first developed in 1988 and has been increasingly used in the field due to several advantages when compared to conventional concrete, including shortened placement time, labor savings, improved compaction, and better encapsulation of rebar [65]. To enhance properties of SCC, material constituents [66, 67], mixture proportions [68], characterization of fresh and hardened properties of SCC including rheology [69, 70], dynamic stability [71], mechanical properties [72] have been investigated However, typical SCC mixes usually have an excessively high cement content, high heat of the hydration, and utilize a high dosage of high-performance superplasticizers and viscosity-modifying agents [68, 73-76]. Developed herein are self-consolidating concrete mixtures with low cement content (less than 250 kg/m^3), and a limited amount of a low range superplasticizer, and without any viscosity modifying agent, with ternary blends of cementing material containing Portland cement, limestone powder and natural pozzolan or fly-ash.

1.2 Objectives and Research Scope

As it is well known, incorporation of the some of SCM (e.g. Class F-fly ash and natural pozzolan) into OPC clinker decelerates the rate of hydration reaction; hence it restricts the replacement level of OPC clinker to satisfy the early age properties. To investigate the effect of high-volume level of substitution of OPC with basaltic ash pozzolan or Class-F fly ash on the self-consolidating concrete, this work comprises multi-scale experimental laboratory study. As an extension of this study, LP was also used to replace OPC, along with the HVNP or HVFA, forming ternary blends. The following properties were measured in fresh concrete samples: slump flow, normal consistency, and setting time. For hardened concrete, the following properties were measured: compressive strength, chloride-ion penetration, water absorption and gas permeability. The replacement of OPC with either SCM or fillers is known to affect the chemical properties and physical characteristics of cement paste. Such effects have strong

influence on fresh and hardened properties of concrete. The effect of a variety of SCM replacements on the fresh and hardened properties of the cement paste and mortar were investigated by following the chemical changes that are a direct result of the addition of SCM or filler. Chemical analysis has been performed on the cement pastes by data analysis of isothermal calorimetry (IC), thermogravimetric analysis (TGA), X-ray diffraction (XRD), scanning electron microscopy (SEM) with energy dispersive spectroscopy (EDS) on the selected cement pastes. Integrating these techniques helps the understanding of the mechanical performance of the mortar samples and brings new insight into the effect of both SCMs and filler on the hydration of OPC.

In addition, the environmental impacts of the selected concrete mixtures were compared using an MS Excel based Life-cycle Assessment (LCA) tool "GreenConcrete LCA" developed by Gursel and Horvath [77]. This cradle-to-gate life-cycle assessment LCA tool estimates direct and supply-chain global warming potential (GWP) in units of CO_2-equivalent (CO_2-eq) emissions and major criteria air pollutants (CO, NO_x, PM_{10}, and SO_2) associated with the use of electricity, fuel, transportation, and production processes taking place within the boundary of concrete production system. In LCA applications, drawing the system boundaries, i.e., decisions on inclusion or exclusion of processes in an analysis, is an essential step [78]. This study incorporates the following parameters in the system boundary: extraction of cement raw materials, manufacturing of cement, extraction and processing of aggregates, manufacturing of superplasticizers, preparation and treatment of fly ash prior to mixing into concrete, extraction and processing of limestone, and concrete batching, and transportation of raw materials and products within the system.

1.3 Organization of the dissertation

The dissertation is divided in four chapters:

Chapter 1 summarizes the motivations of this study and presents the fundamental concepts of supplementary cementitious materials, fillers, and self-consolidating concretes, and explains the objectives and the scope of this study.

Chapter 2 describes the materials used and focuses on the experimental and analytical methods applied on the samples of concrete, mortar and cement paste.

Chapter 3details and discusses the results of experimental and analytical investigations including fresh and hardened properties and environmental assessment of specimens.

Chapter 4 outlines the main results of the research and proposes the areas of future work.

2 Materials and methods

2.1 Materials

Ordinary Portland cement (OPC), basaltic ash pozzolan/natural pozzolan (NP), Class-F fly ash (FA), and limestone powder were used as powder material to produce blended cementitious material in concrete, mortar and cement paste. OPC used in this study meets ASTM Type I/II standard specification. NP and FA was obtained from Jabal Kadaha in Harrat Rahat, Saudi Arabia (Figure 2.1) [79], and the Jim Bridger Power Plant, Wyoming, US, respectively. The mean particle diameters of OPC, NP and FA are 10μm, 17μm, 22.3μm, respectively. The mean particle diameters of limestone powder in concrete (LPC) and limestone powder in mortar and cement paste (LP) were 48.1μm and 19μm, respectively. To reduce the energy required to grind limestone, a coarser limestone powder was used in concrete. All mean particle diameters were determined by using laser granulometry of a Malvern Mastersizer (see Table 2.1 and Figure 2.2). Aggregates used in the concrete include quartzitic sand with fineness modulus of 3.1, pea gravel with maximum size of 12.7mm (½") and basalt with maximum size of 19.0mm (¾") in the concrete specimens. The high-efficiency polycarboxylate-based superplasticizers (ADVA-140M/ADVA-405) with specific gravity of 1.04 and water content of 0.68 were used as <1.5 wt.% cement. The chosen superplasticizers meet the requirements of ASTM C494 as Type A and Type F, and ASTM C1017 as Type I. No viscosity-modifying admixture was used. Graded silica sand satisfying ASTM C778 [80]," with a specific gravity of 2.65 and absorption of less than 0.1% was used in the mortar samples.

Figure 2.1 Schematic map showing the cenozoic lava and cinder cone fields, or harrats, of western Saudi Arabia, adapted from [81], and the site of the basaltic ash from Jabal Kadaha, Harrat Rahat used in the experimental concretes.

Table 2.1 Particle size distribution of ordinary Portland cement (OPC), basaltic ash pozzolan (NP), Class F fly-ash (FA), limestone powder in concrete (LPC), and limestone powder in mortar and paste (LP).

	Mean (μm)	Median (μm)	Mode (μm)
OPC	10.4	11.7	18.5
NP	17.4	13.8	18.6
FA	22.2	12.5	24.4
LPC	48.1	38.7	72.0
LP	18.9	15.5	14.2

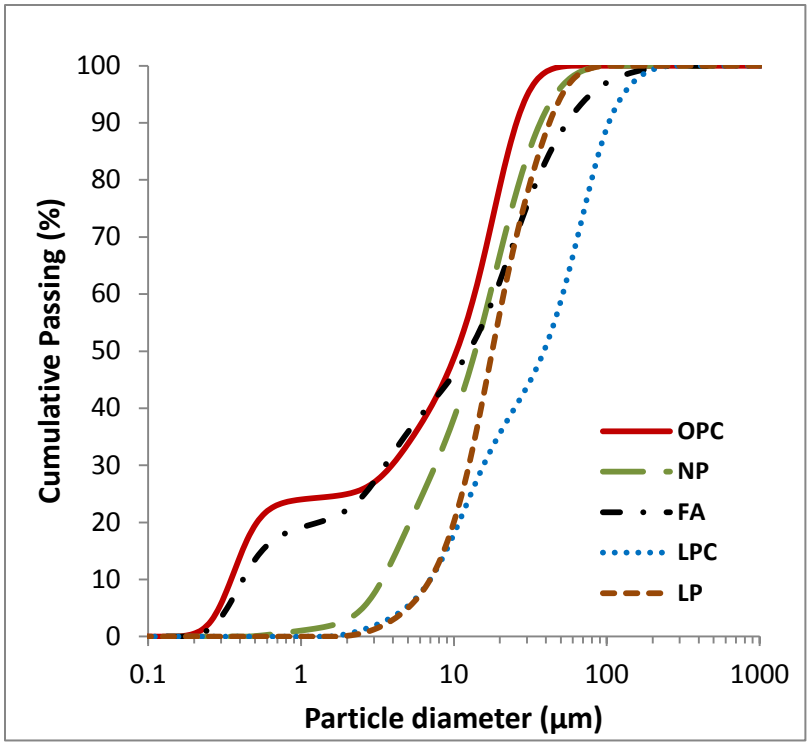

Figure 2.2 Particle size distribution of OPC, NP, FA, LPC, and LP use in the blended cement

The chemical compositions of OPC, limestone powder, NP, and FA determined by XRF are shown in Table 2.2. The XRD measurements on NP, FA and LP used in this study were performed using a PANalytical X'Pert PRO Materials Research Diffractometer. XRD patterns taken at ambient conditions are presented in Figure 2.3 together with schematic diagrams for relevant phases. The NP measurement, the FA measurement and the LP measurement are plotted with the same intensity scales. The NP is rich in anorthite, forsterite and diopside minerals. Although the FA is mainly composed highly amorphous aluminosilicate glass [82], the XRD analysis reveals that it also has several crystalline phases including mainly quartz (SiO_2), but also included hematite (Fe_2O_3), magnetite (Fe_3O_4), mullite ($3Al_2O_3 \cdot SiO_2$), and anhydrite ($CaSO_4$). The XRD analysis of LP showed that it was composed mainly of calcite ($CaCO_3$) and dolomite [$CaMg(CO_3)_2$], and also included quartz, and muscovite. Similar phases were observed in fly ash [83] and limestone [83-85] samples by other researchers.

Table 2.2 Chemical compositions of powder materials (oxides, % by weight).

	OPC	NP	FA	LPC/LP
SiO_2	20.44	46.48	62.0	0.70
Al_2O_3	3.97	14.74	18.90	0.50
Fe_2O_3	4.07	12.16	4.90	0.12
CaO	62.90	8.78	5.98	47.40
MgO	2.42	8.73	1.99	6.80
Na_2O	0.37	3.39	2.41	--
K_2O	0.43	1.27	1.14	--
P_2O_5	0.16	0.63	0.26	--
TiO_2	0.23	2.31	1.09	--
MnO	0.32	0.19	0.04	--
L.O.I.	4.69	1.32	1.30	44.48

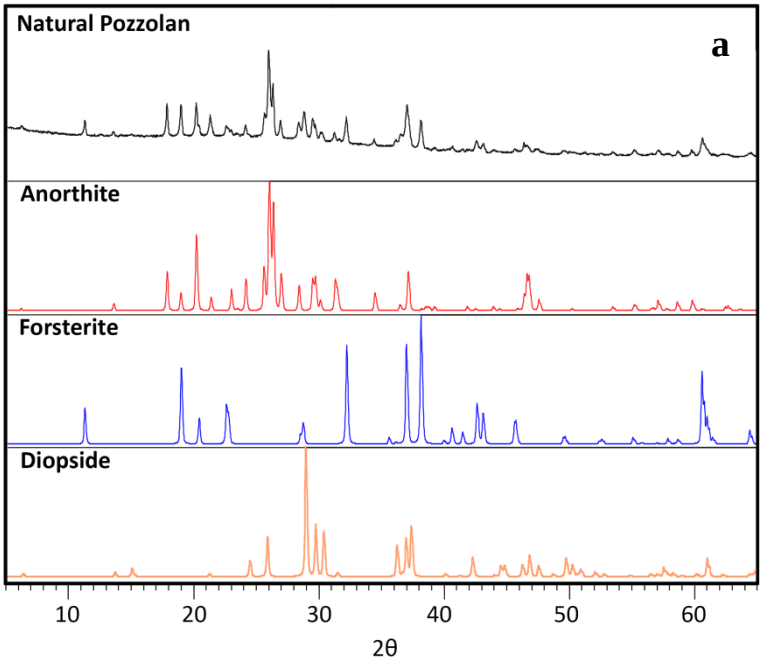

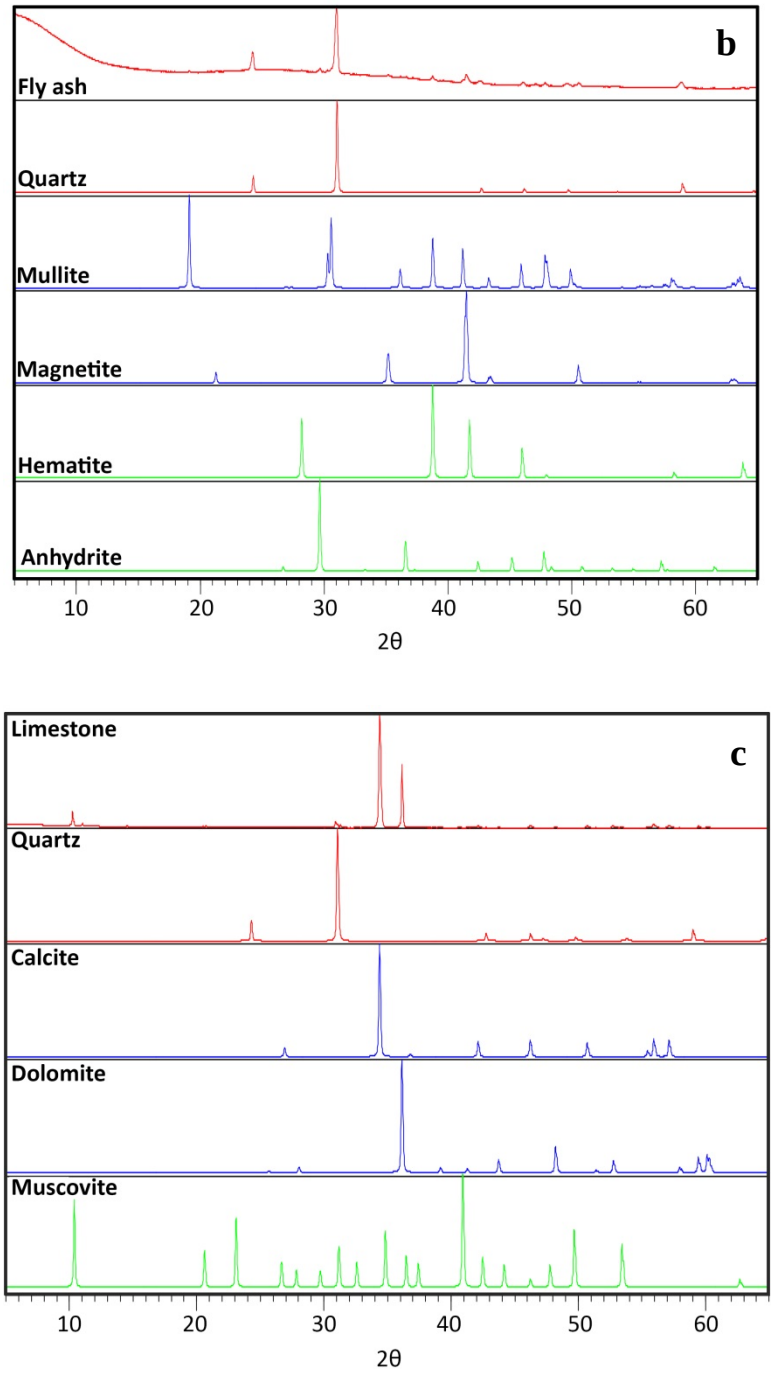

Figure 2.3 X-ray diffraction pattern of (a) NP; the main peaks of anorthite, forsterite, and diopside, (b) FA; the main peaks of anhydrite, mullite, hematite, magnetite, quartz (c) LPC/LP; the main peaks of muscovite, dolomite, calcite, and quartz.

The bulk chemical composition of the Jabal Kadaha NP is typical of an alkali basalt material (Table 2.2). Optical micrographs (Figure 2.4) from petrographic investigations of crushed sand-sized particles of the basaltic ash, which is similar to other Saudi Arabian *harrat* basalts [33, 35, 36]. provide a qualitative assessment of the various glass and crystal components available for pozzolanic reaction in the experimental concretes. The mineralogical composition determined by X-ray diffraction (Figure 2.4a), and confirmed with petrographic observations, indicates a glassy amorphous groundmass, and crystals of plagioclase with an anorthitic composition ($CaAl_2Si_2O_8$), olivine with a forsteritic composition (Mg_2SiO_4), and clinopyroxene with a diopsidic composition ($MgCaSi_2O_6$) (Figure 2.4a, b, c, see [86] for petrographic techniques of mineral identification). Some olivine and diopside crystals have partially dissolved (Figure 2.4a, b, c), and fresh sideromelane glass is generally absent. Rather, the glass has altered to clear, translucent, optically isotropic, gel-palagonite (Figure 2.4d), yellowish-olive brown in plane polarized light [87]. This commonly grades into transitional, glassy, fibro-palagonite, which is dark-dusky brown in plane polarized light, with a fine, fibrous, opaque, texture (Figure 2.4e). The groundmass of lava rock fragments from the volcanic edifice that were entrained in the magma during eruption to the earth's surface, have a strong fibro-palagonite texture (Figure 2.4f).

Resinous, yellow brown gel-palagonite (Figure 2.4d) is the most abundant component of the volcanic ash. Palagonite is a stable alteration product of fresh volcanic glass that has interacted with aqueous solutions on or near the earth's surface, and lost Si, Al, Mg, Ca, Na and K, gained H_2O, and become preferentially enriched in Ti and Fe [87]. These trends are further emphasized in fibro-palagonite, which seems to develop very poorly-crystalline clay mineral not detectable through standard X-ray diffraction analyses [87]. The palagonitization process commonly involves the precipitation of secondary phases, mainly crystalline clay minerals, zeolites, or calcite [87], many of which have pozzolanic properties [32, 34]. Although subaerial alteration of the volcanic glass of Jabal Kadaha NP produced palagonite, there are only occasional secondary authigenic surface coatings. These are thin rims of fluoroapatite ($Ca_5(PO_4)_3F$ and calcite on vesicle surfaces (Figure 2.4f, g, h). The precipitation of fluorapatite may reflect the movement of low-temperature waters locally saturated with respect to fluorine and phosphorous through the ash deposit [88], possibly associated with dissolution of apatite-bearing mantle xenoliths in the basaltic ash [89]. Calcite is a common authigenic mineral in basaltic ash and may be associated with CO_2 that combines with calcium in interstitial ground water. These mineral coatings constitute only a minuscule volume of the NP, and are not present in sufficient quantities to be detected by the X-ray diffraction analysis (Figure 2.4a).

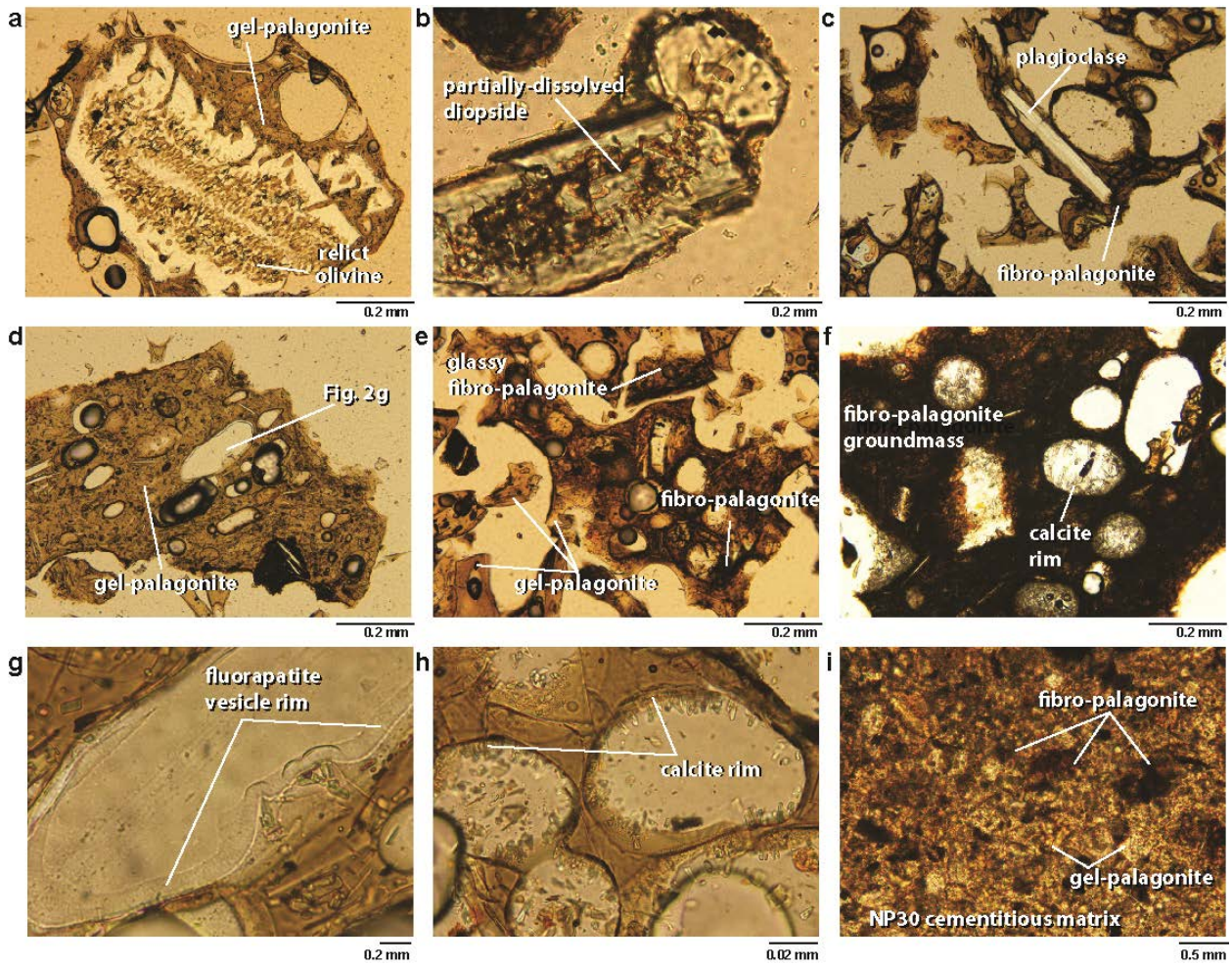

Figure 2.4 Petrographic micrographs of Saudi Arabian basaltic ash pozzolan (NP). Survey of volcanic fragments, plane polarized light: (a) dissolved crystal, probably olivine, (b) etched diopside, (c) intact anorthite, (d) gel-palagonitic glass, (e) transition to fibro-palagonitic glass, (f) fibro-palagonitic groundmass of a lava lithic fragment, with calcite surface coatings in vesicles, (g) gel-palagonite glass (Fig. 2d) with fluoroapatite rims on a vesicle surface, (h) gel-palagonite glass with calcite crystals on vesicle surfaces, and (i) cementitious matrix of the *70OPC–30NP* concrete mix at one year hydration. The dense opaque fabric results from intergrown, amorphous, cementitious hydrates that surround silt to fine sand-sized, partially-reacted gel-palagonite particles. Dark lava lithic fragments with poorly-reactive fibro-palagonite ground mass remain largely intact.

2.2 Methods

2.2.1 Concrete samples

2.2.1.1 Concrete mixture proportions

Concrete mixture proportions with NP and FA are given in Table 2.3 and Table 2.4, respectively. The mixture designs are designated *55OPC–30NP–15LPC*, for example, for the 55 wt.% OPC, 30 wt.% NP, and 15 wt.% LPC mixture. The differences considered for mixture selection were proportion of powder. The water to binder ratio (*w/b*) was held constant at 0.35 for all mixes and the amount of superplasticizer (SP) was added to provide a slump flow diameter between 56-69 cm, and a diameter of 50 cm flow time, T_{50}, between 2 to 5 seconds. The actual *w/b* ratio was 0.36 as the water contribution for the SP increased the overall water content. To reduce the cement content compared to typical SCCs, the total aggregate to fines ratio was fixed at 4:1. The cement replacement (CR) ratio varied from 30% to 65 % by weight for NP mixtures, and 30% to 75% by weight for FA mixtures. For the ternary blends, the LPC content was set as 15 wt.% for NP mixtures, while it was set as 15 wt.% and 25 wt.% for FA mixtures. The ratio of NP or FA was varied between 30 wt.% and 50 wt.% in binary mixtures. The ratio between coarse aggregate and fine aggregate was kept at 1:1. The coarse aggregate consists of 30 wt.% pea gravel and 70 wt.% basalt.

Table 2.3 Concrete mixture proportions with natural pozzolan addition

	(*w/b* = 0.35)	Proportions (by weight)						kg/m^3 of concrete		
	OPC–NP–LPC	OPC	NP	LPC	Aggregates		SP** (%)	Binder	OPC	CR
					Fine	Coarse				
Control mixes	100OPC	1.00	—	—	2.00	2.00	1.43	461	461	0
	85OPC–15LPC	0.85	–	0.15	2.00	2.00	1.43	458	389	69
Binary HVNP blends	70OPC–30NP	0.70	0.30	0.00	2.00	2.00	1.39	453	317	136
	50OPC–50NP	0.50	0.50	0.00	2.00	2.00	1.14	449	224	225
Ternary HVNP–LPC blends	55OPC–30NP–15LPC	0.55	0.30	0.15	2.00	2.00	1.14	451	248	203
	45OPC–40NP–15LPC	0.45	0.40	0.15	2.00	2.00	1.03	448	202	246
	35OPC–50NP–15LPC	0.35	0.50	0.15	2.00	2.00	1.00	446	156	290

* Keys: *w/b*= water to binder ratio; OPC = ordinary Portland cement; NP= Natural pozzolan; LPC = limestone powder in concrete; SP = superplasticizer; CR = cement replacement, HVNP = High-volume natural pozzolan, HVNP-LPC = =High-volume natural pozzolan and limestone.
** High-efficiency polycarboxylate-based superplasticizer (ADVA 140M/ADVA-405)

Table 2.4 Concrete mixture proportions with Class F fly ash addition

	(*w/b* = 0.35)	Proportions (by weight)						kg/m^3 of concrete		
	OPC–FA–LPC	OPC	FA	LPC	Aggregates		SP** (%)	Binder	OPC	CR
					Fine	Coarse				
Control mixes	100OPC	1.00	—	—	2.00	2.00	1.43	461	461	0
	85OPC–15LPC	0.85	–	0.15	2.00	2.00	1.43	458	389	69
	75OPC–25LPC	0.75	–	0.25	2.00	2.00	1.32	456	342	114
Binary HVFA blends	70OPC–30FA	0.70	0.30	0.00	2.00	2.00	1.39	453	317	136
	50OPC–50FA	0.50	0.50	0.00	2.00	2.00	1.14	449	224	225
Ternary HVFA–LPC blends	55OPC–30FA–15LPC	0.55	0.30	0.15	2.00	2.00	1.14	451	248	203
	45OPC–40FA–15LPC	0.45	0.40	0.15	2.00	2.00	1.03	448	202	246
	35OPC–50FA–15LPC	0.35	0.50	0.15	2.00	2.00	1.00	446	156	290
	25OPC–60FA–15LPC	0.25	0.60	0.15	2.00	2.00	1.00	444	111	333
	55OPC–20FA–25LPC	0.55	0.2	0.25	2.00	2.00	1.34	451	248	203
	45OPC–30FA–25LPC	0.45	0.3	0.25	2.00	2.00	1.14	449	202	247
	35OPC–40FA–25LPC	0.35	0.4	0.25	2.00	2.00	1.14	447	156	291
	25OPC–50FA–25LPC	0.25	0.5	0.25	2.00	2.00	1.14	445	111	334

* Keys: *w/b*= water to binder ratio; OPC = ordinary Portland cement; FA= Class F fly ash; LPC = limestone powder; SP = superplasticizer; CR = cement replacement, HVFA = High-volume fly ash, HVFA–LPC = High–volume fly ash and limestone
** High-efficiency polycarboxylate-based superplasticizer (ADVA 140M/ADVA-405)

2.2.1.2 Concrete mixing and casting

A total volume of 22 liters of concrete was prepared in a pan planetary-type mixer for each mixture. First, coarse aggregates and a small amount of water were mixed for 30 seconds. Then cement, natural pozzolan or fly ash, and more water were added and mixed for 1 minute. Limestone powder and the rest of the water were added and mixed for 1 minute before the water reducer was added and mixed again for 1 minute. Fine aggregate was added and mixed for 3 minutes. During that time, the mixer was stopped if necessary, and the bottom of the mixer was scraped to remove fine particles.

The slump flow test was performed on the prepared mixture (Section 3.3.2). When the concrete mixture met the desirable slump flow diameter and T_{50}, it was returned to the mixer and mixed for an additional minute before casting. If the slump flow time was too low or too high, the concrete was returned to the mixer, mixed for an additional minute and the water reducing admixture was adjusted until workability looked to be sufficient. Then the slump flow test was performed once more. If the concrete was then satisfactory in terms of consistency and cohesiveness, it was remixed for an additional minute before casting. Otherwise, it was discarded and a new trial mixture was prepared with a proper amount of water-reducer admixture.

Once the concrete mixture was prepared, the following samples were cast: eighteen 75×150 mm cylinders and three 100×200 mm cylinders in two lifts without mechanical vibration. Light shaking was allowed as the only method of consolidation. Cylinders were immediately covered with plastic wrap and left undisturbed for 24 hours under the ambient laboratory conditions. The cylinders were then demolded and placed in an environmental chamber at 100% relative humidity and room temperature (23±2°C) until testing in accordance with ASTM C 192 [90].

2.2.1.3 Slump flow test

To assess the properties of the fresh concrete, the slump flow test (Figure 2.5) was carried out according to ASTM C1611 [91] and the flow diameter and T_{50} time was recorded. To evaluate for SCC characteristics, the flow diameter and T_{50} were checked at 550–700 mm and 2–5 seconds, respectively [79, 92, 93]. In addition, segregation and bleeding were checked qualitatively by observing aggregate density and excess liquid near the slump flow perimeter.

Figure 2.5 Slump flow test of self-consolidating concrete

2.2.1.4 Compressive strength test

Compressive strength of concrete was determined according to ASTM C39 [94] at 7, 28, and 91 days, and one year on 75×150 mm cylinders. The results reported in this study present the mean values of three samples for each mixture and curing period. Rubber pads were used to cap all 7-day samples and 14-day samples (ASTM C1231 [95]), while all others were capped with sulfur mortar (ASTM C617 [96]). The compressive strength of cylinders was measured under a stress rate control machine until significant softening was observed. The maximum load value was taken as the compressive strength. To keep the coefficient of variation (ratio of standard deviation to mean) at less than 10% for each mixture and curing period, the outliers were identified and removed from the data. The cylinder size was preferred for convenience and economy, yet testing 75×150 mm concrete cylinders with 19.0 mm maximum size aggregate undervalue compressive strength by 2.94%, compared to the standard 100×150 mm concrete cylinders due to the "wall effect" [97, 98]. For that reason, the correction factor of 102.94% was used in compressive strength calculations.

2.2.1.5 Non-steady state chloride migration test

To determine the resistance of one-year-old concrete samples to chloride penetration, a non-steady state chloride migration test was performed in accordance with Nordtest Method, NT BUILD [99]. The 100×200 mm cylinder samples were sawed into 50 ± 2 mm-thick sections, and brushing and washing away any burrs from the surfaces, and then cured in the fog room until the testing date.

Three specimens were tested for each mixture. They were preconditioned by vacuuming in the saturated $Ca(OH)_2$ solution and then settled between a catholyte solution (10% NaCl) and an anolyte solution (0.3 N NaOH). The specimens were tested under a 30 V electrical potential for 24 hours (Figure 2.6a). Each specimen was then split axially into two pieces, and a 0.1 M $AgNO_3$ solution was sprayed on the freshly split surfaces where the areas containing chloride ions colored white. The chloride penetration depth was measured on photographic images of the specimens enlarged with image-processing software at seven points over 70 mm distance from the white silver chloride precipitation. From the mean penetration depth, the non-steady state chloride migration coefficient D_{nssm} (2) was calculated, as described in NT BUILD 492 [99], using:

$$D_{nnsm} = \frac{RT}{zFE} \cdot \frac{x_d - \alpha\sqrt{x_d}}{t} \qquad 1$$

where

$$E = \frac{U - 2}{L}$$

and

$$\alpha = 2\sqrt{\frac{RT}{zFE}} \cdot erf^{-1}\left(1 - \frac{2c_d}{c_0}\right)$$

where D_{nssm} is the non-steady-state migration coefficient, m^2/s; z is the absolute value of ion valence for chloride, $z = 1$; F is the Faraday constant, $F = 9.648 \times 10^4$ J/(V·mol); U is the absolute value of the applied voltage, V; R is the gas constant, $R = 8.314$ J/(K·mol); T is the average value of the initial and final temperatures in the anolyte solution, K; L is the thickness of the specimen; x_d is the average value of the penetration depths, m; t is the test duration in seconds; erf^{-1} is the inverse of the error function; c_d is the chloride concentration at which the color of the concrete changes, and c_d generally equals 0.07 N (N is the molar concentration divided by an equivalence factor) for OPC concrete; and c_0 is the chloride concentration in the catholyte solution, about 2 N. Three specimens were tested for each mixture, and the average was calculated.

2.2.1.6 Water absorption test

A water absorption test was carried out on the one-year-old concrete specimens, 100 mm in diameter and 50 mm in thickness, in accordance with the ASTM C948 [100]. The specimens were immersed in 21°C water and weighed every 24 hours until obtaining saturated-surface dry (SSD) weight stabilization, which requires less than 0.5% weight difference between two successive measurements. The last weight obtained of specimens was designated as *B*. Then, the specimens were dried at 100–110 °C in oven, and weighed every 24 hours. Once a weight loss of less than 0.5% of previously measured weight was obtained, the specimen was cooled in a vacuum desiccator to room temperature. The weight of the specimen in room temperature was designated as *C*. The water absorption was determined as follows:

$$Water\ absorption\ (\%)\ = \frac{B - C}{C} x100 \qquad 2$$

2.2.1.7 Gas permeability test

The gas permeability test was performed on the one-year-old oven-dried specimens according to the CEMBUREAU method [101] to determine the gas permeability coefficient (Figure 2.6b). Nitrogen gas was applied to the specimens at five particular gas pressures in the range from 0.5 bar (0.05 MPa) to 2.5 bar (0.25 MPa), in 0.5 bar (0.05 MPa) increments. Flow times of nitrogen gas were recorded until a steady-state flow was obtained. The steady-state condition was reached once the difference between two successive flow times was less than 3% within 5 minutes. For each gas pressure stage, the gas permeability coefficient, K_g, was calculated using the Hagen-Poiseuille relationship for laminar flow of a compressible fluid through a porous medium under steady-state conditions [102], so that:

$$K_g = \frac{2P_0 QL\mu}{A(P^2 - P_a^2)} \qquad 3$$

where K_g is the gas permeability coefficient (m^2); Q is the volume flow rate of the fluid ($m^3\ s^{-1}$); A is the cross-sectional area of the specimen (m^2); L is the thickness of the specimen in the direction of flow (m); μ is the dynamic viscosity of the nitrogen at test temperature (N s m^{-2}); P is the inlet (applied) pressure (absolute) (N m^{-2}); P_a is the outlet pressure assumed in this test to be equal to atmospheric pressure (N m^{-2}); and P_0 is the pressure at which the volume flow rate is determined, assumed in this test to be atmospheric pressure (N m^{-2}).

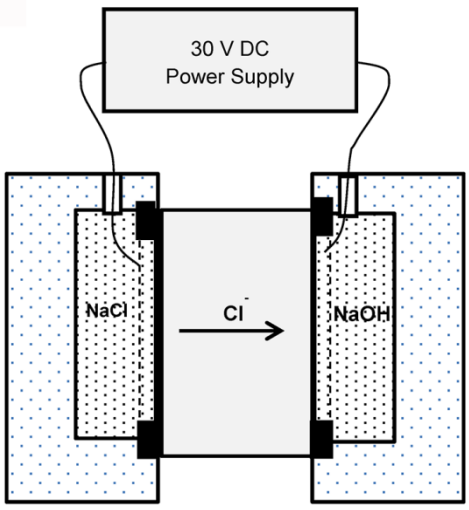

(a)

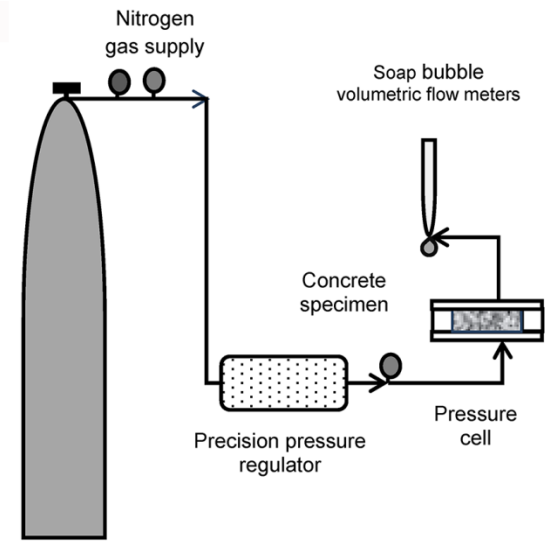

(b)

Figure 2.6 Schematic diagrams of experimental testing devices. (a) Test set-up of the chloride migration test, and (b) typical setup for the gas permeability test.

2.2.2 Mortar samples

2.2.2.1 Mortar mixture proportions

Mortar cubes (40×40×40 mm) with binder–sand–water proportions of (1/3/0.5) were prepared in accordance with ASTM C305 – 12 [103]. The percentage of cement replacement material ranged from 30% to 65% by weight (Table 2.5). NP and FA content were varied between 30% and 50%. For the ternary blends, LP was kept at a constant 15%. The combinations of Portland cement-based binary and ternary blends were shown in Table 2.5. The corresponding cements, for instance, were labelled as *55OPC–30NP–15LP* for the 55%OPC, 30%NP and 15%LP by weight. The cubes were immediately covered with plastic wrap and stored into a fog room at a relative humidity of greater than 95% for 24 hour. The samples were cured in $Ca(OH)_2$ saturated solution at 23±2 °C after demolding them.

Table 2.5 Composition of binders in mortar specimens

	Materials (wt. %)		
	OPC	NP/FA	LP
100OPC	100	–	–
85OPC–15LP	85	–	15
70OPC–30NP/FA	70	30	–
50OPC–50NP/FA	50	50	–
55OPC–30NP/FA–15LP	55	30	15
45OPC–40NP/FA–15LP	45	40	15
35OPC–50NP/FA–15LP	35	50	15

2.2.2.2 Normal consistency and setting time

The binary and ternary cement blends and control mixtures were tested for normal consistency in accordance with ASTM C187 [104]. The cement pastes were proportioned and mixed to normal consistency, and thereafter the Vicat needle penetration test was conducted to obtain the initial and the final time of setting in accordance with ASTM C191 [105].

2.2.2.3 Compressive strength test

The compressive strength of the samples was determined on three mortar prisms for each testing age (one day, three days, seven days, 14 days, 28 days, 91 days, 180 days, and one year) according to ASTM C109/C19M [106]. The strengths of three mortar specimens were then averaged. The samples are being cured to test at the age of two year.

2.2.3 Cement pastes

2.2.3.1 Mixture proportions of cement pastes

To study the time-dependent hydration process XRD, thermogravimetric analysis (TGA), isothermal calorimetry (IC) and scanning electron microscopy (SEM) was used up to the reaction time of seven days, 28 days and 91 days on the selected specimens. Table 2.6 contains the proportions of powder materials used in paste. All the powder materials are homogenized by dry mixing.

Table 2.6 Composition of binders in the specimens of cement paste

	Materials (wt. %)		
	OPC	NP/FA	LP
100OPC	100	–	–
85OPC–15LP	85	–	15
70OPC–30NP/FA	70	30	–
55OPC–30NP/FA–15LP	55	30	15

2.2.3.2 Mixing and casting of cement pastes

The paste specimens were prepared with distilled-water to binder ratio (*w/b*) of 0.50 by hand-mixing, and cast into cylindrical molds measuring ϕ2.54×2.54 cm plastic cylinders and stored at 23±2 °C in 100% relative humidity until testing age. The paste specimens, then, were immersed in isopropanol to stop the hydration process, vacuum-dried, and kept under carbonation-free conditions until testing.

2.2.3.3 X-ray powder diffraction (XRD)

X-ray powder diffraction (XRD) spectra of raw materials and hydrated cement paste specimens were obtained using a PANalytical X'ert PRO with X'Celerator ® position sensitive detector. The finely-ground samples of cement paste were loaded into metal sample holders and placed into the diffractometer (Figure 2.7). XRD measurements were operated with Co Kα radiation (wavelength of 1.789 Å) at 40 mA and 40 kV. XRD acquisition was carried out in continuous scan mode over the range 5 to 65° 2θ with a step width of 0.0170° (i.e. 3527 steps) and a counting time of 4.08 s, corresponding to a total acquisition time of 4 hours. PANalytical X'Pert HighScore Plus was used to analyze the data.

Figure 2.7 Placing finely-ground samples of cement paste mixtures into the diffractometer.

2.2.3.4 Thermal analysis

2.2.3.4.1 Isothermal calorimetry (IC)

The heat of hydration of cement is measured by calorimetry, and the hydration behavior of the exothermic reaction is observed. The heat generated by the reaction tends to have characteristic thermal pattern. Once the heat evolution is plotted over time, it is comparatively easy to define the chemical reactions that have occurred, an estimate of the heat evolved and the rate of heat evolved at any given time in the reaction. Yet, the pattern is dependent on the properties of the cement and will differ on addition of supplementary cementitious materials and chemical admixtures such as superplasticizers.

Isothermal conduction calorimetry has been used to assess the effects of SCM and additives to the hydration reaction [47, 107, 108]. While fly ash samples indicate little to no effect of the hydration other than a small amount of retardation of hydration of alite ([109] cited [110]), slag blends demonstrates an acceleration of the hydration reaction as well as an increase in the heat evolved [110, 111].

The hydration kinetic of cement mixtures was investigated. To this end, a series of cement pastes was prepared with binders that their compositions were described in Table 2.6. The mixtures had *w/c* 0.35 and 0.50. All pastes were mixed in a vacuum mixer (Twister evolution) at 450 rpm. The first step of dry mixing was 30 s for all mixtures. In the next step, the 90% of the water was added and mixed for 1.5 min. In the last step, the rest of the water was added, and the pastes were mixed further 3 min.

The heat flow was measured with a Thermometric TAM Air conduction calorimeter, capable of eight parallel measurements in eight separate measuring cells. About 5.4 g of freshly mixed paste were weighed into a glass vial with a 25.4 mm of internal diameter, corresponding to about 5-

mm thick paste layer. The glass vial was sealed and placed into the calorimeter and the heat flow was measured for about 162 hours. During the experiment, isothermal conditions (20±0.02℃) were maintained in the measuring cells. The hydration heat flow and the cumulative hydration heat, normalized to the cement weight in the samples are shown in the resulting plots.

2.2.3.4.2 Thermogravimetric analysis (TGA)

Thermogravimetric Analysis (TGA) was used to follow the hydration reaction, to determine the amount of CH and the presence of other phases in the cementitious matrix, and to calculate the pozzolanic reaction. The equation X was used to calculate the amount of bound water (H) in the paste where w_{40} and w_{550} is the weight of acetone washed - dry sample at 40 °C and 550 °C, respectively. The bound water indicates decomposition of hydrates such as AFm and AFt phases, and C–S–H in cement paste [112]. The amount of portlandite and calcite was found by the weight loss between 400 °C and 550 °C, and the weight loss between 600 °C and 900 °C. The exact temperature range was determined by the tangent method [113].

$$H = \frac{w_{40} - w_{550}}{w_{550}} \quad 4$$

Under the thermal treatment, cementitious material goes through physical and/or chemical changes such as weight, dimension, or crystalline transition. DTA detects these variations as a function of temperature. An endothermal change and exothermal change is represented by a trough and a peak, respectively. These exothermal and endothermal effects are characterized by their temperature range and used to determine the phases present [114]. DTA is commonly used with TGA, as TGA determines the weight change as the sample undergoes heating at a uniform rate. This weight change, caused by the release of gasses on heating, gives a good indication of the phases present, as most phase in cement alter at different temperatures.

The pastes described in Table 2.6 were studied with thermogravimetric analysis (TGA). The ground samples of between 15±1 mg were placed in the alumina crucible of a SDT Q600, for both TGA and DTA in the presence of flowing nitrogen gas at a flow rate of 100 ml/min. The sample was then heated from 30 - 1000°C at a heating rate of 20°C/min. A thermogravimetric (TG) curve is produced under these conditions. An example of TGA curve of percentage weight loss against time is shown in Figure 2.8. Due to decompostion of CH and $CaCO_3$, the weight loss can be calculated using this curve by the following method.

As:

$$Ca(OH)_2 \rightarrow CaO + H_2O \quad (5)$$

Molecular weight: 74 56 18

The sample may go through carbonation which will result in one mole of CH producing one mole of CO_2 in the following process.

$$Ca(OH)_2 + CO_2 \rightarrow CaCO_3 + H_2O \text{ (carbonation)} \quad (6)$$

Molecular weight: 74 44 100 18

$$CaCO_3 \rightarrow CaO + CO_2 \text{ (decarbonation)} \quad (7)$$

Molecular weight: 100 56 44

Therefore, as equation 7 will lead on to equation 8, the total $Ca(OH)_2$ is proportional to,

$$74/18 \times A + (74/100 \times 100/44 \times B) \quad (8)$$

or,

$$74/18 \times A + (74/44 \times B) \quad (9)$$

where A is the weight loss of one mole of water (18g/mol) from one mole of $Ca(OH)_2$ (74g/mol), due the dehydration of CH, and B is the weight loss of one mole of CO_2 (44g/mol) also from CH, due to decarbonation of $CaCO_3$. Both A and B are calculated using the TGA curve show in Figure 2.8, and are the difference in weight between approximately 410-540ºC and 600-780 ºC respectively. The weight change occurs within a range of temperatures and not at one set point as it depends on each cement system [15].

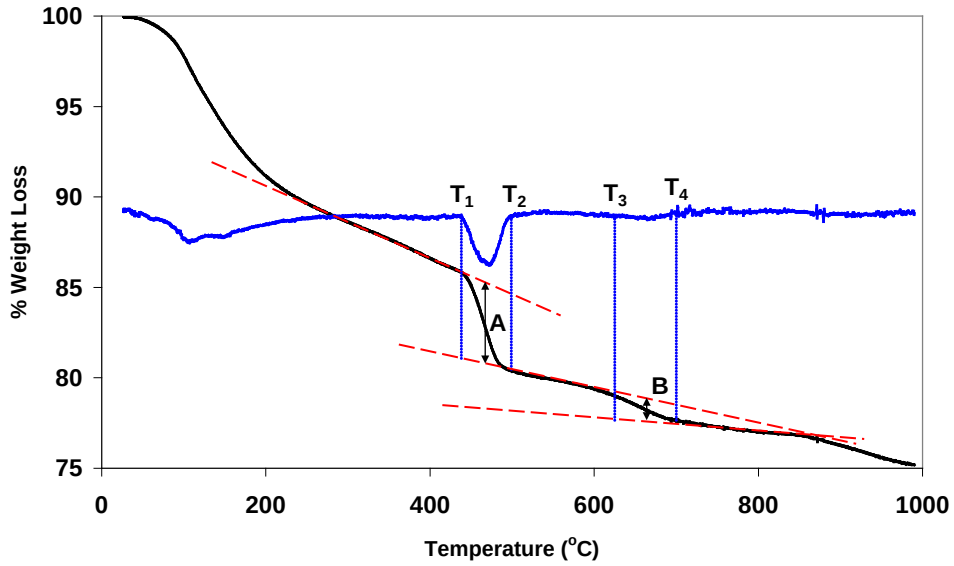

Figure 2.8 Example demonstrating the calculation of A and B in the TG curve [115]

The dotted blue lines correspond to the derivative of the weight loss curve, where these lines cross the weight loss curve is the point that a tangent is drawn shown as the red lines on this example. The tangents were used to calculate the midpoint of the weight loss curves so that the average percentage weight loss could be calculated. The weight loss was then substituted in to equation 7. The total amount of CH calculated was then divided by the percentage of sample left in the crucible (residue value) after the required temperature had been reached. This gives an estimated percentage of CH as ignited weight. This could then determine the extent of carbonation, if at all present, and the extent of the hydration reaction [15].

2.2.3.5 Scanning Electron Microscope (SEM)

SEM is able to provide a high resolution image with sufficient contrast that is required to distinguish the observed phases over the background of sample. A beam of electrons is generated by a thermionic emission and directed to the specimen. This incident or primary electron beam interacts with the sample which results in many forms of radiation being released as illustrated in Figure 2.9. A select few of the resulting signals are used in electron microscopy. Some of the beam will not interact with the sample and so remain unscattered, but the majority of the beam will and then undergoes either, elastic or inelastic scattering. Elastically scattered electrons will undergo a change in direction but have no detectable energy loss, it is predominantly these electrons that produce diffraction patterns. Inelastic scattering refers to electrons which upon interaction with the sample will change direction and lose some energy, resulting in secondary effects incidents. The energy lost will be transferred to the electrons or atoms in the sample in the form of heat [116, 117], but some may escape and have an effect which is detectable outside of the sample, these are called secondary effects. Secondary effects include emitted secondary electrons backscattered electrons, and characteristic X-rays ([117] cited [15]). With its high resolution, SEM provides a much clearer delineation of ultra-fine phases and intricate details in

the microstructure than the optical microscope, which has proven most useful in research dealing with concrete attack. CH crystals appear in many different shapes and sizes, but with the aid of EDX analysis identification is relatively simple. Other phases such as Calcium Sulfoaluminate Hydrates are more continuous in their morphology: AFt forms needle-like crystals in the vacant spaces during early hydration, and AFm appear as hexagonal platy crystals. Early-formed AFm tends to crystallize in clusters, rosettes of irregular plates, whereas those formed later grow into well developed, but very thin hexagonal plates.

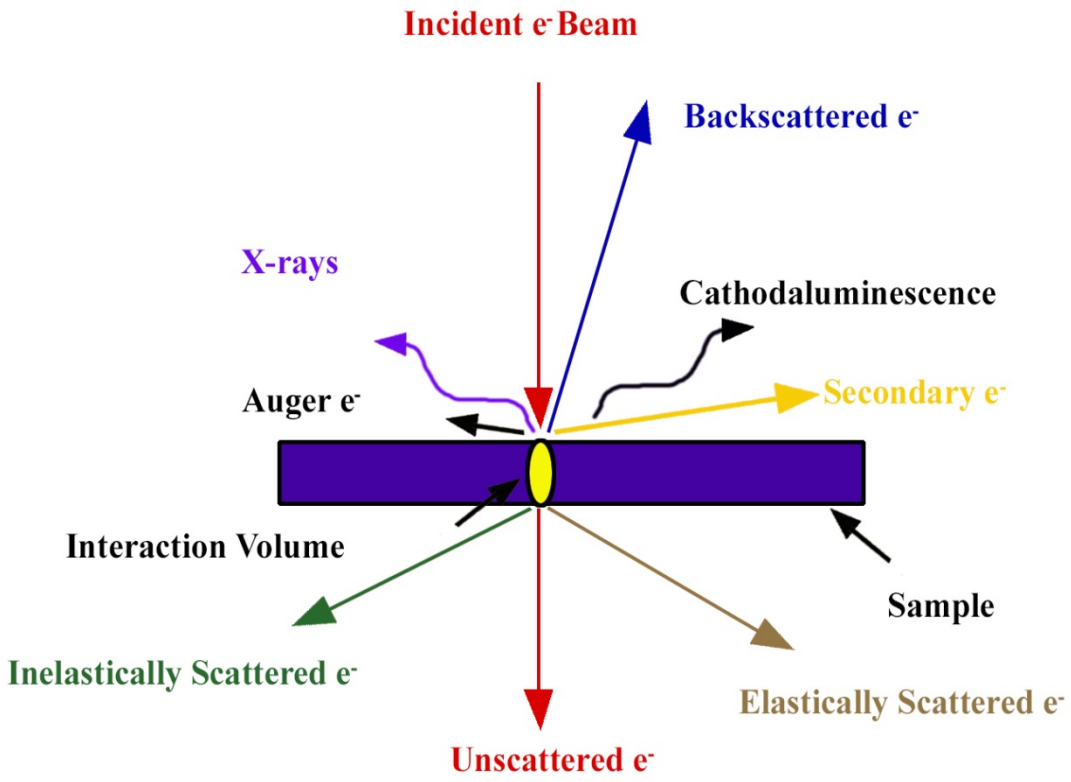

Figure 2.9 Schematic representation of the signals resulting from the electron beam interaction with a specimen ([118] cited in [15]

SEM with energy dispersive X-ray analysis (SEM- EDS), was performed on approximately 200µm thick slices of hardened paste, dried via solvent exchange using propanol before being resin impregnated with EPO-TEK 301-2 from Epoxy Technology. The demoulded resin impregnated pastes were then ground and polished using a Dayton Mico –3µ and ¼ µ, until level and smooth, before being carbon coated to a thickness of approximately 15nm, to prevent changing under the SEM beam. The anhydrous material was placed on a carbon film for the same reason. An EDAX TSL energy dispersive x-ray spectrometer on the Zeiss EVOMA10 Scanning Electron Microscope was operated with beam energy of 15 keV, beam current of 850 pA, and counting time of 10 seconds with 3500 counts per second, reported as relative atomic concentrations. The working distance was set between 6-9.5 mm for backscattered (BSE) imaging and 10-15 mm for EDS analysis. For microstructural morphology, 2 k and 20 k

magnification on BSE–SEM images were chosen to show homogenous microstructures of the paste.

2.2.4 Analytical procedures

A life-cycle approach systematically studies the environmental impacts of concrete by the quantification of resource inputs and environmental burdens (life-cycle inventory compilation), and estimates the impacts of these inputs and burdens on humans and nature (impact analysis), and identifies areas where improvements are possible. Therefore, LCA is particularly crucial for a methodical analysis of the cradle-to-gate environmental impacts of concrete production given the high volumes of concrete use, the growing importance of environmentally sustainable infrastructure decisions, and the fact that once concrete is put in a structure certain environmental factors are static for many years [119].

2.2.4.1 LCA methodology

The LCA approach is a methodological framework that assesses the environmental impacts and resources (including raw materials, energy, etc.) used throughout a product's life-cycle from raw material acquisition through production, use, maintenance, recycling, and ultimate disposal. ISO 14040 series are accepted as providing a consensus framework, terminology, and some methodological choices for performing a LCA [120, 121]. The LCA consists of four major stages, as illustrated in Figure 2.10.

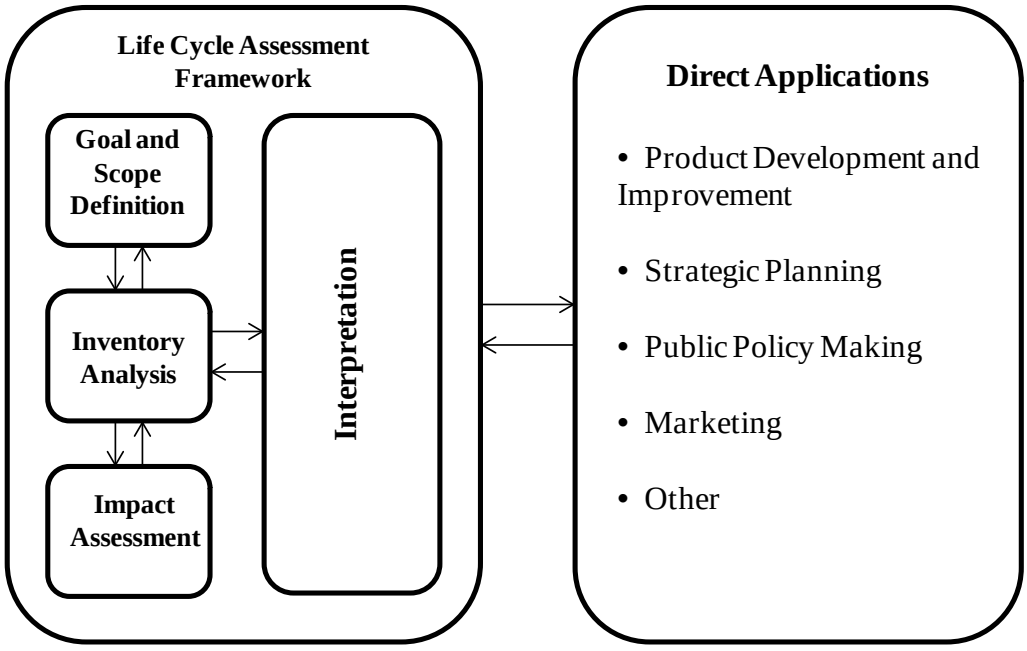

Figure 2.10 Stages and applications of an LCA, adapted from [121-123]

The goal and scope definition of an LCA provides a description of the product system in terms of the system boundary and functional unit. The functional unit, measured in the cubic meter of ready-mixed concrete, is the basis for comparison throughout the study [120, 121, 124]. In the GreenConcrete LCA tool, the system boundary starts with the extraction of cement and concrete raw materials, and covers major material production and preparation processes (e.g., cement, aggregates, admixtures, fly ash, and limestone), transportation of materials within the system, mixing of concrete materials at the batching plant, and ends at the gate of the concrete plant with the final product being the concrete mixture ready to be used at the construction site.

The life-cycle inventory (LCI) stage estimates the consumption of resources and quantities of waste flows and emissions caused by or otherwise attributable to a product's life-cycle. The processes within the life-cycle and associated material and energy flows as well as other exchanges represent the product system and its total inputs and outputs from and to the natural environment, respectively. Within the scope of the study, GWP (in CO_2-eq) as well as major criteria air pollutants that include CO, NO_X, PM_{10}, and SO_2 were estimated.

The life-cycle impact assessment (LCIA) stage evaluates the potential human and ecological effects of energy, water, and material consumption and the environmental releases identified in the inventory analysis. This stage involves classification, characterization, and normalization of impact categories. For the purpose of this study, concrete production GWP, that is relative to that of 1 kg of the reference gas CO_2 (in CO_2-eq) is calculated based on IPPC guidelines as follows [125, 126]:

$$GWP_{100_{YEAR}} = 1 \times CO_2 + 21 \times CH_4 + 310 \times N_2O \qquad 10$$

The life-cycle interpretation is the last stage of the LCA process. It is a systematic technique to "identify, quantify, check, and evaluate information from the results of the LCI and the LCIA, and communicate them effectively" [78, 121, 123, 127]. Results from the GreenConcrete LCA are discussed as part of the interpretation stage in following sections.

2.2.4.2 Environmental assessment of concrete mixtures

This study used a concrete production LCA tool named as GreenConcrete LCA [77] to assess the environmental profiles of concrete mixtures. The concrete incorporated with FA was included in this work as it was locally available. The tool evaluates both direct and supply-chain environmental impacts of each process during the production of concrete and concrete-making materials. For example, when a process involves the use of electricity, the tool provides not only direct electricity generation impacts but also supply-chain impacts that encompass the construction and operation of a power plant, as well as the life-cycle impacts of the major resources used in the construction of the plant, the operation of the plant, and so on. Moreover, integration of regional variations and technological alternatives in the material production processes within the tool offers a wide range of applicability and flexibility for cement and concrete manufacturers in the United States and worldwide.

Table 2.7 and Table 2.8 summarize the LCA inputs used in the GreenConcrete LCA tool regarding the production technologies, geographic locations, electricity grid mix percentages,

transportation distance and mode selection, as well as type of material choices , based on a real case scenario [59].

Table 2.7 Assumptions for the concrete mix production LCA calculations*

User-Input Data:	**Assumption**	
Type of cement	Type I	
Type of SCMs	Fly ash, limestone	
Type of admixture	Superplasticizer	
Electricity grid mix for:	**Location**	
Cement supplier	California, US	
Fine aggregates supplier	California, US	
Coarse aggregates supplier	Canada, average	
Gypsum supplier	California, US	
Limestone supplier	California, US	
Fly ash supplier	Wyoming, US	
Transportation details for:	**Mode**	**Distance (km)**
Cement raw materials to cement plant	Truck_Class 8b (Model 2005)	1
Gypsum to cement plant	Truck_Class 8b (Model 2005)	200
Cement to concrete plant	Truck_Class 8b (Model 2005)	60
Fine aggregates to concrete plant	Truck_Class 8b (Model 2005)	50
Coarse aggregates to concrete plant	Water_Barge and Truck_Class 8b (Model 2005)	1,000 km by barge and 10 km by truck
Admixture to concrete plant	Truck_Class 8b (Model 2005)	1,000
Fly ash to concrete plant	Rail	1,000
Limestone to concrete plant	Truck_Class 8b (Model 2005)	130
Technology options for:	**Type of technology selected**	**Distance (m)**
Cement raw materials prehomogenization	Dry, raw storing, preblending	
Cement raw materials grinding	Dry, raw grinding, ball mill	
Cement raw meal blending/homogenization	Dry, raw meal blending, storage	
Clinker pyroprocessing	Preheater/Precalciner kiln with US average kiln fuel mix [75]	
Clinker cooling	Reciprocating grate cooler (modern)	
Cement finish milling/grinding/blending	Roller press	
Cement PM control technology	ESP	
Conveying within the cement plant	Screw pump	20 m between process stations
Concrete batching plant loading/mixing	Mixer loading (central mix)	
Concrete batching plant PM control	Fabric filter	

* For further details see GreenConcrete LCA tool (Website: http://greenconcrete.berkeley.edu/).

Table 2.8 Electricity grid mix percentage by source of energy adapted from EIA [128, 129] for United States and from CEA [130] for Canada

User-Input Data	California (%)	Wyoming (%)	Canada (%)
Coal	1	91	19
Natural gas	55	1	6
Fuel oil	0.1	0.1	3
Petroleum coke	1		
Nuclear	16		13
Hydropower	14	2	58
Biomass	3		
Geothermal	6		
Solar	0.3		1
Wind	3	5	

* Percentages may not add up to 100% because rounding of the numbers during calculations.

3 Results and Discussion

3.1 Concrete samples

3.1.1 Flowability of fresh concrete

The slump flow diameter (ds) and T50 times of the concrete mixtures containing NP and FA are presented in Tables 3.1 and Table 3.2, respectively. According to the slump flow results, all mixtures met the specified SCC requirements; see Table 3.3 [131]. The visual stability index (VSI) values of the mixtures were evaluated between zero and one: zero shows no evidence of segregation or bleeding, and one showed segregation and slight bleeding as a sheen on the concrete mass, in accordance with ASTM C1611 [91]. Due the constant water content and variable use of water reducing agent, the impact of NP and LPC or FA and LPC replacement on flowability is not clearly discernible. However, it was noted that generally the necessary water-reducer content, and T50 decreased, or ds increased with the addition of NP or FA to the mixtures (Table 3.1 and Table 3.2). Remarkably, the 100OPC control concrete had a lower flow diameter and higher flow times, as compared with the more workable 70OPC–30NP concrete or 50OPC–50FA concrete, even though the amount of water reducer used in the 100OPC concrete was 32% and 25% greater, respectively

Table 3.1 Slump flow diameter and T_{50}.

OPC–NP–LPC (%)	d_s (mm)	T_{50} (sec)	SP (%)
100OPC	584	4.5	1.43
85OPC–15LPC	667	3.1	1.08
70OPC–30NP	686	3.8	1.03
50OPC–50NP	622	4.4	1.43
55OPC–30NP–15LPC	635	4.5	1.22
45OPC–40NP–15LPC	673	4.5	1.22
35OPC–50NP–15LPC	648	4.7	1.12

Table 3.2 Slump flow diameter and T_{50}.

OPC–FA–LPC	d_s (mm)	T_{50} (sec.)	SP (%)
100OPC	584	4.5	1.43
85OPC–15LPC	622	4.4	1.43
75OPC–25LPC	559	4.6	1.32
70OPC–30FA	610	4.5	1.43
50OPC–50FA	660	3.8	1.14
55OPC–30FA–15LPC	622	3.6	1.14
45OPC–40FA–15LPC	572	3.2	1.03
35OPC–50FA–15LPC	635	2.6	1.00
25OPC–60FA–15LPC	667	2.8	1.00
55OPC–20FA–25LPC	635	4.0	1.34
45OPC–30FA–25LPC	622	3.8	1.14
35OPC–40FA–25LPC	653	3.0	1.14
25OPC–50FA–25LPC	692	3.5	1.14

Table 3.3 Specifications and recommended values for SCC [63]

Workability characteristic	Test Methods	Recommended Values
Deformability and flow rate (filling ability, unrestricted flow)	Slump flow	Hwang et al .620 mm to 720 mm EFNARC: 650 mm to 800 mm JSCE: 600 mm to 700 mm PCI: ≥ 660 mm Swedish Concrete Association: 650 mm to 750 mm
	T_{50}	EFNARC: 2-5 seconds PCI: 3-5 seconds Swedish Concrete Association: 3-7 seconds

3.1.2 Compressive strength test

3.1.2.1 Compressive strength of HVNP

Figure 3.1 and Table 3.4 show that changing the mixture proportions of NP and LPC has a strong influence on the rate of strength development of the experimental concretes. The binary *70OPC–30NP* mixture results in concrete with only slightly lower strengths compared to the *100OPC* control concrete at all test ages (Figure 3.1a). However, the *50OPC–50NP* mixture produced a lower rate of strength development, about 25% less than the control at 1 year. Even so, the 28-day and one-year strength values, 34 MPa and 57 MPa, respectively, are adequate for most structural applications.

The ternary blends with 45–55% OPC replacement contain 15% LPC in addition to NP and OPC; they produce concretes with very good long-term compressive strength (Figure 3.1c). The *55OPC–30NP–15LPC* and *45OPC–40NP–15LPC* concretes show higher long-term strengths than the *85OPC–15LPC* control. At 90 days hydration, for example, the *55OPC–30NP–15LPC* concrete had compressive strength, 49 MPa, similar to the *85OPC–15LPC* control mixture and at one year hydration, the *55OPC–30NP–15LPC* concrete had a compressive strength, 60 MPa, a bit higher than the control mixture, 53 MPa. At 28 days hydration, however, the strengths of *55OPC–30NP–15LPC* and *35OPC–50NP–15LPC* concretes were 39 MPa and 23 MPa, respectively. These values are 9% and 47% less than the *85OPC–15LPC* control, and indicate relatively poor performance for the *35OPC–50NP–15LPC* blend.

Although the *50OPC–50NP* binary mixture showed slightly higher strength, 34 MPa, than the *45OPC–40NP–15LPC* ternary mixture, 30 MPa, at 28 days hydration, both mixtures exhibited nearly identical strengths at 90 days and one year hydration, 43 MPa and 57 MPa, respectively. This suggests the large volume ternary mixtures with LPC did not interfere with long-term strength development, and that 55% wt. replacement of OPC with a finely ground NP–LPC mixture can be a viable solution to producing SCCs with good long-term strength development.

This seems to be the result of adequate pozzolanic activity of NP at up to 40% OPC replacement and a relatively reduced dilution effect of 15% LPC replacement of OPC [62, 132].

Table 3.4 Average compressive strength (MPa).

OPC–NP–LPC	Compressive Strength (MPa)			
	7 days	28 days	91 days	365 days
100OPC	43.9	53.9	66.3	77.1
85OPC–15LPC	28	43.2	49.7	53
70OPC–30NP	39.9	53.9	64.9	73.1
50OPC–50NP	21.9	34.3	42.2	56.8
55OPC–30NP–15LPC	24	39.4	48.9	59.7
45OPC–40NP–15LPC	16.4	30.5	42.9	56.6
35OPC–50NP–15LPC	11.1	23	30.6	42.4

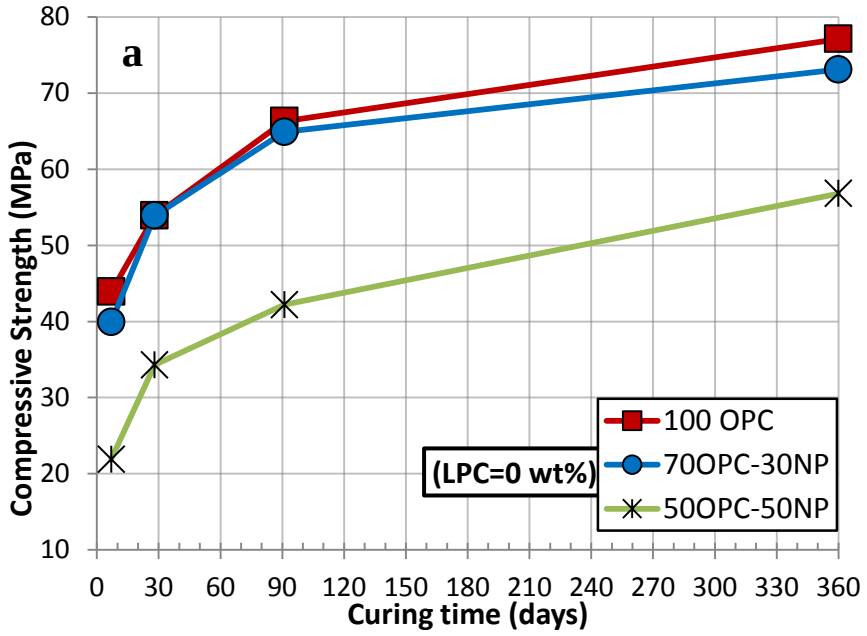

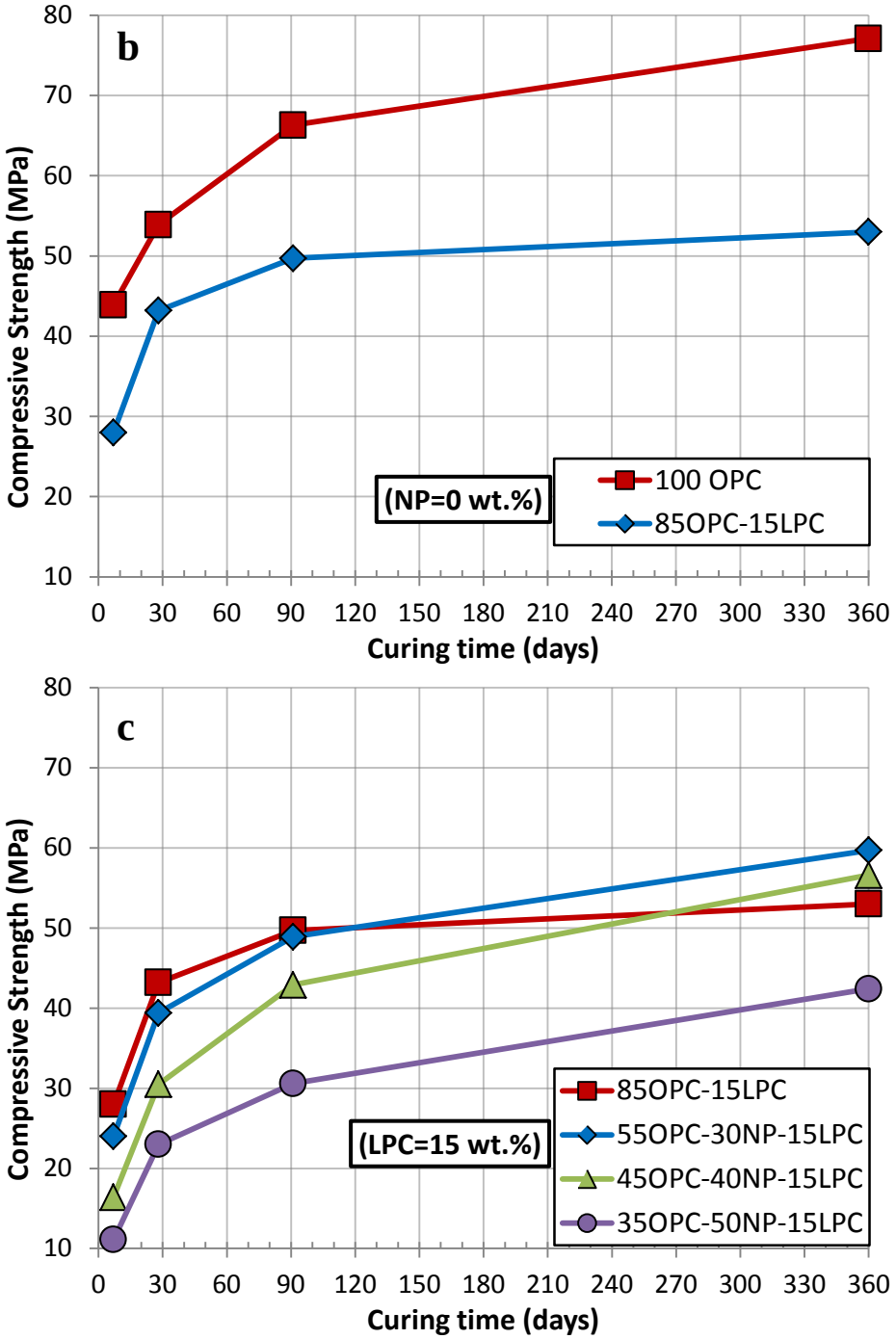

Figure 3.1 Results of compressive strength tests of the experimental OPC–NP–LPC concretes. (a) OPC–NP binary cement blends, (b) OPC and OPC–LPC control blends (c) OPC–NP–LPC ternary cement blends.

3.1.2.2 Compressive strength of HVFA

Table 3.5 presents the average compressive strength for all concrete mixtures, while Figure 3.2 shows the results in graphic form. As it can be readily observed, a wide range of strengths are attainable depending on the specific replacement ratios and curing time specified for a given

project. Similarly, a given strength can be obtained using a variety of mixtures and cement replacement ratios. For example, a strength level of 30 MPa can be obtained either at 28 days with a total cement replacement level of up to 55% (either using 15% LPC+ 40% FA or 25% LPC + 30% FA), or at 56 days with a replacement level of up to 65%, or at 91 days with a cement replacement level as high as 75%. Higher strengths can also be easily achieved. The 45% replacement mixture with 30% FA and 15% LPC reached approximately 42 MPa at 28 days, growing to about 54 MPa at 91 days.

The early age data are very similar for the 15% LPC and 25% LPC series. At 7 days, FA–LPC mixtures ranged between 9 MPa for 75% replacement and 20 MPa for 45%. At 28 days, these mixtures reached 19 MPa for 75% replacement and approximately 40 MPa for 45%. At 56 days, this range was 24 MPa to 44 MPa. Finally, at 90 days the FA–LPC mixtures obtained a minimum of 31 MPa and up to 54 MPa for the 30-15 mixture.

As expected, at a fixed *w/b* ratio as used herein, increased FA content led to relatively lower early strengths but higher strength gain rates, as shown in Figure 3.2, which plots σ_c' against time.

Note the remarkable synergistic effect between limestone powder and fly ash shown in Figure 3.2 (a) and (b) compared to the control mixtures, shown in Figure 3.2 (c), in which the addition of fly ash led to reduced compressive strength. In several cases, the compressive strength actually increased for the limestone series mixtures when Portland cement was replaced by fly ash up to a certain amount. For the 25% limestone series with 20% fly ash (45% total replacement ratio), at 28 days the strength was 8% higher than the zero fly ash mixture (with only 25% replacement); the strength was kept increasing over time. With 30% fly ash in both cases (15% and 25% limestone powder), the strength was only slightly lower than the zero fly ash mixtures at 28 days, and it exceeded them at 56 days. At one year the strength of *55OPC–30FA–15L* was slightly higher than the one of *85OPC–15LPC*. This suggests that the more sustainable product can be obtained with more cement replacement by fly ash. Investigating the influence of fine additives on the viscosity of cement paste, Diamantonis et al [133] also observed a synergistic effect in a mixture with 20% limestone powder and 20% fly ash. The authors concluded that the synergy between the materials can lead to a higher packing density that in turn results in a denser microstructure - a hypothesis which is also supported by Liu and Yan [93].

Table 3.5 Average compressive strength (MPa).

OPC–FA–LPC	Compressive Strength (MPa)			
	7 days	28 days	91 days	365 days
100OPC	43.9	53.9	66.3	77.1
85OPC–15LPC	28.0	43.2	49.7	53.0
75OPC–25LPC	22.2	33.6	38.7	42.2
70OPC–30FA	35.6	51.0	64.6	71.8
50OPC–50FA	27.9	41.6	54.8	64.8
55OPC–30FA–15LPC	21.5	37.5	47.3	56.8
45OPC–40FA–15LPC	17.1	33.9	46.2	56.5
35OPC–50FA–15LPC	12.9	26.0	39.3	49.0
25OPC–60FA–15LPC	10.3	20.6	29.4	39.5
55OPC–20FA–25LPC	19.6	36.3	42.9	54.2
45OPC–30FA–25LPC	14.9	31.5	43.3	55.3
35OPC–40FA–25LPC	12.4	28.9	41.8	50.4
25OPC–50FA–25LPC	10.1	20.6	32.8	38.0

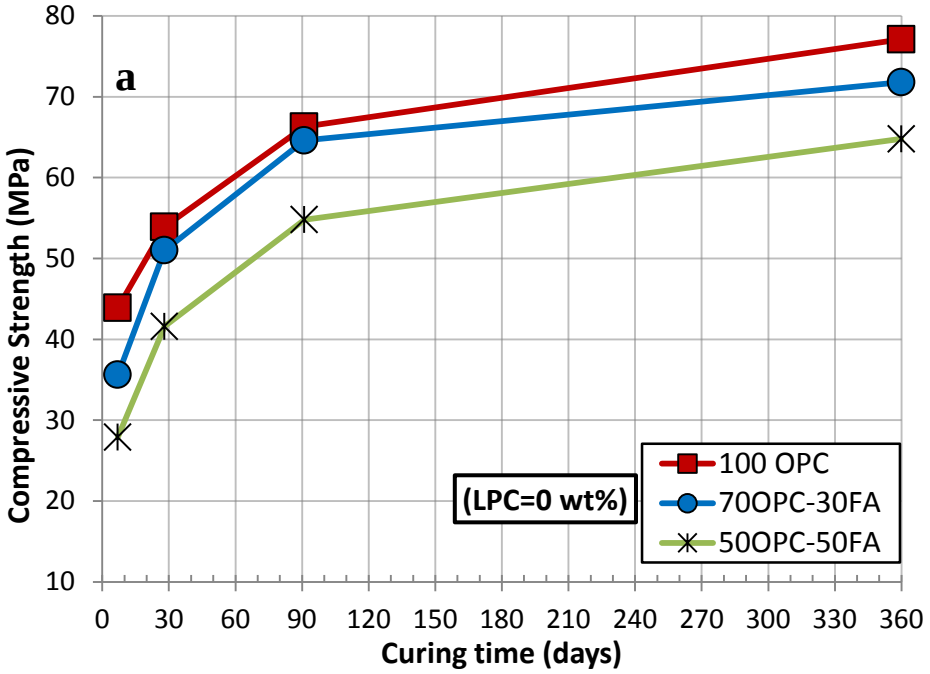
a
Compressive Strength (MPa)
Curing time (days)
(LPC=0 wt%)
100 OPC
70OPC-30FA
50OPC-50FA

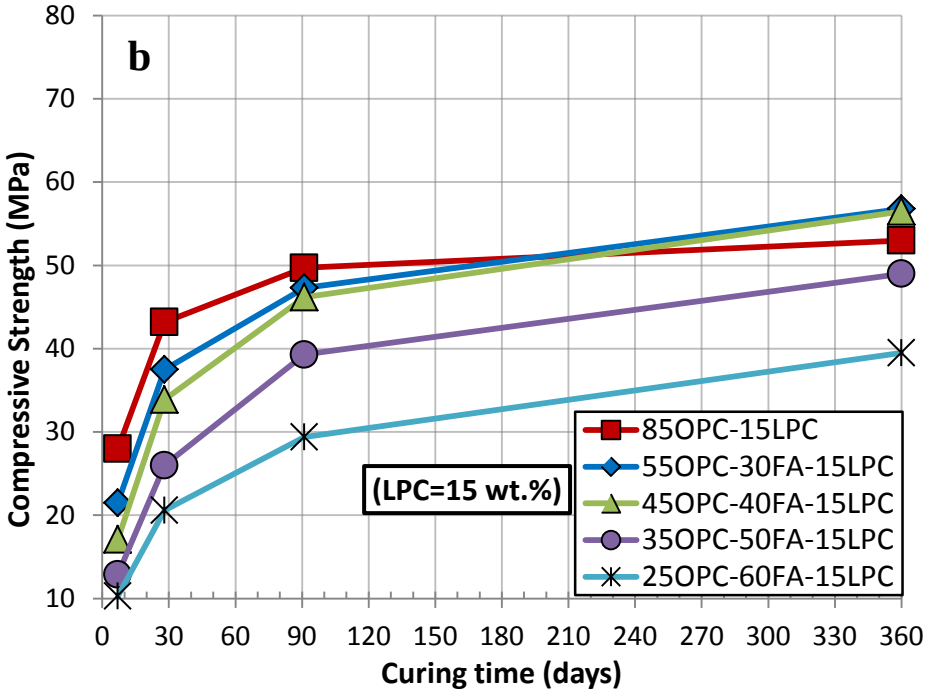
b
Compressive Strength (MPa)
Curing time (days)
(LPC=15 wt.%)
85OPC-15LPC
55OPC-30FA-15LPC
45OPC-40FA-15LPC
35OPC-50FA-15LPC
25OPC-60FA-15LPC

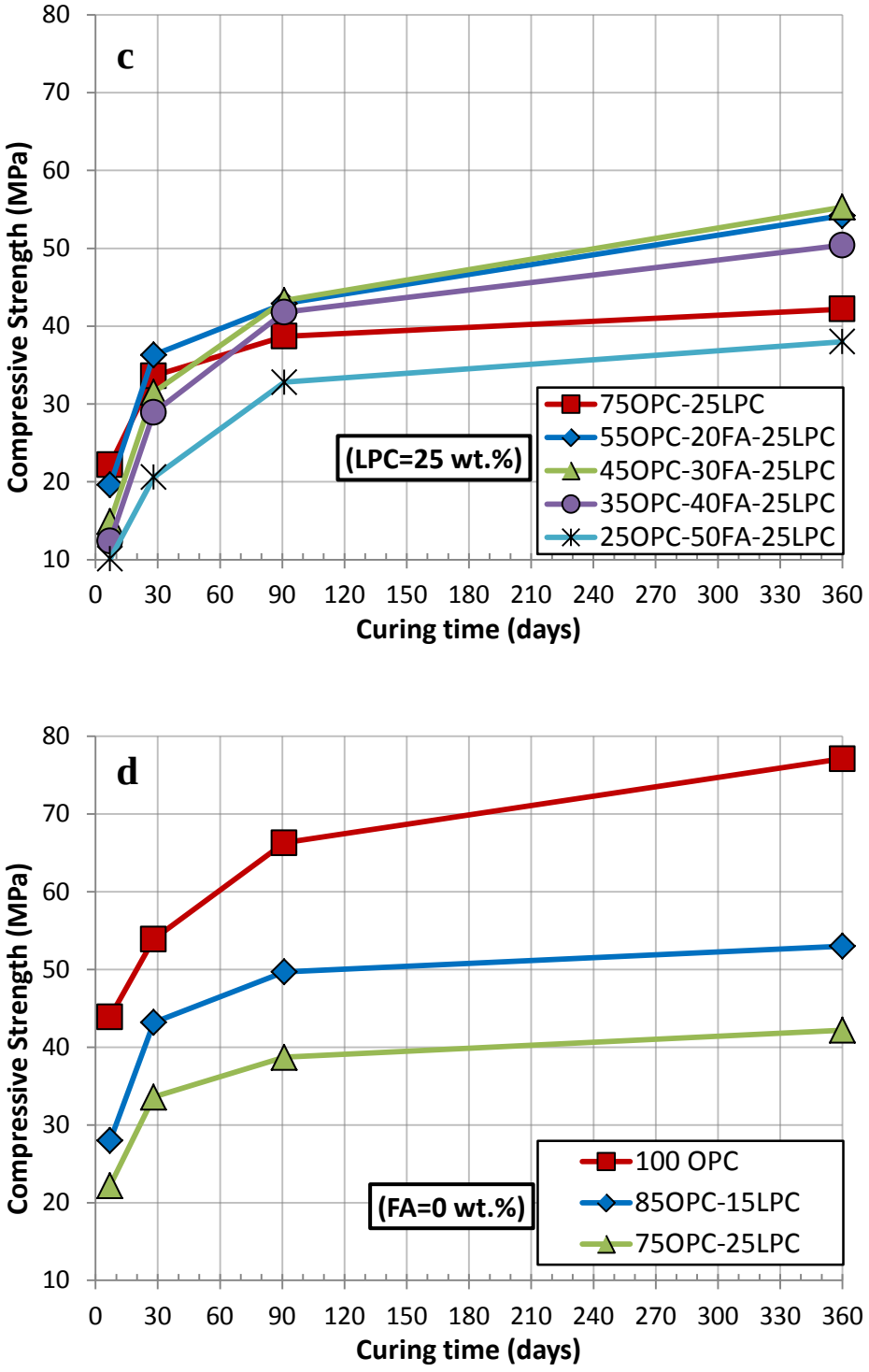

Figure 3.2 Compressive strength development over time. (a) binary mixtures (without limestone powder) (b) 15% LPC series, (c) 25% LPC series, (d) control mixtures. Mixtures with higher FA content gain strength steadily over time.

3.1.2.3 Comparison of compressive strength of HVNP and HVFA

The effects of changing the mixture proportions of cementing materials on the rate of strength development of concrete are shown in Figure 3.3. The binary mixture containing 30% NP or FA by wt. resulted in concrete with slightly lower strengths compared to the control concrete after seven days of curing. The concrete containing a cementing material mixture with 50 wt.% NP or FA registered a much lower rate of strength development when compared with control specimens. This suggests that the large volume of NP/FA replacement in binary mixtures contain a greater proportion of anhydrous phases; however, the 28-day and 91-day strength values 41MPa and 55MPa for the FA specimens and 34MPa and 42MPa for the NP specimens, which are adequate for most structural applications. Among the binary mixtures, the specimens replaced with 30 wt.% NP produced 6% higher strength than the one with 30% FA at 28 days, while they had similar strength at 91 days. However, the specimens replaced with 50 wt.% NP produced 18% and 23% lower strength than the one with 50 wt.% FA at 28 and 91 days, respectively. Perhaps this is because the pozzolanic reactivity of FA is higher than that of NP. In the case of ternary blended cements containing 15 wt.% LPC, the larger amount of NP/FA addition led to reduced compressive strength compared to the control specimen that has only 15 wt.% LPC replacement at early ages. This could be attributed to the slower rate of pozzolanic reaction and dilution effect of LPC on cementitious process associated with highly-replaced OPC hydration [79]. However, 30 wt.% NP or FA replacement in the ternary mixture showed identical strength to that of the control specimen, which contains 85 wt.%OPC–15 wt.%LPC, at later ages. This suggests that 30 wt.% NP or FA replacement with OPC and LPC did not affect with long-term strength development. The comparison between FA and NP among the ternary mixtures in Figure 3.3 shows that 30 wt.% NP replacement had marginally higher strength than the 30 wt.% FA replacement, whereas 40% and 50 wt.% NP replacement had lower strength than the corresponding FA replacements up to 28 days. This could be associated with the pozzolanic activity of FA at 50 wt.% OPC replacement being higher than the NP in the ternary mixtures.

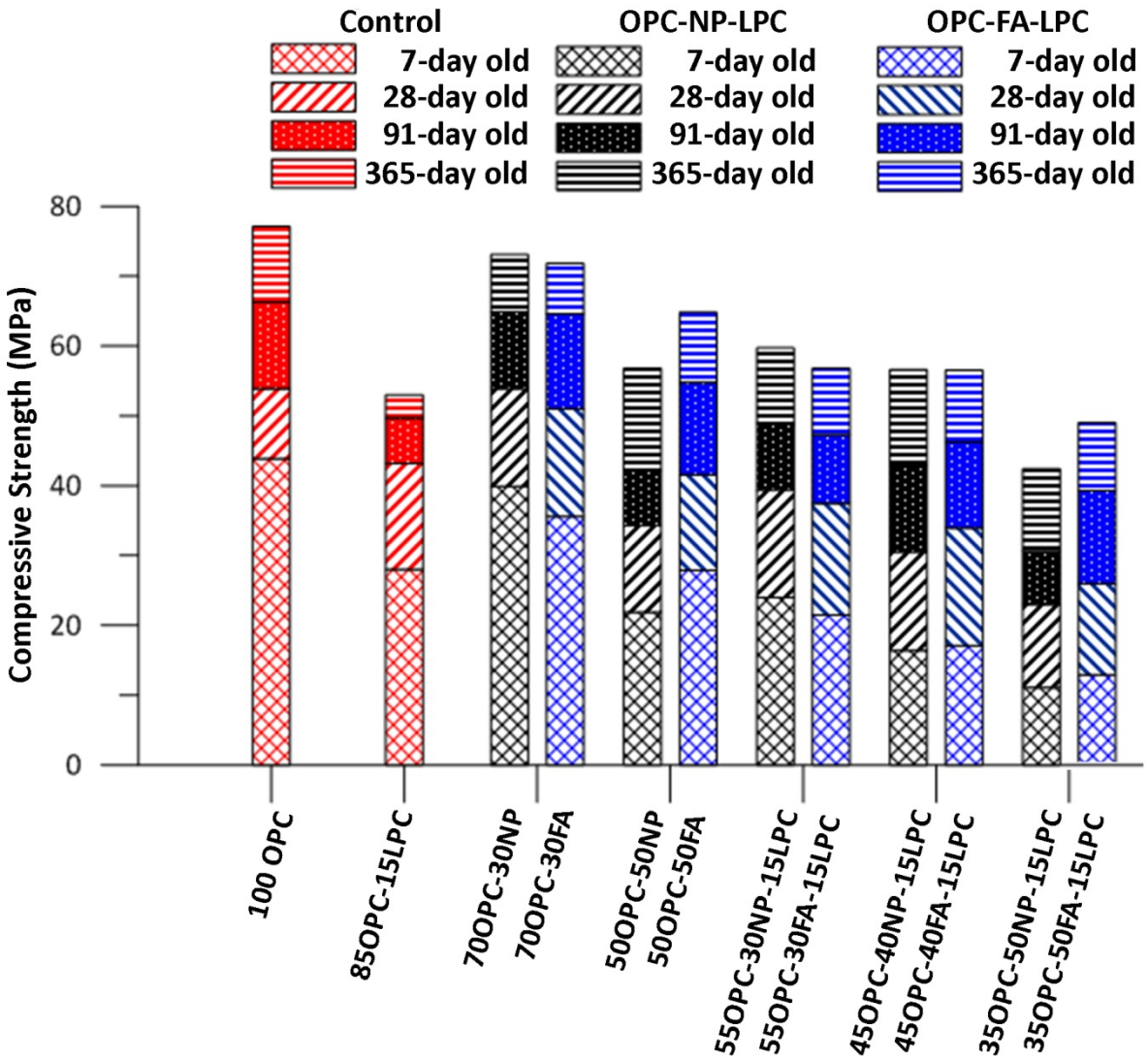

Figure 3.3 Compressive strength development over time (days).

3.1.3 Durability Properties

3.1.3.1 Coefficient of chloride migration

3.1.3.1.1 Coefficient of chloride migration of HVNP

The mixing ratio of finely ground NP, and NP–LPC as OPC replacement seems to have a strong influence on the chloride migration coefficient of the experimental concretes. All the concretes with blended cement mixtures demonstrated a higher resistance to chloride migration relative to the *100OPC* and *85OPC–15LPC* controls (Figure 3.4). Based on standard guidelines [134], the chloride penetration resistance of the *70OPC–30NP* binary mixture and ternary mixtures with a 30NP and 40NP ranges from very high to high (Figure 3.4 and Table 3.6). The low porosity of Saudi basaltic cinders measured by Sabtan and Shehata [33] may help to reduce the permeability of the resulting concrete. Furthermore, hydration of fine volcanic ash granulates obstructs voids and pores, leading to pore size reduction and smaller effective chloride diffusivity [135]. The *55OPC–30NP–15LPC* and *45OPC–40NP–15LPC* mixture show very high chloride penetration resistance, while the *50OPC–50NP* binary mixture and the *35OPC–50NP–15LPC* ternary mixture show high resistance to chloride penetration. Concrete with 40 wt.% volcanic ash replacement for OPC also shows low chloride ingress [135]. This suggests that both binary NP and ternary NP–LPC blends could improve resistance to chloride migration and, possibly, the overall durability and corrosion resistance of the resulting concretes. This could be the result of a pore refinement effect associated with 15% LPC replacement of OPC, related to the possible formation of carbo-aluminates and the reduction of ettringite transformation to monosulfate in the ternary mixtures [46, 136].

Table 3.6 Resistance against chloride penetration based on non-steady state migration testing [47].

Chloride Diffusion D ($\times 10^{-12}$ m^2/s)	Concrete Resistance
> 15	Low
10–15	Moderate
5–10	High
2.5–5	Very high
< 2.5	Extremely high

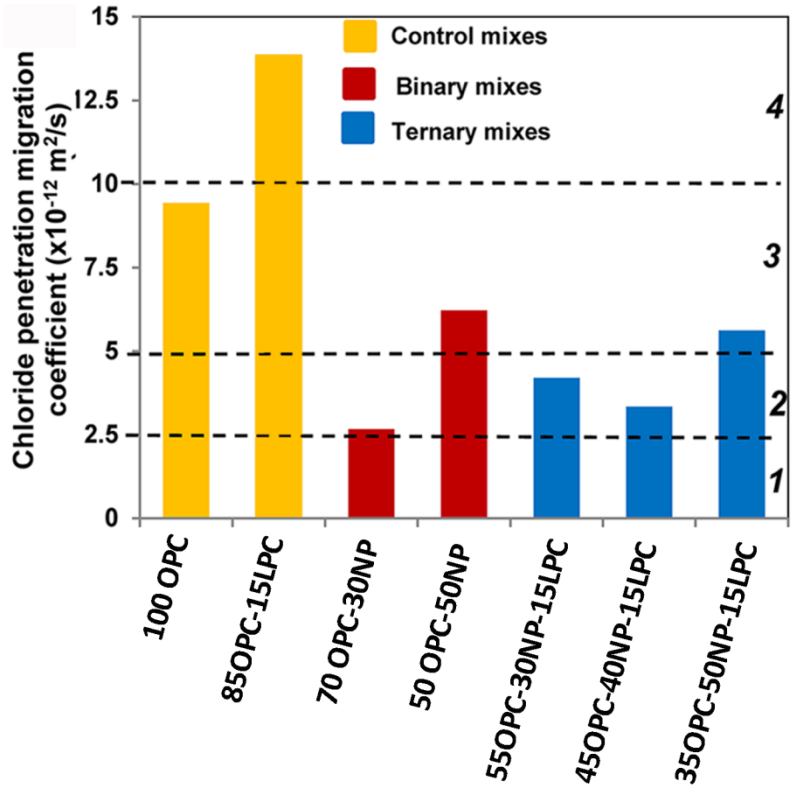

Figure 3.4 Non-steady state chloride migration coefficient of OPC–NP–LPC concretes at 1 year as a function of cement replacement of the concrete mixture. Zones 1, 2, 3 and 4 indicate extremely high to moderate resistance to chloride penetration (Table 3.6).

3.1.3.1.2 Coefficient of chloride migration of HVFA

Figure 3.5 demonstrates that the mixing ratio of FA and FA–LPC as a cement replacement had a strong effect on the chloride migration coefficient of the experimental concretes. All the concretes with blended cement mixtures demonstrated a higher resistance to chloride migration relative to the *100OPC* and *85OPC–15LPC* and *75OPC–25LPC*. Based on standard guidelines [134], the chloride penetration resistance of the OPC–FA binary mixtures and OPC–FA–LPC ternary mixtures ranged from extremely high to very high (Figure 3.5 and Table 3.6). This result suggests that hydration of FA and LPC impedes voids and pores, leading to pore size reduction and smaller effective chloride diffusivity.

The *50OPC–50FA* showed higher resistance to chloride penetration than the *70OPC–30FA*. This suggests that the more the FA replacement, the more chloride penetration resistance for the binary mixtures. However, the *35OPC–50FA–15LPC* showed lower resistance to chloride penetration than the *45OPC–40FA–15LPC*, whereas the *45OPC–40FA–15LPC* presented higher resistance to chloride penetration than *55OPC–30FA–15LPC*. This indicates that 65% and above 65% replacement for the ternary mixtures lowers the resistance to chloride migration.

Significantly, for the same ratio of cement replacement with FA and LPC, the ternary *35OPC–40FA–25LPC* mixture results in higher chloride resistance compared to *35OPC–50FA–15LPC* mixture. This indicates that the 25% LPC replacement had the added advantage of improving chloride resistance in ternary blends.

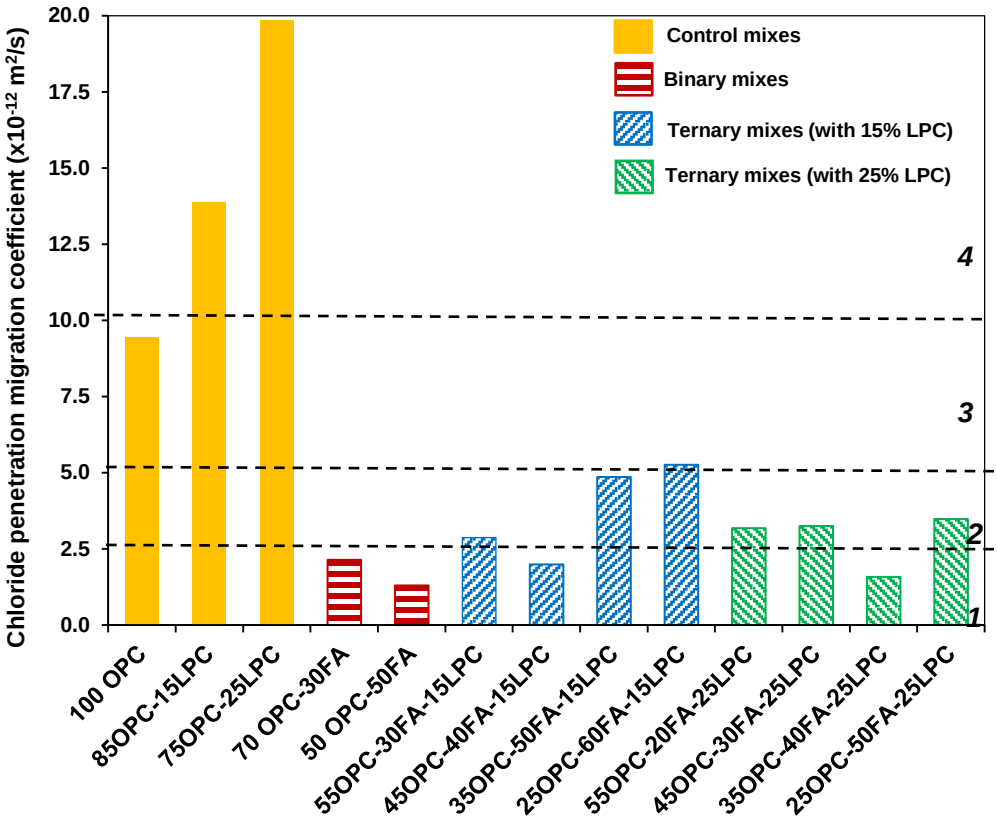

Figure 3.5 Non-steady state chloride migration coefficient of OPC–FA–LPC concretes at 1 year as a function of cement replacement of the concrete mixture. Zones 1, 2, 3 and 4 indicate extremely high to moderate resistance to chloride penetration (Table 3.6).

3.1.3.1.3 Comparison of chloride-migration coefficient of HVNP and HVFA

The effect of changing the mixing ratio of NP/FA, and NP–LPC/FA–LPC as a Portland cement replacement on the chloride migration coefficient of concrete is shown in Figure 3.6. All mixtures made with blended cements demonstrated higher resistance to the chloride migration compare to the control mixtures. Based on standard guidelines [134] , the chloride penetration resistance of the binary and ternary mixtures ranges from extremely high to high (Table 3.6). This result suggests that hydration of NP/FA and NP/FA–LPC impedes voids and pores, leading to pore size reduction and smaller effective chloride diffusivity. The concretes produced with FA and FA–LPC demonstrated higher chloride migration resistance compared to the concrete produced with NP and NP–LPC with the exception of *55OPC–30FA–15LPC* which showed slightly lower resistance to chloride migration. The increased amount of FA replacement increased the resistance to chloride migration in binary and ternary mixtures with the exception of *35OPC–50FA–15LPC*. This could be the result of an effective pore refinement of pozzolanic reaction up to 50% FA in binary mixtures and up to 40% FA and 15% LPC replacements of OPC associated the possible formation of carboaluminates and the reduction of ettringite transformation to monosulfate in the ternary mixtures. However, the increased amount of NP in

binary and ternary mixtures decreased the chloride migration resistance. In general, the concrete mixtures with ternary cement showed greater resistance to chloride migration compared to the mixtures with binary cement for a similar cement replacement configuration for the mixtures with NP. This could be the result of LPC which acts as an inert calcareous filler and a limited participant in the hydration process [38-40].

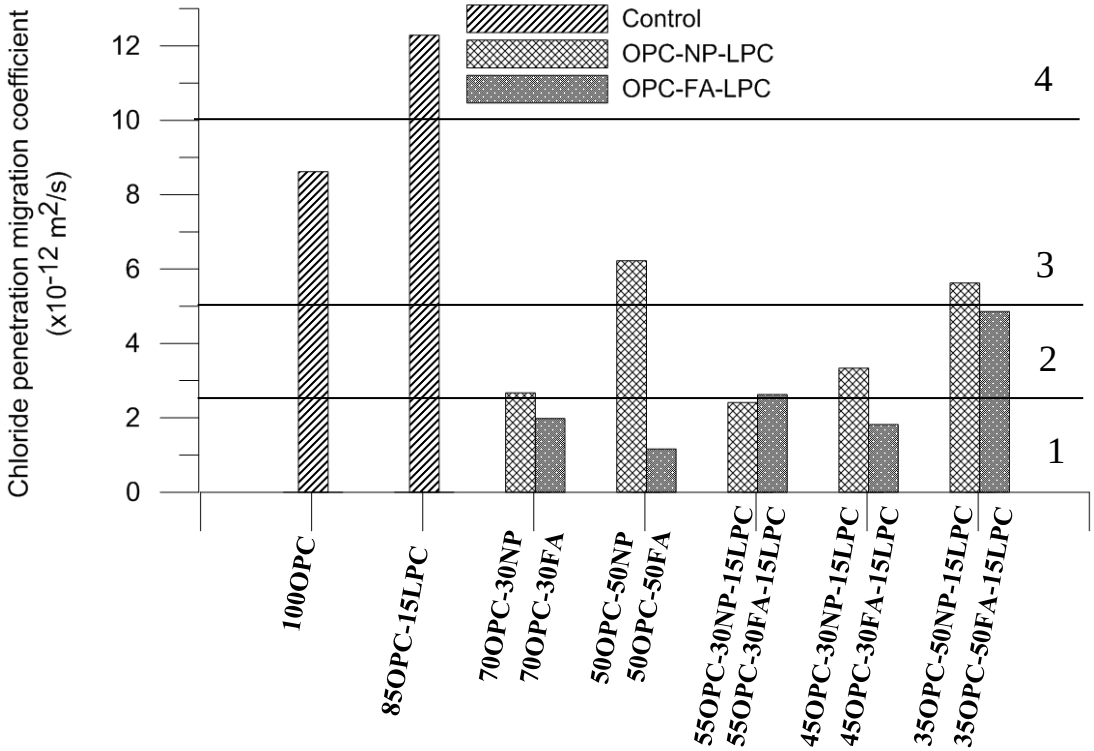

Figure 3.6 Non-steady state chloride migration coefficient as a function of cement replacement of the concrete mixtures of OPC–NP–LPC and OPC–FA–LPC at 1 year. Zones 1, 2, 3 and 4 indicate extremely high, very high, high, moderate resistance to chloride penetration, respectively according to guidelines presented in [134]. All ratios listed as wt.% OPC–NP–LPC and OPC–FA–LPC.

3.1.3.2 Water absorption test

3.1.3.2.1 Water absorption of HVNP

Variations in the cement replacement mixtures also influence the water absorption of the experimental concretes (Figure 3.7). For both the binary and ternary blends with <50OPC replacement, water absorption is less than to the *100OPC* and *85OPC–15LPC* controls. This may, perhaps, reflect lower overall porosity. At 55–65% OPC replacement, water absorption is greater than the controls, but at only 2.5–3.5 wt.% it is still within acceptable limits. Water absorption describes a material's ability to take in water as a consequence of capillary suction, which is a function of size, distribution, shape, tortuosity, and continuity of its pores [137]. More than 55% OPC replacement in the ternary mixtures may induce an increased capillary porosity. This could be attributed to higher water absorption capacity associated with the vesicles of the basalt ash [33], and also the dilution effect of the LPC on OPC hydration [45].

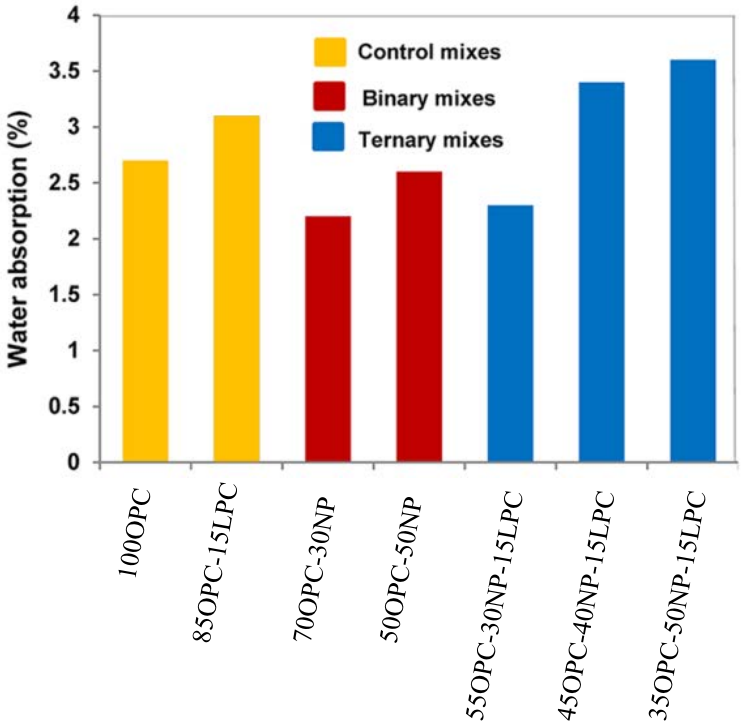

Figure 3.7 Relationship between water absorption and cement replacement of OPC–NP-LPC concretes at 1 year. All ratios listed as wt.% OPC–NP–LPC.

3.1.3.2.2 Water absorption of HVFA

Figure 3.8 shows that alterations in the cement replacement mixtures have a strong influence on the water absorption of the experimental concretes. The *70OPC–30FA* and *50OPC–50FA* binary mixtures displayed lower water absorption compared to the control mixtures and ternary mixtures due to possible lower porosity. For the control specimens and ternary blends, the more LPC replacement resulted in more water absorption, with the exception of the *55OPC–20FA–25LPC* which had lower absorption than the *55OPC–30FA–15LPC*. In general, by the increasing the ratio of FA replacement resulted in the higher water absorption in the binary and ternary mixtures.

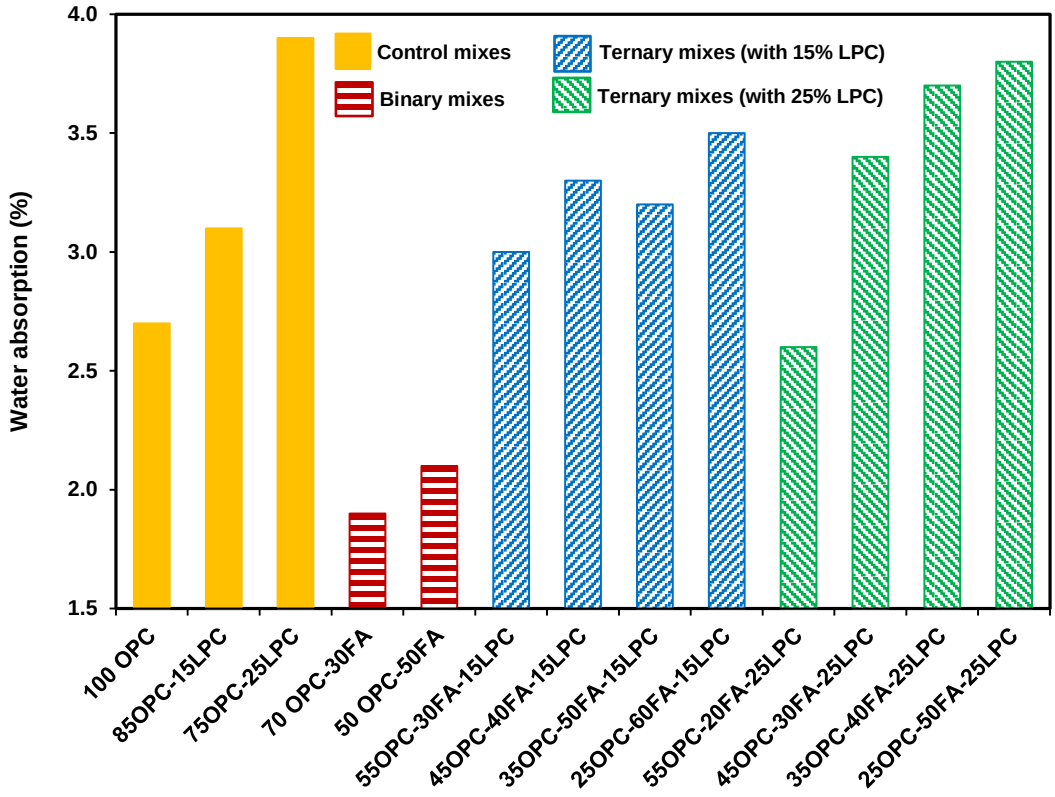

Figure 3.8 Relationship between water absorption and cement replacement of OPC–FA–LPC concretes at 1 year. All ratios listed as wt.% OPC–FA–LPC.

3.1.3.2.3 Comparison of water absorption of HVNP and HVFA

The effect of varied ratio of OPC replacement with NP/FA, and NP-LPC/FA-LPC on the water absorption of concrete samples is presented in Figure 3.9. The binary and ternary mixtures containing NP showed higher water absorption compared to the corresponding mixtures containing FA with the exception of *55OPC–30NP-15LPC*. This can be associated with the higher water absorption capacity of NP particles [33, 138] relative to FA, which is also observed as an increased water demand for the normal consistency in Section 3.2.1.3. The binary concrete mixtures containing either OPC–NP or OPC–FA had lower water absorption compared to the control *100OPC*, indicating possible lower capillary porosity. Among the ternary mixtures containing 40% or 50% NP/FA along with 15% LPC demonsrated higher water absorption relative to the control *85OPC–15LPC*, while 30% NP/FA and 15% LPC had lower water absorption. This can be attributed to the slower rate of pozzolanic reaction in the high-volume of OPC replacement due to the delayed pore refinement in the ternary mixtures. However, it should be noted that the capillary absorption can be influenced by the drying at 105°C as drying at elevated temperature can introduce micro-cracks in the samples [139, 140].

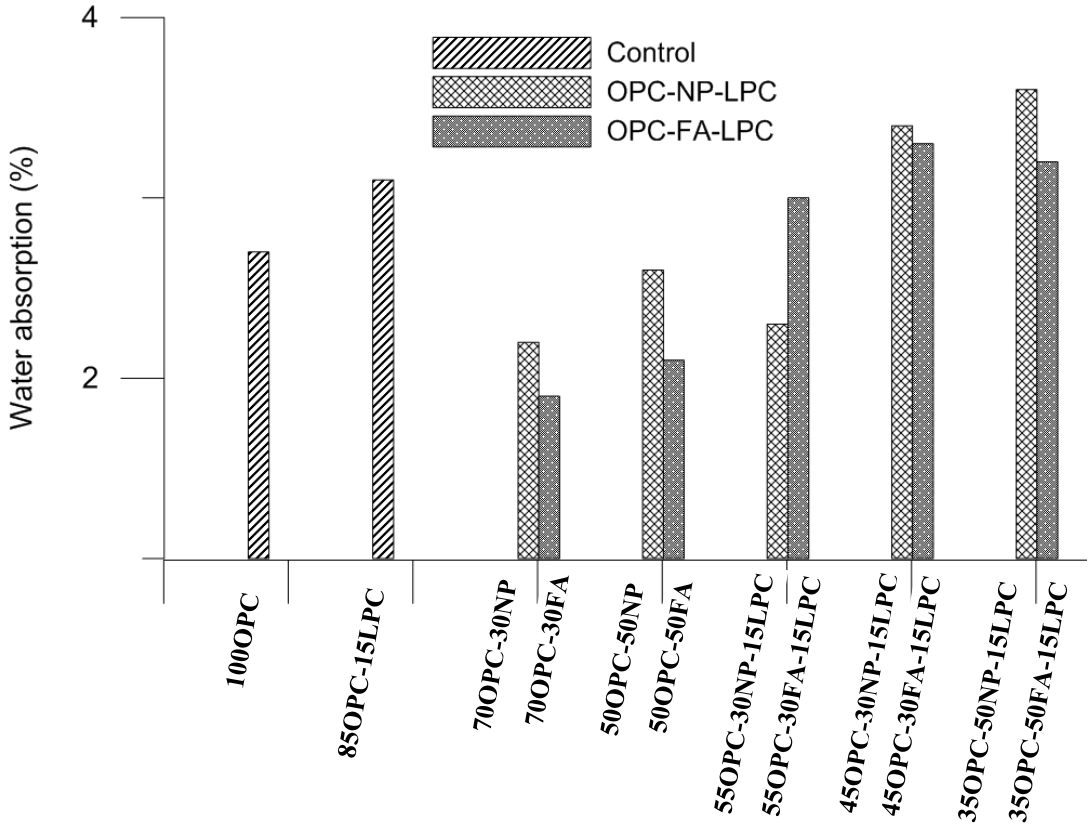

Figure 3.9 Relationship between water absorption and cement replacement of OPC–NP–LPC and OPC–FA–LPC concretes at 1 year. All ratios listed as wt.% of OPC–NP–LPC and OPC–FA–LPC.

3.1.3.3 Gas permeability test

3.1.3.3.1 Gas permeability of HVNP

Variations in the NP and NP–LPC mixture proportion seem to influence the coefficient of gas permeability in the experimental concretes (Figure 3.10). The greater the amount of OPC replacement with NP, the lower the apparent gas permeability in both the binary and ternary cement systems, with the exception of the *45OPC–40NP–15LPC* specimens. These appear to be anomalous tests, which could have developed microcracks during the drying process; they have good compressive strength and low chloride penetration.

Adding LPC may increase the gas permeability, as shown by the 85–15–0 control mixture, but this does not seem have a systematic effect. Although a correlation has been observed between resistance to chloride penetration and decreased gas permeability of concrete subjected to short-term air or oven drying, this effect weakens with longer drying periods [131, 141-145]. This is demonstrated for the specimens tested here at one year hydration: increasing NP replacement of OPC in the binary and ternary mixtures generally decreases gas permeability, while it increases the chloride penetration coefficient, which is the more straightforward measurement. The apparently reduced drying shrinkage of the concrete with increased NP may be related to the refinement of pores through pozzolanic reaction, which obstructs water evaporation [146], and also a higher amount of unreacted ash, which could act as aggregate that restrains shrinkage [147].

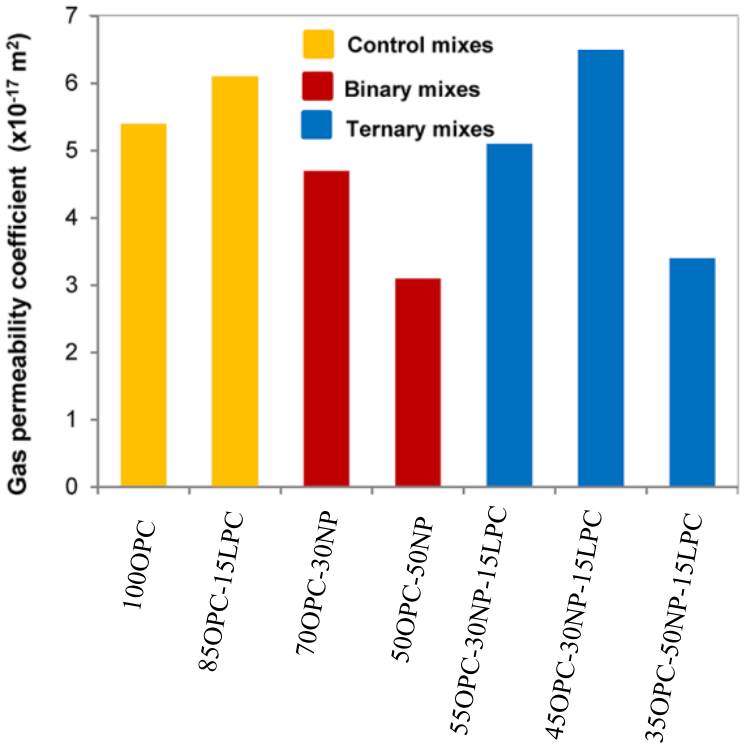

Figure 3.10 Gas permeability coefficient of in function of cement replacement of OPC–NP–LPS concrete mixtures at 1 year. All ratios listed as wt.% OPC–NP–LPC.

3.1.3.3.2 Gas permeability of HVFA

Figure 3.11 indicates that FA and FA–LPC mixtures had a strong influence on the coefficient of gas permeability in the experimental concretes. Greater amounts of cement replacement with FA lower the gas permeability in both the binary and ternary cement systems, with the exception of the *45OPC–40FA–15LPC* and *35OPC–40FA–25LPC* mixtures. Adding LPC acts to increase the gas permeability with the exception of the *45OPC–30FA–25LPC* that has 10% lower gas permeability than the *45OPC–40FA–15LPC*; note that gas permeability is affected by drying procedure [131, 142-144]. Although there is a correlation between resistance to chloride penetration and gas permeability of concrete subjected to short-term air or oven drying, this correlation weakens with longer drying periods [145]. This is demonstrated for the specimens tested here with the CEMBUREAU method: even though increasing FA replacement of OPC in the binary and ternary mixtures generally decreased gas permeability, it increased the chloride penetration coefficient for the 50% and more FA replacement in ternary blends, which is the more straightforward measurement. Long-term drying in the gas permeability tests may have introduced artifacts into the specimens that obscure the meaning of the experimental results. Thus, microcracks induced in the concrete during longer drying periods may result in higher gas permeability in specimens with less OPC replacement [79, 131, 142-145].

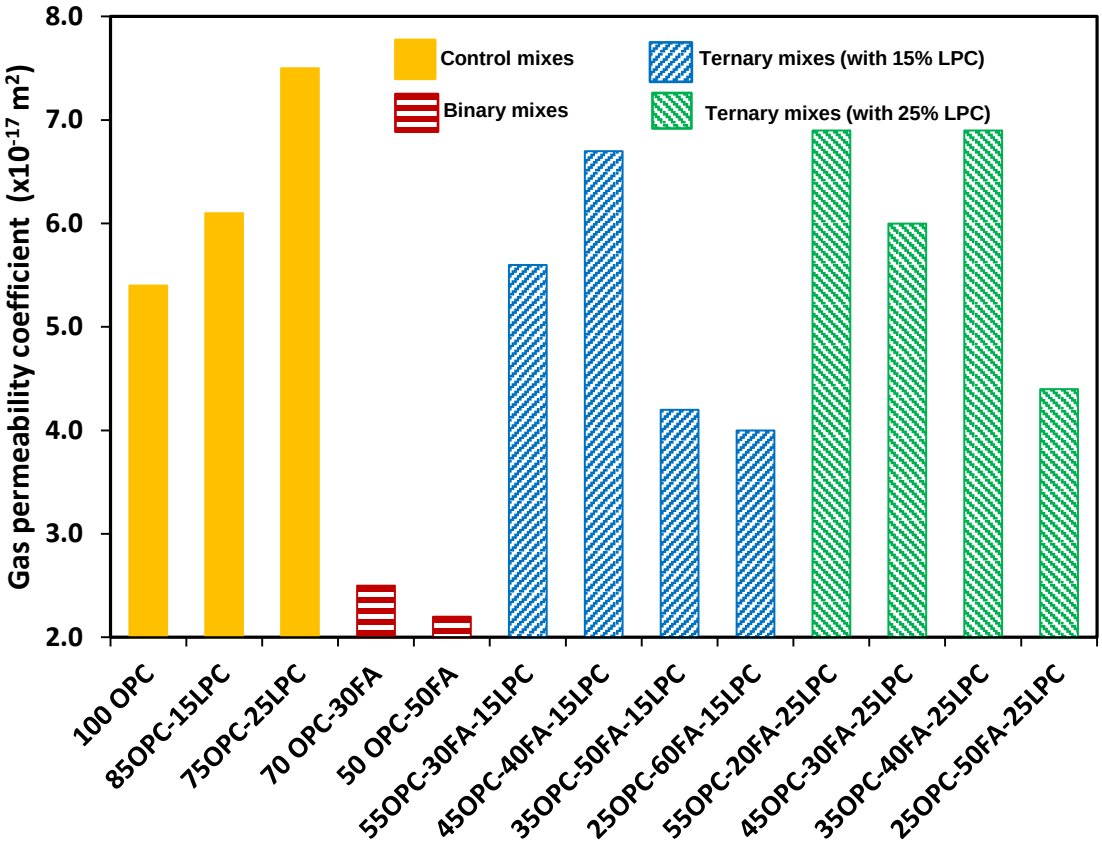

Figure 3.11 Gas permeability coefficients in function of cement replacement of OPC–FA–LPS concrete mixtures at 1 year. All ratios listed as wt.% OPC–FA–LPC.

3.1.3.3.3 Comparison of gas permeability of HVNP and HVFA

Figure 3.12 shows that NP/FA and NP/FA–LPC mixtures have a strong influence on the coefficient of gas permeability in the experimental concretes. Greater amounts of Portland cement replacement with NP/FA lower the gas permeability in both the binary and ternary cement systems, with the exceptions of the *45OPC–40FA–15LPC* and *45OPC–40NP–15LPC*. These seem to be anomalous tests, which could have developed microcracks during the drying process; they have good compressive strength and low chloride penetration [79]. In general, addition of LPC into the mixture increased the gas permeability. The comparison of FA and NP as a cement replacement in terms of gas permeability suggests that the mixtures with NP exhibited lower resistance to gas permeability compared to FA in binary cement system, whereas, NP-LPC showed higher resistance to gas permeability compared to FA–LPC. It should be noted that the gas permeability is affected significantly by drying procedure [143, 145, 148, 149]. While there is a correlation between gas permeability of concrete subjected air drying or short-term oven drying and chloride penetration of concrete, the correlation weakens with longer drying periods, as demonstrated for the specimens tested according to the CEMBEREU method. Sugiyama *et al*. [145] suggested that micro-cracks induced in concrete by longer drying periods result in higher gas permeability. The investigation of microstructure of the specimens is planned as a second phase of the project.

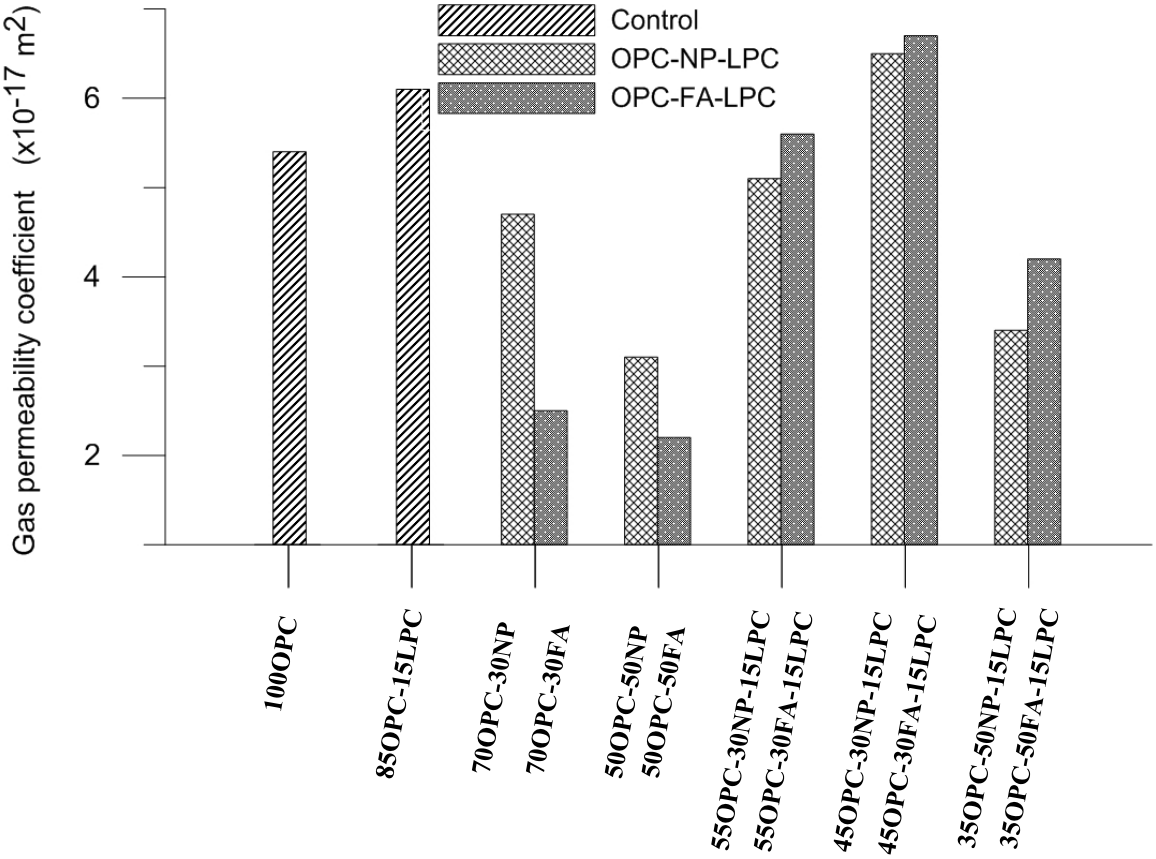

Figure 3.12 Gas permeability coefficient in function of cement replacement of the concrete mixtures at 1 year.

3.2 Mortar samples

3.2.1 Normal consistency and setting time

3.2.1.1 Normal consistency and setting time of HVNP

The water to cementitious material ratios needed for normal consistency are shown in Figure 3.13 along with initial and final times of setting of the cementitious mixtures. The water demand of *70OPC–30NP* and *50OPC–50NP* was 6% and 10% higher than that of control *100OPC*, respectively. The ternary blends of *55OPC–30NP–15LP*, *45OPC–40NP–15LP* and *35OPC–50NP–15LP* demonstrated 6%, 2%, and 6% more water demand than the control *85OPC–15LP*. This highlighted that the inclusion of NP in the blends increased the water requirement in the cement paste. It is observed that the addition of 15% LP in control *100OPC* slightly increased the water demand.

The results shown in Figure 3.13 demonstrate that variation in mixture proportions of NP had a significant effect on the initial and final times of setting. Both the blends of binary and ternary cementitious material had longer time of settings compared to control specimens. With an increase in NP content, both initial and final time of setting increased in binary mixtures. The final setting times of samples *70OPC–30NP* and *50OPC–50NP* were 22% and 57% longer than that of control *100OPC*, respectively. Moreover, the ternary blends of *55OPC–30NP–15LP*, *45OPC–40NP–15LP* and *35OPC–50NP–15LP* increased the final setting times by 30%, 30%, and 35%, respectively, compared to that of control *85OPC–15LP*. Lastly, the addition of 15% LP in control *100OPC* did not interfere the times of settings.

Table 3.7 Setting time of the mixtures

	OPC–NP–LP	*w/b* for normal consistency	Setting time, minutes	
			Initial	Final
Control	100OPC	0.25	136	185
mixtures	85OPC–15LP	0.25	134	185
Binary HVNP	70OPC–30NP	0.25	128	185
blends	50OPC–50NP	0.23	189	260
Ternary	55OPC–30NP–15LP	0.22	353	420
HVNP–LP	45OPC–40NP–15LP	0.24	267	315
blends	35OPC–50NP–15LP	0.22	282	345

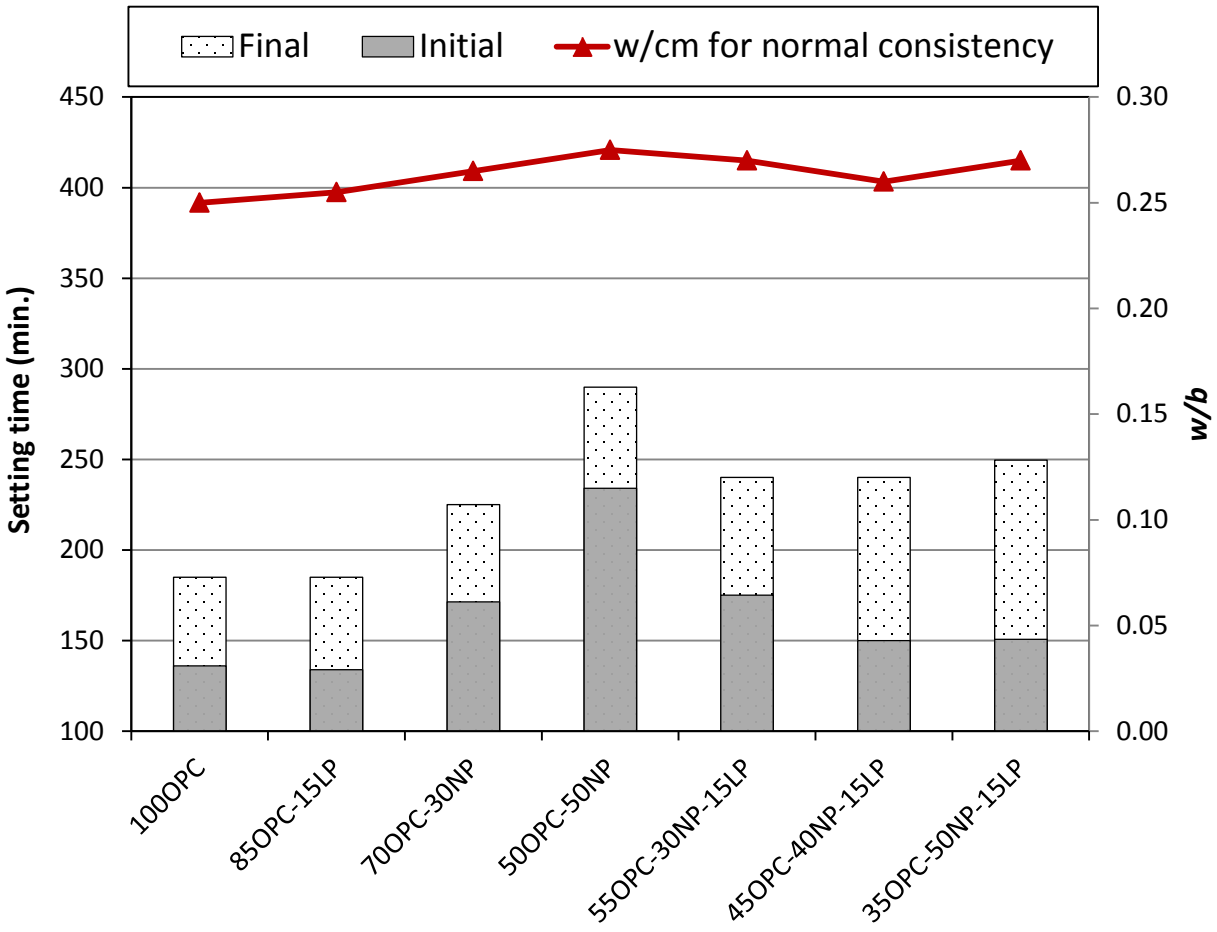

Figure 3.13 . *w/b* for normal consistency, and initial and final times of setting of the cement blends containing NP

3.2.1.2 Normal consistency and setting time of HVFA

Water-to-cementitious material ratios desired for normal consistency and initial and final times of setting of cement blends are shown in Table 3.8 and Figure 3.14. Water demand of *70OPC–30FA* and *50OPC–50FA* was 8% and 12% lower than that of control *100OPC*, respectively. The ternary *25OPC–60FA–15LP* blends showed 19% less water demand than the control *85OPC–15LP*. This indicates that addition of FA in the cement system greatly decreased the water demand in cement paste. In general, a LP increase in the cement blends requires slightly more *w/b* for the normal consistency. The water demand of *45OPC–30FA–25LP*, for instance, was approximately 5% higher than that of *45OPC45–40FA–15LP*.

Figure 3.14 shows that changing the mixture proportions of FA and LP had a strong influence on the initial and final times of setting. Binary and ternary blends showed longer setting times compared to the control specimens. The larger amounts of cement replacement with FA elevate the initial and final setting times in both of the binary and ternary cement systems. Significantly, the final setting times of *70OPC–30FA* and *50OPC–50FA* were about 1.4 and 2.3 times longer than the control *100OPC*. When the 30FA mixtures are compared, the *70OPC–30FA* had much lower initial and final setting times than the *55OPC–30FA–15LP* and *45OPC–30FA–25LP*. However, when compared to *50OPC–50FA*, the cement replacement with LP in ternary mixtures lowered the setting times. For example, the final setting time of *45OPC–40FA–15LP* and *45OPC–30FA–25LP* was almost 18% and 29% shorter than that of *50OPC–50FA*, respectively.

Table 3.8 Setting time of the mixtures

	OPC–FA–LP	*w/b* for normal consistency	Setting time, minutes	
			Initial	Final
Control mixtures	100OPC	0.25	136	185
	85OPC–15LP	0.25	134	185
	75OPC–25LP	0.25	128	185
Binary HVFA blends	70OPC–30FA	0.23	189	260
	50OPC–50FA	0.22	353	420
Ternary HVFA–LP blends	55OPC–30FA–15LP	0.24	267	315
	45OPC–40FA–15LP	0.22	282	345
	35OPC–50FA–15LP	0.22	340	360
	25OPC–60FA–15LP	0.21	278	390
	55OPC–20FA–25LP	0.24	214	270
	45OPC–30FA–25LP	0.23	245	300
	35OPC–40FA–25LP	0.22	285	345
	25OPC–50FA–25LP	0.22	359	405

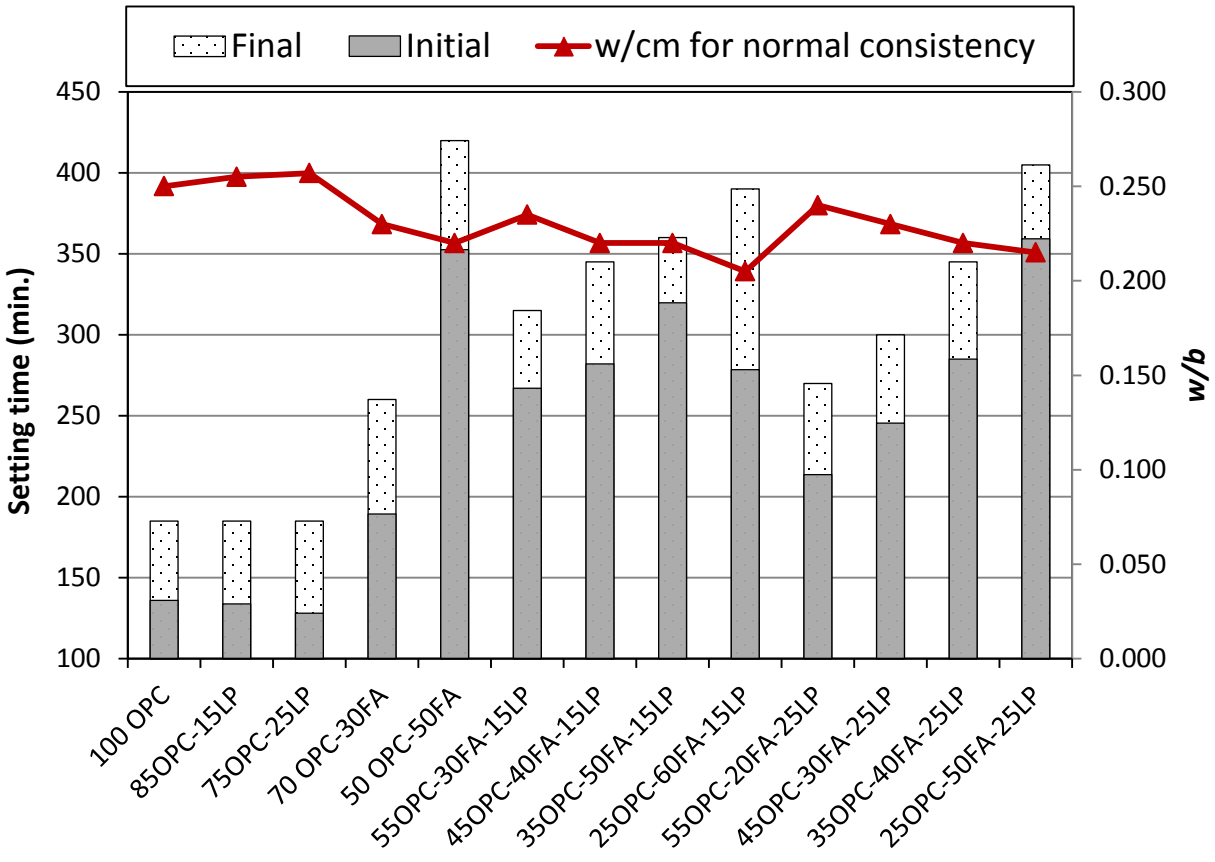

Figure 3.14. *w/b* for normal consistency, and initial and final times of setting of the cement blends containing FA

3.2.1.3 Comparison of normal consistency and setting time of HVNP and HVFA

Water demand of *70OPC–30FA* and *50OPC–50FA* was 8% and 12%, respectively lower than that of control *100OPC*. The ternary *35OPC–50FA–15LP* blend showed 14% less water demand than the control *85OPC–15LP*. This indicates that addition of FA in the cement system greatly decreased the water demand in cement paste compared to NP addition. All binary and ternary NP mixtures required more water than that of FA to have normal consistency. This has been attributed to the spherical shape of FA that contributes to increment of workability.

Figure 3.15 shows that alteration in the mixture proportions of FA and LP had a strong influence on the initial and final times of setting. Binary and ternary blends showed longer setting times compared to the control specimens and corresponding mixture with NP. The larger amounts of cement replacement with FA elevate the initial and final setting times in both of the binary and ternary cement systems. Significantly, the final setting times of *70OPC–30FA* and *50OPC–50FA* were about 1.4 and 2.3 times longer than the control *100OPC*. This also means that *70OPC–30FA* and *50OPC–50FA* setting times were 19% and 70% longer than that of *70OPC–30NP* and *50OPC–50NP*, respectively. When the 30FA mixtures are compared to each other, the *70OPC–30FA* had a lower initial and final setting time than the *55OPC–30FA–15LP*. However, *50OPC–50FA* had a higher setting time than the ternary mixtures of *45OPC–40FA–15LP* and *35OPC–50FA–15LP*. For example, the final setting time of *45OPC–40FA–15LP* was almost 18% shorter than that of *50OPC–50FA*. All binary and ternary NP mixtures had shorter time of initial and final settings more water than that of FA to have normal consistency.

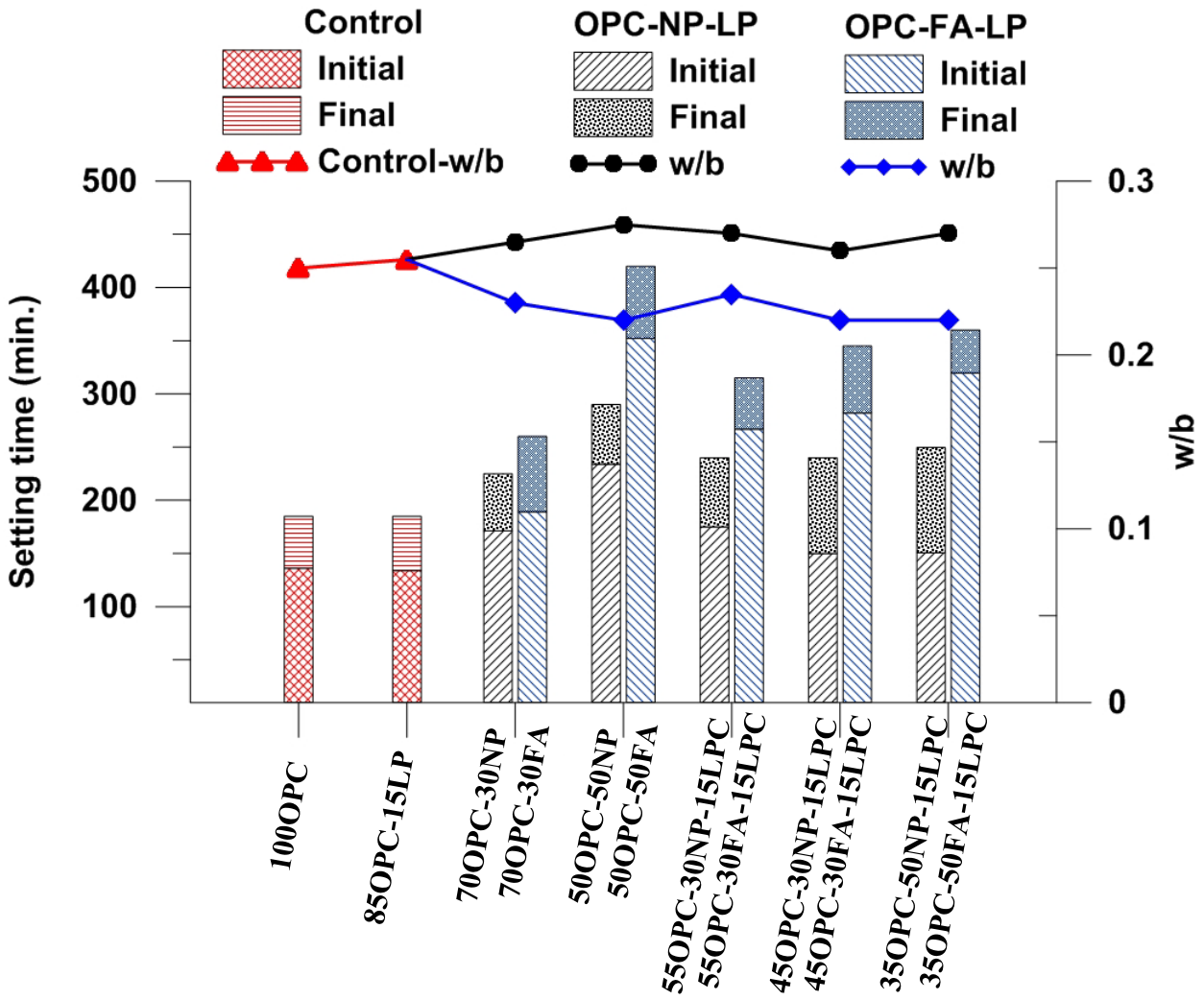

Figure 3.15 *w/b* for normal consistency and initial –final times of setting of the cement blends

3.2.2 Compressive strength of mortar specimens

3.2.2.1 Compressive strength of HVNP mortars

The results for compressive strength of mortar specimens incorporating with NP at different ages are shown in Figure 3.16. The control sample *100OPC* shows greater strength compared to *85OPC–15LP* at all test ages. The strength of *85OPC–15LP* was 40% and 28% less than that of control *100OPC* at 1 day and 3 days, respectively, while it was 2% less at 7 days (Fig. 3.16a). This seems to be a favorable early age result from the use of LP which was observed after 3 days. Yet, *85OPC–15LP* produced 12% less strength than *100OPC* mixture at 1 year.

The varied proportions of NP in mixtures had substantial effect on the strength evolution of the mortar specimens. When compared to the control *100OPC* mortar, the binary *70OPC–30NP30* mortar produced significantly lower strength up to 28 days; whereas it produced 11% higher strength than the control at 1 year. The binary *50OPC–50NP* showed lower strength than control *100OPC* and the binary *70OPC–30NP* and at all testing ages. However, the rate of strength development of *50OPC–50NP* increased over the time (Fig. 3.16b).

All ternary mixtures had developed lower strength than control *85OPC–15LP* up to 1 year of hydration. Moreover, the more replacement of OPC with NP in ternary mixtures, the greater the reduction in the strength, when compared with the control *85OPC –15LP*, with the exception of *45OPC–40NP–15LP* at 1 year which had slightly higher strength than that of *55OPC–30NP–15LP*. Again, *45OPC–40NP–15LP* produced the highest rate of strength development in 1 year among the all ternary blends. The significant–strength recovery of ternary blends in comparison with control *85OPC–15LP* was observed at 180 days and later ages due to the pozzolanic activity which is discussed in section 3.3. At 180 days, for instance, the strength of control *85OPC–15LP*, *55OPC–30NP–15LP* and *45OPC–40NP–15LP* was 34 MPa, 30 MPa, and 28 MPa, respectively.

While the ternary *55OPC–30NP–15LP* had considerably higher strength than the binary *50OPC–50NP* up to 14 days hydration, they had similar strength at 28 days of hydration. Moreover, *55OPC–30NP–15LP* had lower strength than the binary *50OPC–50NP* after 90 days of hydration (Figure 3.16–d). This result shows that the larger volume of replacement with binary mixture (OPC–NP) had higher strength development in the long term compared to the one with ternary mixture (OPC–NP–LP). This result can be attributed to the retarded pozzolanic reactivity of NP in the high volume of OPC replacement.

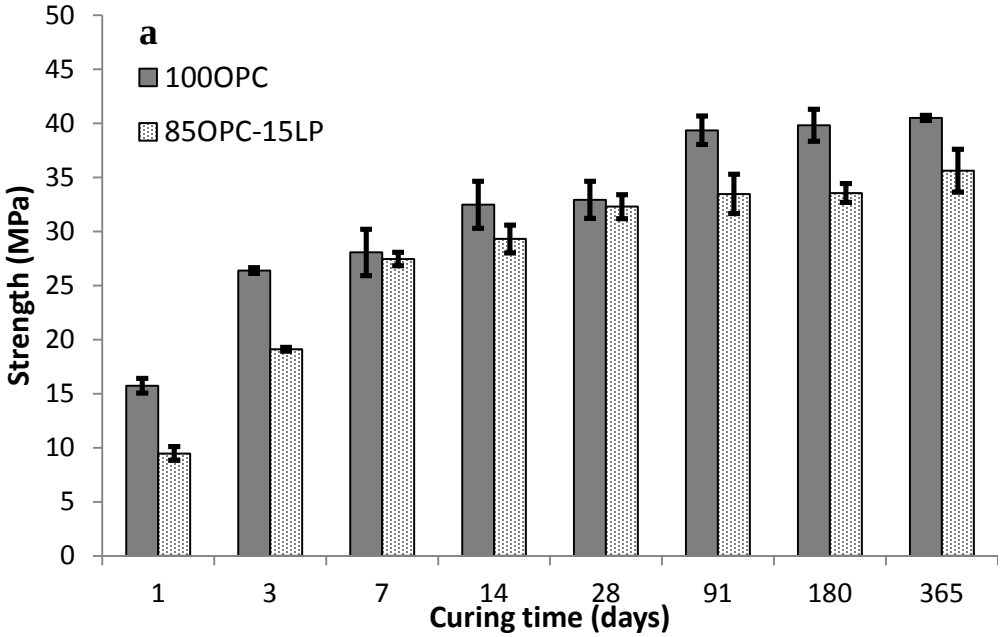
a
100OPC
85OPC-15LP
Strength (MPa)
Curing time (days)
0
5
10
15
20
25
30
35
40
45
50
1
3
7
14
28
91
180
365

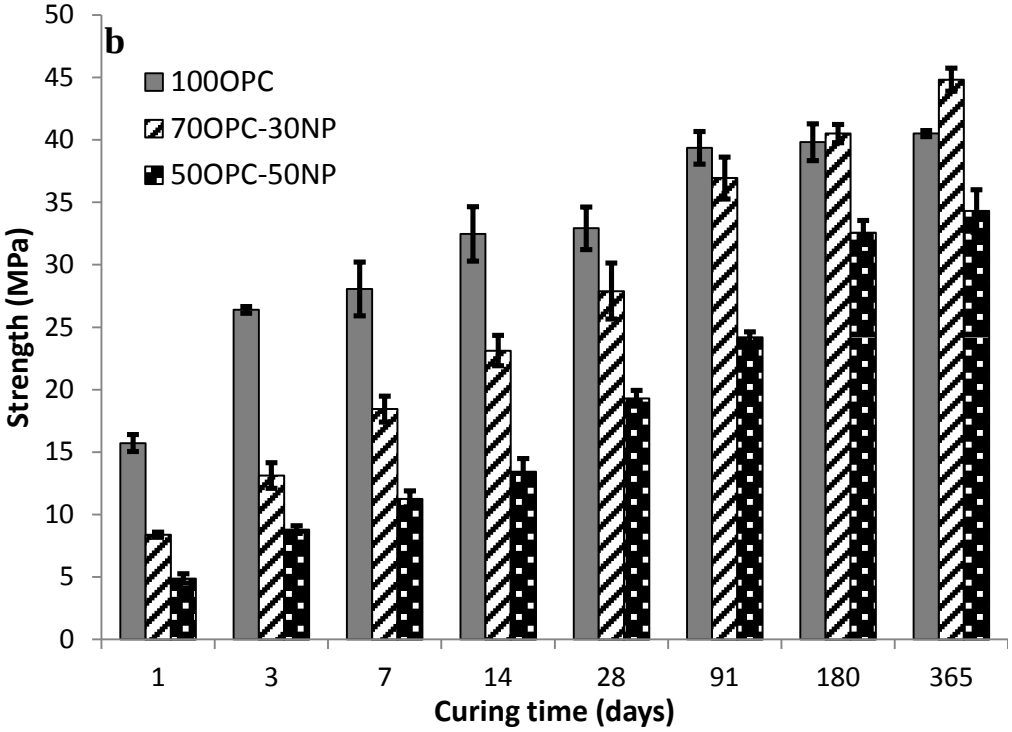
b
100OPC
70OPC-30NP
50OPC-50NP
Strength (MPa)
Curing time (days)
0
5
10
15
20
25
30
35
40
45
50
1
3
7
14
28
91
180
365

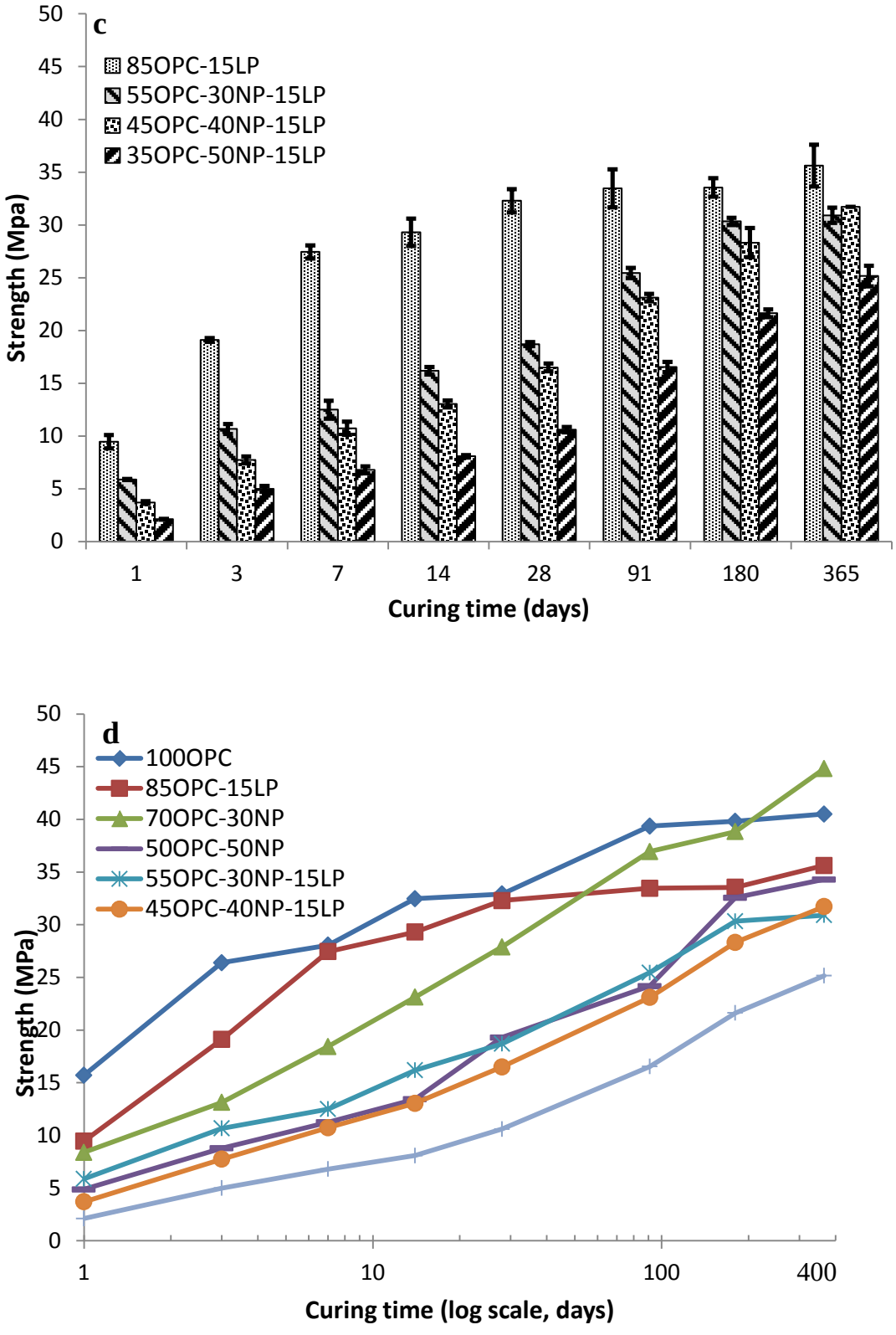

Figure 3.16 Compressive strength development of mortar specimens containing NP over time (a) control (b) binary (c) ternary (d) all specimens.

3.2.2.2 Compressive strength of HVFA mortars

Figure 3.17 shows the compressive strength development of mortar specimens containing FA over time. The binary specimens of *70OPC–30FA* and *50OPC–50FA* had lower strength at early ages, while they had slightly higher strength at 28 days and 91 days, respectively, compared to the control *100OPC* (Figure 3.17a). In addition, the strength of *70OPC–30FA* was 21% higher than *100OPC* at 91 days of hydration, showing that the dilution effect of FA was overcame by pozzolanic reaction. Also, *50OPC–50FA* produced 11% higher strength than *100OPC* at 1 year. Note that *50OPC–50FA* developed lower strength than *70OPC–30FA* at all testing ages; however, the rate of strength development of *50OPC–50FA* further increased with respect to *70OPC–30FA* after 180 days of hydration. This can be attributed to the delayed strength contribution of pozzolanic reaction in the high-volume of fly-ash replacement. It is also interesting to see that 1 year strength of *50OPC–50FA* of mortar sample was higher compared to the control *100OPC*, whereas *50OPC–50FA* of concrete sample was still lower compared to the control *100OPC* of concrete sample (Section 3.1.2.2). It could be attributed the curing condition of mortar sample which were cured in saturated $Ca(OH)_2$ solution and the varying mixture content of mortar and concrete specimens in terms of binder to aggregate ratios.

The effect of different replacement ratio of FA with OPC on the strength development of ternary mixtures is presented in Fig 3.17b. All ternary mixtures had produced lower strength up to 28 days of hydration, whereas *55OPC–30FA–15LP* and *45OPC–40FA–15LP* developed higher strength than the control 85*OPC–15LP* at 91 days of hydration and later ages. For instance, at 91 days of hydration *55OPC–30FA–15LP* and *45OPC–40FA–15LP* had 20% and 6% higher strength. At one year of hydration they had 18% and 24% higher strength compared to 85*OPC–15LP*, respectively. However, *35OPC–50FA–15LP* produced 16% and 11% lower strength compared to the control mortar. The substantial-strength recovery of ternary blends relative to the control 85*OPC–15LP* was at 91 days and later ages of hydration.

The strength development of all specimens is plotted in Fig 3.17c, with curing time in a base-10 log scale. The ternary specimens, with the exception of *35OPC–50FA–15LP* had slightly higher strength than the binary specimen of *50OPC–50FA* at 14 days of hydration. However, *50OPC–50FA* had had slightly higher strength than *55OPC–30FA–15LP* and *45OPC–40FA–15LP* at 1 year of hydration. This can be attributed with the delayed contribution of pozzolanic reaction of FA in the high-volume of replacement with OPC relative to *55OPC–30FA–15LP* and *45OPC–40FA–15LP*.

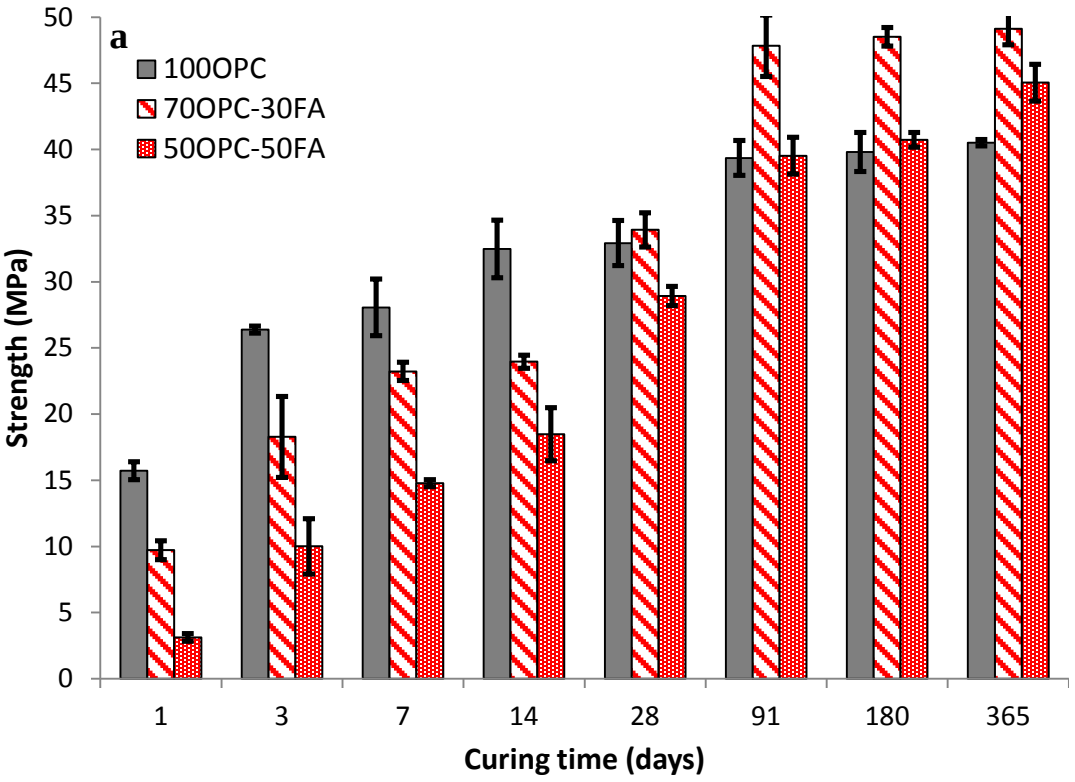
a
100OPC
70OPC-30FA
50OPC-50FA
Strength (MPa)
0
5
10
15
20
25
30
35
40
45
50
1
3
7
14
28
91
180
365
Curing time (days)

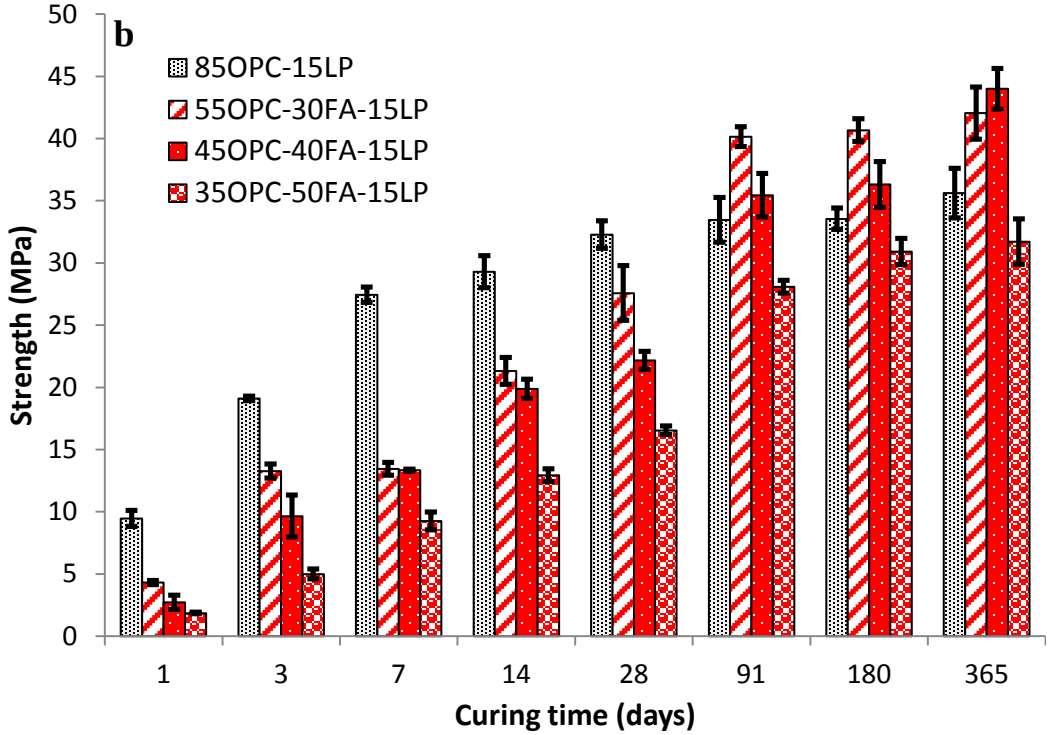
b
85OPC-15LP
55OPC-30FA-15LP
45OPC-40FA-15LP
35OPC-50FA-15LP
Strength (MPa)
0
5
10
15
20
25
30
35
40
45
50
1
3
7
14
28
91
180
365
Curing time (days)

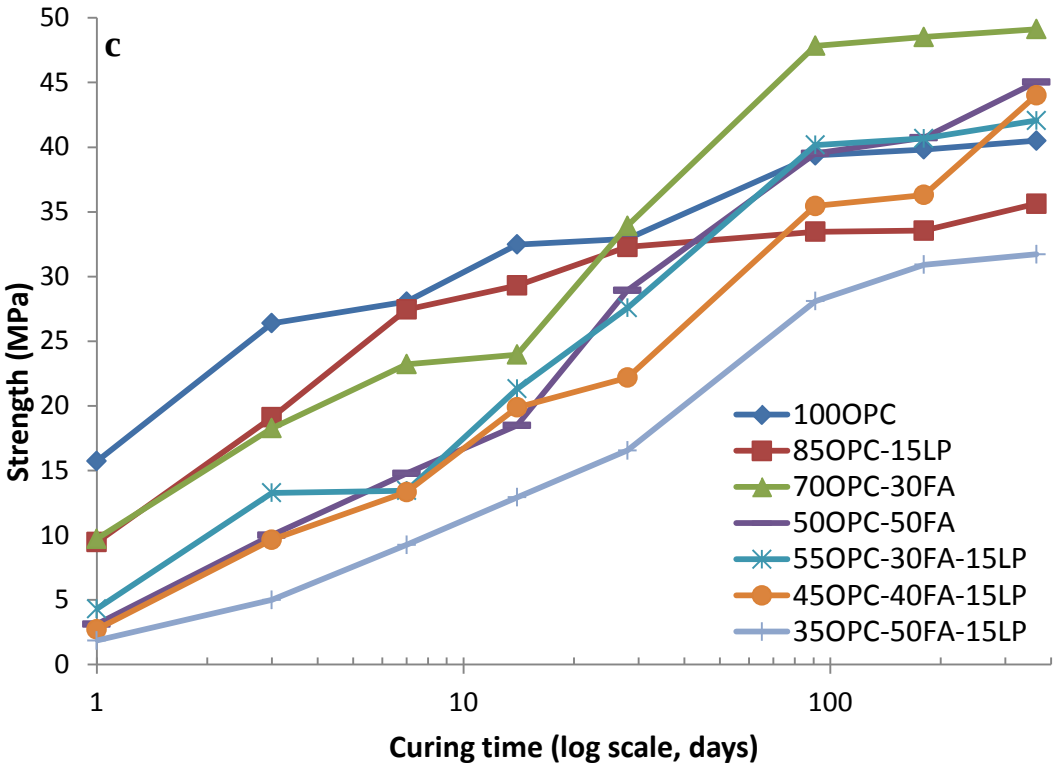

Figure 3.17 Compressive strength development of mortar specimens containing FA over time (a) binary (b) ternary (c) all specimens.

3.2.2.3 Comparison of compressive strength between HVNP and HVFA mortars

Figure 3.18 presents the compressive strength for all binary mortar mixtures with NP and FA and control *100OPC*. As it can be readily observed, with the exception of 1-day strength of *50OPC–50FA* all binary FA samples had higher strength than NP samples up to 1 year.

While the sample *70OPC–30FA* produced higher strength than the control *100OPC* after 28 days of curing, *70OPC–30NP* produced higher strength than the control after 180 days of curing. The mortar containing a cementing material mixture with 50 wt. % FA had a higher strength than control specimens at 180 day. However, the specimen with 50% NP had much lower rate of strength development when compared with 50%FA and control specimens. This suggests that the pozzolanic activity of FA is higher than NP.

In the case of ternary blended cements containing 15 wt. %LP, the increased NP/FA content led to relatively lower early strength. However, the sample *45OPC–40FA–15LP* had higher strength than *55OPC–30FA–15LP* at 1 year of curing (Figure 3.18b). This could be attributed to the slower rate of pozzolanic reaction at early ages but higher rates of strength gain in the long term.

In general FA specimens had higher strength than NP specimens at all ages except 1 day of curing. This could be related with the higher pozzolanic activity of FA than that of NP in the ternary mixtures and delayed setting time of FA specimens at 1 day. At 91 days and later ages 30

wt.% and 40 wt.% FA replacement in the ternary mixture showed higher strength than that of the control specimen, which contains 85 wt.% OPC–15 wt.% LP. This suggests that up to 40 wt.% FA replacement with OPC and LP did not affect with long–term strength development.

It is important to note here the synergistic effect between LP and FA shown in Figure 3.18 (a) and (b) compared to the control mixtures, shown in Figure 3.18(a), in which the addition of LP led to reduced compressive strength. In several cases, the compressive strength actually increased for the LP series mixtures when Portland cement was replaced by FA up to 40%. For the 30 wt.% FA and 40 wt.% FA along with 15% LP (45% and 55% total replacement ratios) the strength was 20% and 6% higher than the reference mixture of *85OPC-15LP* at 91 days. This suggests that the more sustainable product can be obtained over time, with increased cement replacement by FA and LP together. The reason for this outcome was discussed in section 3.1.2.2.

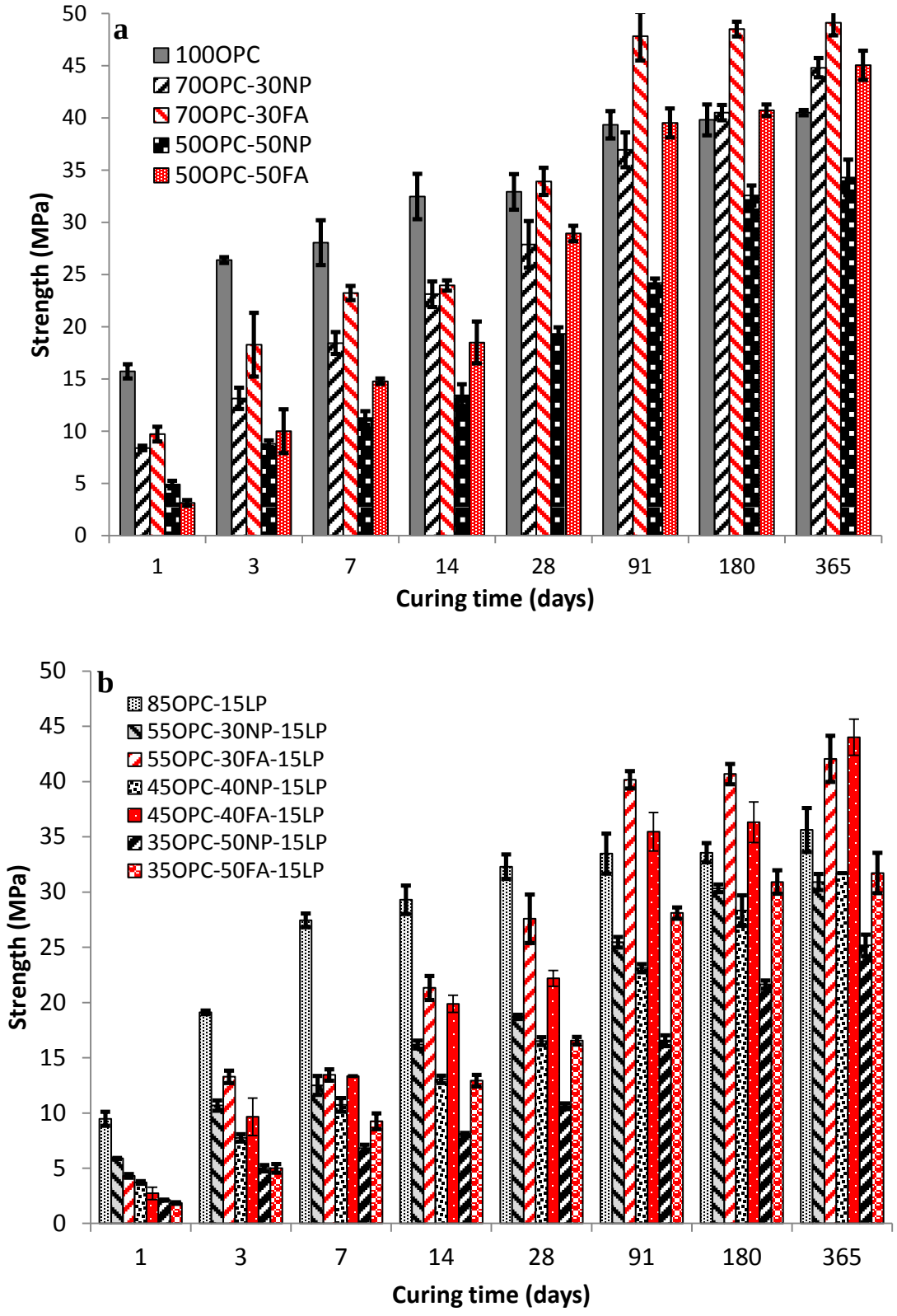

Figure 3.18 Compressive strength development of (a) binary OPC–NP/FA–LP (b) ternary OPC–NP/FA–LP mortar specimens over time

3.3 Cement paste samples

3.3.1 X-ray powder diffraction (XRD)

3.3.1.1 X-ray powder diffraction of HVNP pastes

XRD patterns of two cement pastes, one containing 100% OPC, and the other containing 85% OPC and 15% LP at different ages of hydration are shown in Figure 3.19a and Figure 3.19b, respectively. The XRD measurements are plotted with the same intensity scales. In *OPC100* and *OPC85–LP15,* after 91 days of hydration, belite and ferrite are the anhydrous phases still present. *OPC85–LP15* also has calcite after 91 days. The hydration products of *OPC100* were ettringite, monosulfate and portlandite, while the addition of 15% LP produced hemicarbonate and monocarbonate in *OPC85–LP15*. In *OPC100,* the ettringite peak, visible at 7 days had significantly reduced by 28 days and disappeared by 91 days, at which time a monosulfate peaks become clearly visible. However, in agreement with the other finding [43], the amount of ettringite did not reduce, and monosulfate was not observed over time in *OPC85–LP15*. Underlying reasons for the characterization of monosulfate in *OPC100* over time is that at the time of depletion of calcium sulfate and in the absence of calcite, the ettringite will react with aluminate and ferrite to form monosulfate [150]. Portlandite was present in both samples, and the peaks of portlandite increased at later ages due to the hydration reaction of silicates [3]. Figure 3.19b shows that carboaluminate hydrates have been precipitated at 7 days (Hc at 12.2° and 25.2° 2θ; d-spacing (d) = 8.4 Å and 4.1 Å, and Mc at 13.6° and 27.3° 2θ; d = 7.5 Å and 3.8 Å) in *OPC85–LP15* showing that the existence of calcite in composition led to remaining aluminates, after all gypsum was used, react with calcite to form hemicarbonate and monocarbonate [150]. In addition, monosulfate is less stable than monocarbonate [150]. Thus, ettringite did not decompose to form monosulfate in *OPC85–LP15*. Hemicarbonate disappeared at 91 days of hydration, monocarbonate peaks increased prominently after 28 days, since monocarbonate is thermodynamically more stable of the two [151].

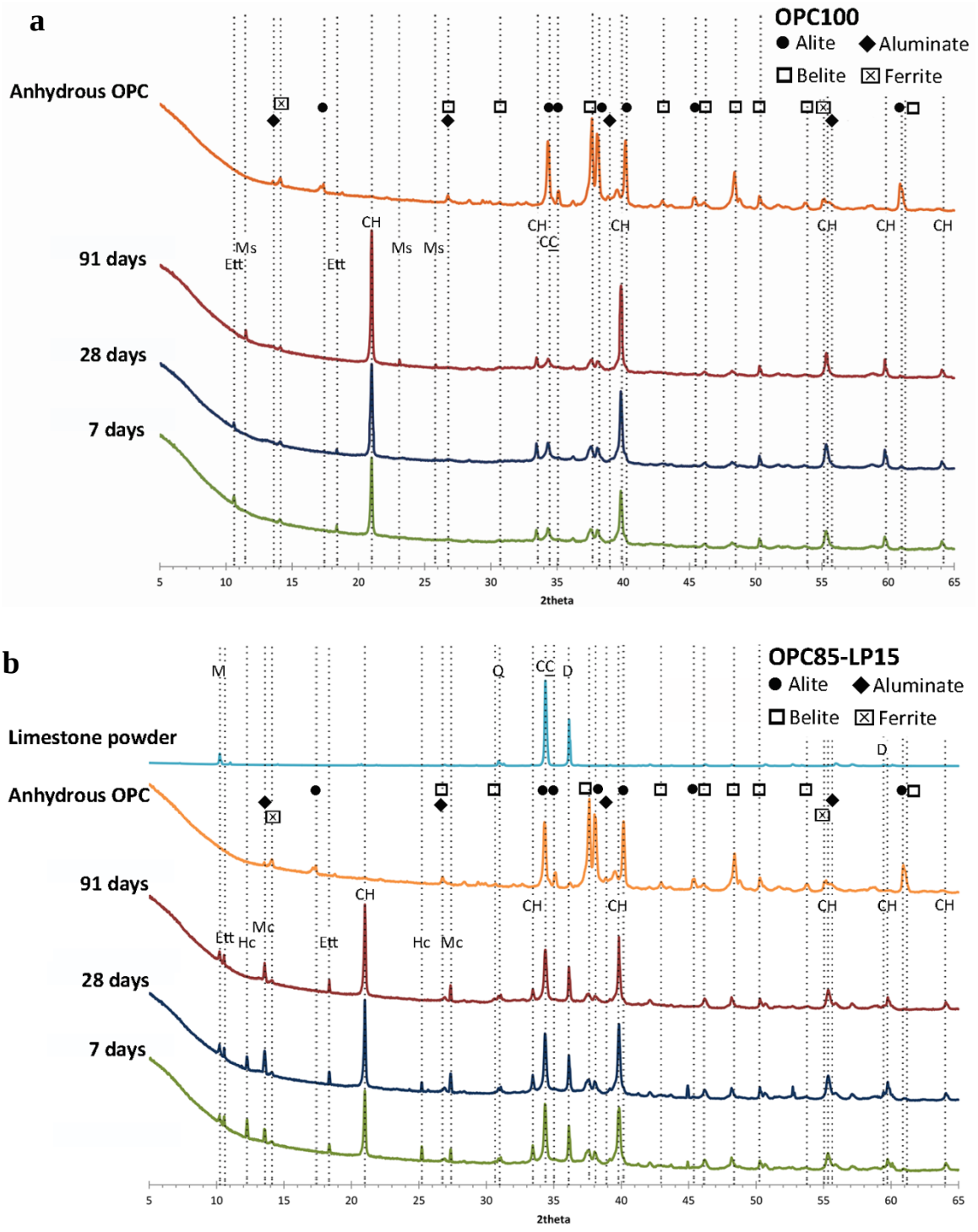

Figure 3.19 Phase composition observed by XRD in a hydrated cement paste at 7, 28 and 91 days a) *OPC100* b) *OPC85–LP15*. The main peaks of ettringite (Ett), monosulfate (Ms), portlandite (CH), hemicarbonate (Hc), monocarbonate (Mc), muscovite (M), quartz (Q), calcite (CC) and dolomite (D) are designated. The XRD measurements are plotted with the same intensity scales.

Figure 3.20 presents the XRD patterns of cement pastes containing 30% NP replacement (*OPC70–NP30*) and 30%NP–15%LP (*OPC55–NP30–LP15*) replacement of OPC at 7, 28 and 91 days. At 28 days and longer the presence of monosulfate was observed in *OPC70–NP30*. This

shows that ettringite became unstable after 7 days of hydration in binary blends (70%OPC and 30%NP), and the unreacted aluminates and ferrites reacted with ettringite to produce monosulfate. While monosulfate first was observed at 91 days in *OPC100*, it was detected at 28 days in sample containing 30%NP and 70%OPC. The earlier detection of monosulfate can be attributed to the lower pH in the pore solution of the sample ([152] cited in [153]) *OPC70–NP30* at 28 days which may destabilize the ettringite. The reason of low pH is because of portlandite consumption due to the pozzolanic reaction of NP. The work of Codina *et al.* indicates that low pH resulting from pozzolanic reaction of fly ash or silica fume decomposed the ettringite [154]. However, in the ternary cement containing *55OPC–30NP–15LP* monosulfate was not seen up to 91 days which confirming that LP made ettringite stable in ternary blends. Ettringite was found at all ages in both *OPC70–NP30* and *OPC55–NP30–LP15*, whereas the peaks of ettringite reduced slightly in *OPC70–NP30* with time. Portlandite peaks did not increase at 28 days of hydration in *OPC70–NP30* compared to that of the 7 days hydration sample, while they decreased at 28 days for *OPC55–NP30–LP15*. The earlier reduction of portlandite in ternary cement could be attributed the enhanced nucleation sites (filler effect) for pozzolanic reaction by means of limestone powder. It was observed that portlandite peaks reduced at 91 days of hydration for *OPC70–NP30*. In pure cement pastes, hemicarbonate and monocarbonate were not observed in *OPC70–NP30*. However, the hemicarbonate was observed at 7 days in *OPC55–NP30–LP15*; however its amount was reduced at 28 days and disappeared at 91 days of hydration. The peak of monocarbonate first was detected at 7 days and the intensity of monocarbonate peak increased with time. Thus, it could be concluded that sulphates were replaced by calcites during the formation of ettringite [47] in ternary blended cement.

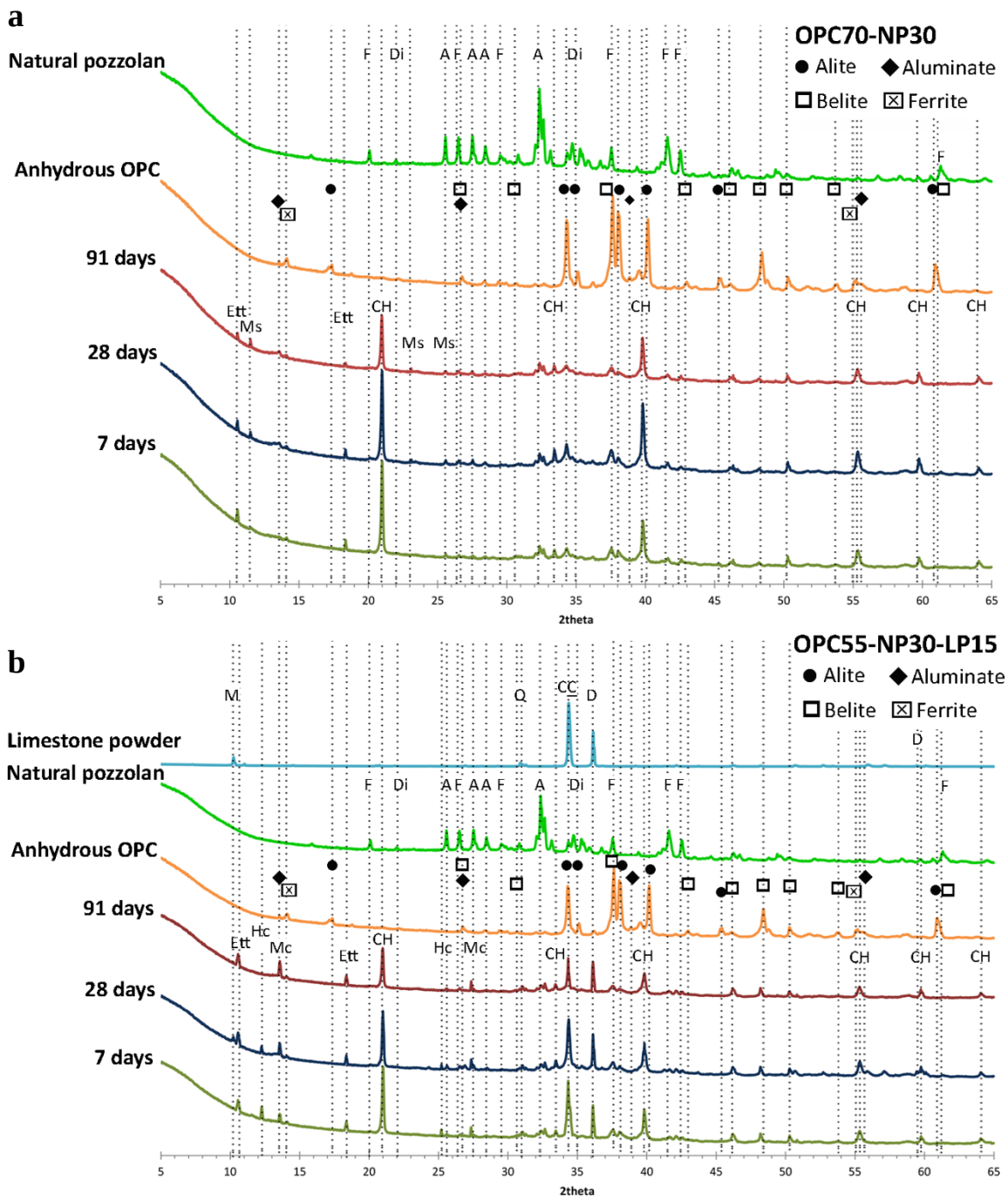

Figure 3.20 Phase composition observed by XRD in a hydrated cement paste at 7, 28 and 91 days a) OPC70–NP30 b) *OPC55–NP30–LP15*. The main peaks of ettringite (Ett), monosulfate (Ms), portlandite (CH), calcite (CC), hemicarbonate (Hc) and monocarbonate (Mc), forsterite (F), diopside (Di), anorthite (A), muscovite (M), quartz (Q), calcite (CC) and dolomite (D) are designated. The XRD measurements are plotted with the same intensity scales.

3.3.1.2 X-ray powder diffraction of HVFA pastes

Figure 3.21 shows the XRD patterns of cement pastes containing 30% FA replacement (*OPC70–FA30*) and 30%FA–15%LP (*OPC55–FA30–LP15*) replacement of OPC at different ages of hydration. In the absence of LP, monosulfate was first observed at 28 days in *OPC70–FA30*, while it was not detected in *OPC55–FA30–LP15* during all ages of hydration. The intensity of ettringite peaks decreased with time in *OPC70–FA30* due to the high aluminum oxide and low sulfur trioxide content of fly ashes that, confirming previous works ([155-159] cited in [153]). However, the intensity of ettringite peaks was prominent in *OPC55–FA30–LP15* up to 91 days. As previously mentioned, limestone powder makes stable ettringite because the aluminates react with calcite [150]. For the sample containing only 30% FA replacement and 30% FA–15% LP replacement, the amount of portlandite reduced at 28 days of hydration, and the decrease was more prominent for *OPC55–FA30–LP15*. Hemicarbonate and monocarbonate were detected at 7 days of hydration in *OPC55–FA30–LP15*. The intensity of hemicarbonate peak was decreased after 7 days and vanished at 91 days, whereas monocarbonate peak was more distinct after 7 days of hydration. Note that the reduction of the intensity of portlandite peaks was slightly more obvious at 28 days in *OPC70–FA30* and *OPC55–FA30–LP15* than *OPC70–NP30* and *OPC55–NP30–LP15*, respectively. This shows that pozzolanic reactivity of blended cement composed of fly ash was better than those containing natural pozzolan. This result agrees with the TGA analysis of blended cement over the time which will be discussed in Section 3.3.2.2.

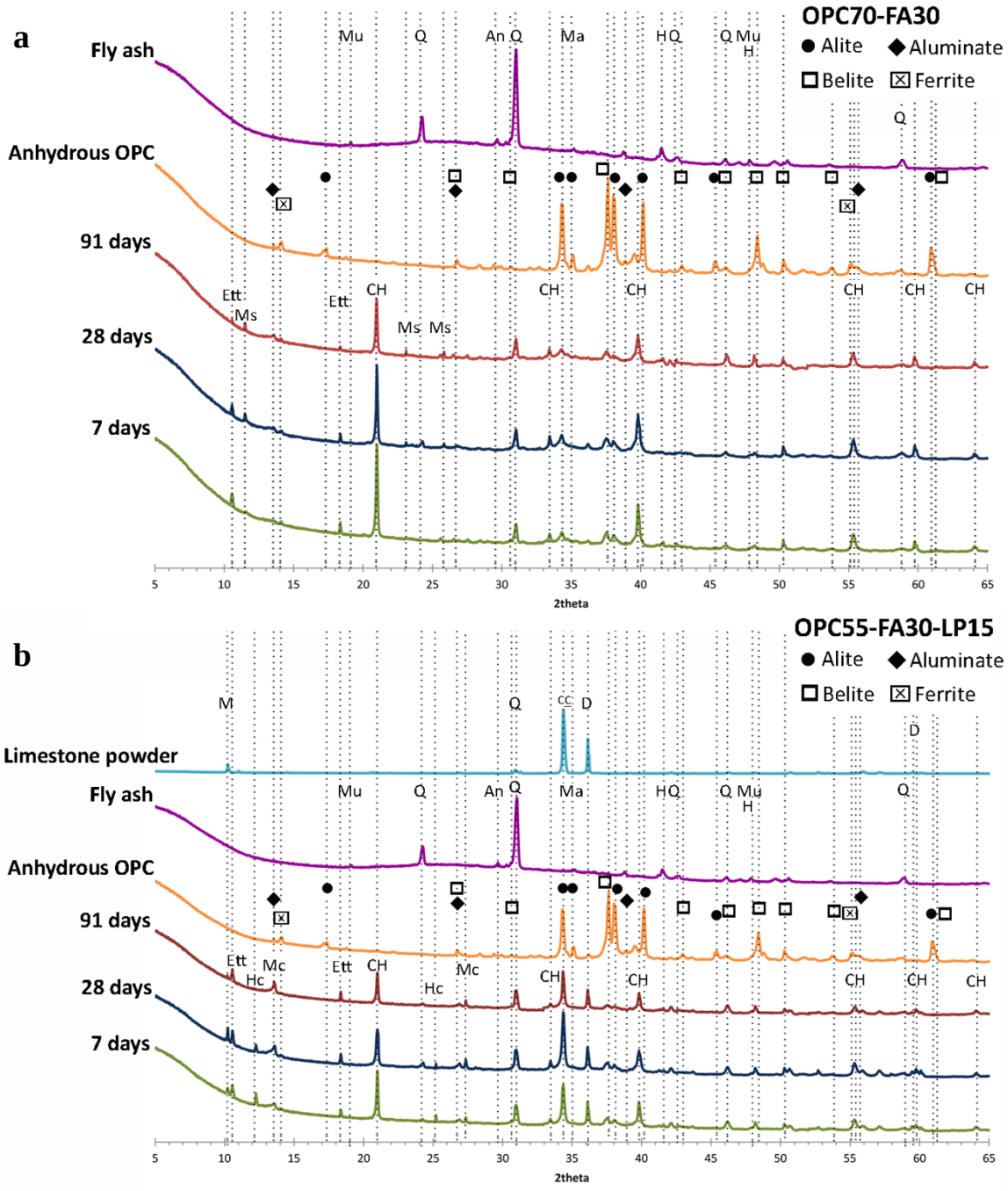

Figure 3.21 Phase composition observed by XRD in hydrated cement paste at 7, 28 and 91 days a) *OPC70–FA30* b) *OPC55–FA30–LP15*. The main peaks of ettringite (Ett), monosulfate (Ms), portlandite (CH), calcite (C$\underline{C}$), hemicarbonate (Hc) and monocarbonate (Mc), mullite (Mu), quartz (Q), anhydrite (An), magnetite (Ma), hematite (H), muscovite (M), quartz (Q), calcite (C$\underline{C}$) and dolomite (D) are designated. The XRD measurements are plotted with the same intensity scales.

3.3.2 Thermal analysis

3.3.2.1 Isothermal calorimetry (IC)

3.3.2.1.1 Isothermal calorimetry of HVNP pastes

Figure 3.22a shows the heat flow of blended cement containing limestone powder and/or natural pozzolan which was normalized to OPC content, and the cumulative heat flow normalized to both OPC content and binder content are shown in Figure 3.22b and Figure 3.22c, respectively. The induction period, which is the period after the first release of heat once the cement came into contact with water, was not changed when OPC was substituted by LP at 15% (*85OPC–15LP*); however, the slope of heat evolution curve was slightly steeper during the acceleration period as compared to the control mix containing 100% OPC. The main peak and second peak (visible only as a shoulder for *100OPC* in Figs 3.22a) which is associated with the reaction of silicate and aluminate phases, respectively, was increased and slightly accelerated (shifted to the left) with respect to *100OPC*. Appropriately, the cumulative heat per mass of OPC was higher for the *85OPC–15LP* than *100OPC* at 160 hr (Fig. 3.22b). The cause of acceleration and amplification of the heat flow when 15% limestone powder was blended with OPC is attributed to the filler effect created by the limestone powder, which means that more space for reaction of OPC at the same water to binder ratio, assuming that the limestone powder did not produce more hydration products, but instead created more nucleation sites for the hydration products of OPC [153]. In addition, the second peak was higher than the main peak of *85OPC–15LP*, while the main peak of *100OPC* was higher than second peak. It can be attributed to the filler effect of limestone powder and the participation of aluminate phases [153, 160] in chemical reactions result in the formation of carboaluminate hydrates [150, 161, 162]. Figure 3.22c shows that the cumulative heat per mass of cementing material was lower for the *85OPC–15LP* than for *100OPC* at 160 hr due to the dilution effect of limestone powder on the clinker. Even so, the cumulative heat of blended cement (*85OPC–15LP*) per gm of binder at 24 hr was about 91% of the cumulative heat of *100OPC*.

The induction period was slightly delayed when OPC was substituted by 30% and 50% natural pozzolan (*70OPC–30NP* and *50OPC–50NP*); on the other hand, the slope of heat evolution was steeper during the acceleration period when compared to the control mix containing 100% OPC. The second peak of *70OPC–30NP* and *50OPC–50NP* was higher than the ones of main peak. They were more amplified and slightly accelerated as compared to the ones of *100OPC*. Accordingly, the cumulative heat per mass of OPC was higher for *70OPC–30NP* than *100OPC* at 160 hr (Fig. 3.22b). The observed acceleration period, the sharpened peaks and the increased cumulative heat was greater, as the replacement of OPC with NP was increased from 30% to 50%. Therefore, the data suggest that the acceleration and amplification of the heat flow when finely-ground natural pozzolan was added into OPC promote the filler effect and nucleation site at early ages. The effect of pozzolanic reaction is negligible in the first days as it is highly dependent on the alkalinity of the pore solution which forms with the progress of silicates reaction. This is in agreement with a previous study [113]. The cumulative heat per mass of binder was lower as replacement of OPC with NP increased with the increasing dilution effect of Portland-cement clinker. The cumulative heat emitted per gm of binder during the first 24 hr was

about 77% and 60% of the cumulative heat of hydration of *100OPC* for *70OPC–30NP* and *50OPC–50NP*, respectively.

The addition of LP in the ternary blends containing NP and OPC further accelerated the heat evolution and amplified the main peak and the second peak as compared the control *100OPC*, and binary *70OPC–30NP* and *50OPC–50NP*, while the dormant period was not extended compared to binary mixtures. The maximum heat evolution of second peaks became more prominent on the ternary mixtures of *55OPC–30NP–15LP* and *45OPC–40NP–15LP* as NP content increased. Therefore, it seems that the addition of limestone powder to OPC and OPC–NP mixtures did not have negative effect on the reaction of aluminate phases; instead the reaction of the aluminate phases was accelerated. Accordingly, the cumulative heat of hydration of *55OPC–30NP–15LP* per gm of OPC was greater than *100OPC* and *70OPC–30NP*, whereas it was similar to the one of *50OPC–50NP*; while, the cumulative heat of hydration of *45OPC–40NP–15LP* per gm of OPC was the highest among the other mixtures. It can be attributed to the presence of limestone powder in the ternary mixtures as a result of filler effect and more nucleation sites. It is important to note that the cumulative heat of *55OPC–30NP–15LP* and *45OPC–40NP–15LP* per mass of binder at 24 hr was about 67% and 56% of the cumulative heat of control *OPC100* (Table 3.9) showing the dilution effect of Portland-cement clinker.

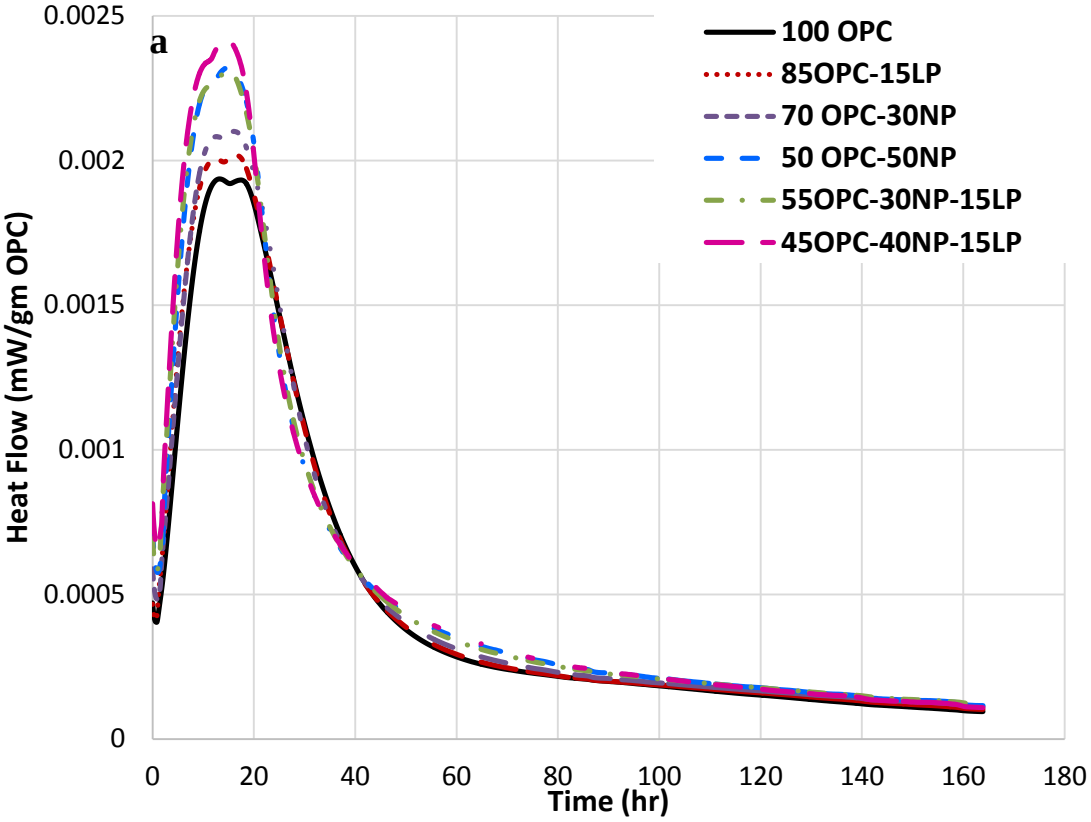
a
0.0025
0.002
0.0015
0.001
0.0005
0
Heat Flow (mW/gm OPC)
0
20
40
60
80
100
120
140
160
180
Time (hr)
100 OPC
85OPC-15LP
70 OPC-30NP
50 OPC-50NP
55OPC-30NP-15LP
45OPC-40NP-15LP

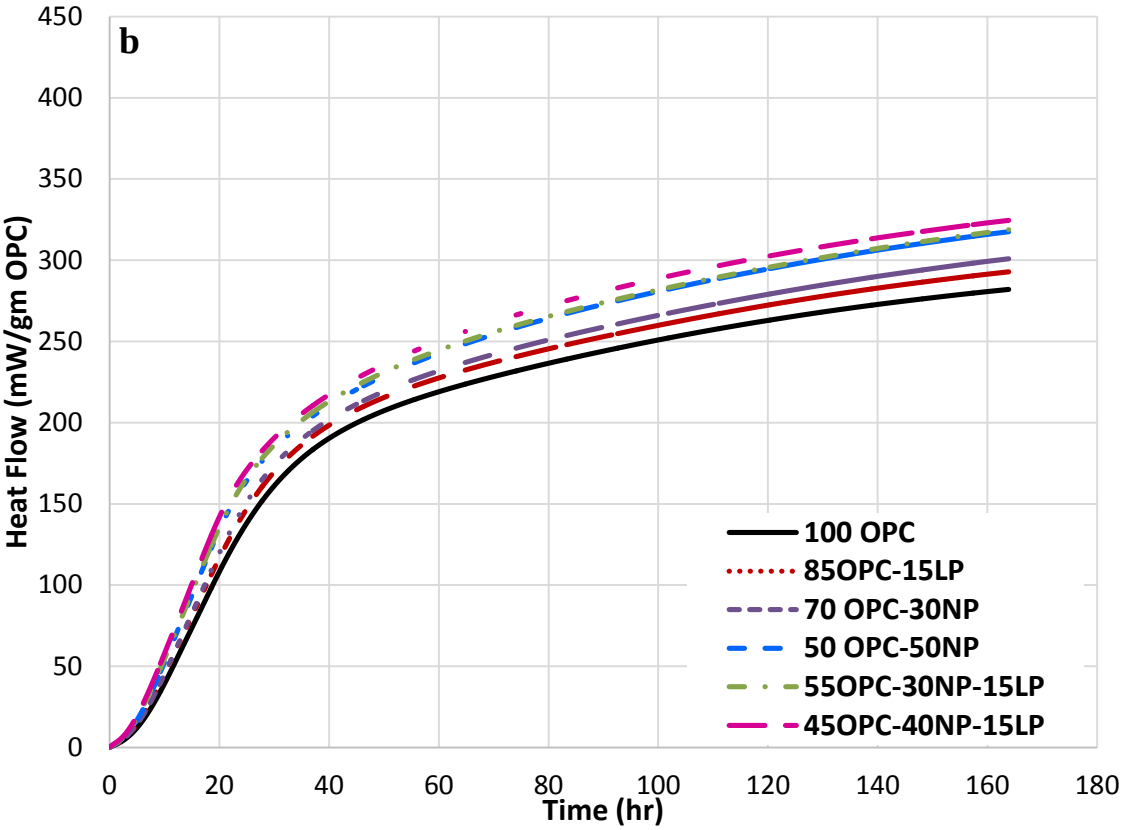
b
450
400
350
300
250
200
150
100
50
0
Heat Flow (mW/gm OPC)
0
20
40
60
80
100
120
140
160
180
Time (hr)
100 OPC
85OPC-15LP
70 OPC-30NP
50 OPC-50NP
55OPC-30NP-15LP
45OPC-40NP-15LP

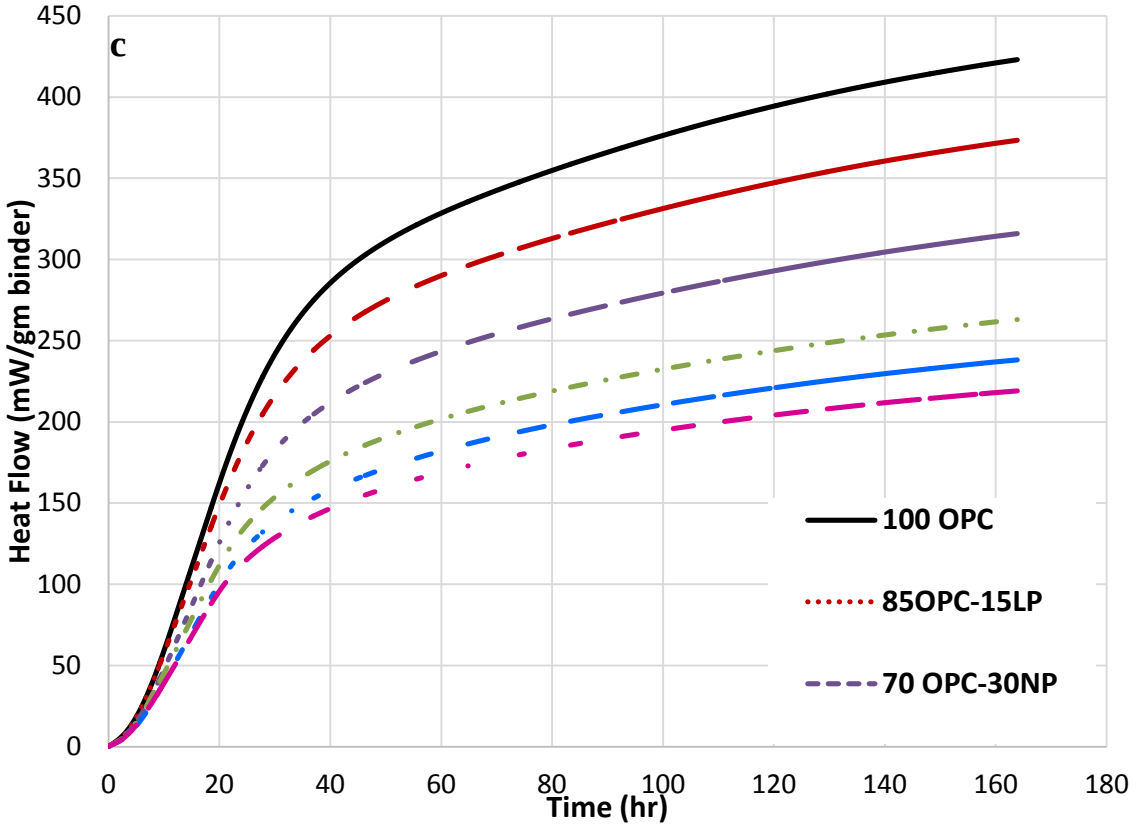

Figure 3.22 Isothermal calorimetry of cement blends containing natural pozzolan and/or limestone powder (a) Heat flow and (b) cumulative heat flow is normalized to the OPC content denoted as (mW/gm OPC) and (c) cumulative heat flow is normalized to the binder content denoted as (mW/gm binder)

Table 3.9 Cumulative heat per gram of binder and normalized cumulative heat to the one of OPC100

	Cumulative heat (mW/gm binder)	Normalized cumulative heat (%)
100OPC	199.2	100.0%
85OPC–15LP	180.5	90.6%
70OPC–30NP	152.9	76.7%
50OPC–50NP	119.5	60.0%
55OPC–30NP–15LP	132.6	66.6%
45OPC–40NP–15LP	112.2	56.3%
70OPC–30FA	124.6	62.6%
50OPC–50FA	75.8	38.1%
55OPC–30FA–15LP	108.4	54.4%
45OPC–40FA–15LP	80.6	40.4%

3.3.2.1.2 Isothermal calorimetry of HVFA pastes

Figure 3.23 shows the heat flow of cement blends containing LP and/or FA that was normalized to OPC content and cumulative heat flows that were normalized to both OPC content and binder content. The induction period was retarded when OPC was substituted by FA in the binary mixtures and ternary mixtures, and the main peak and second peak was delayed. However, the first peak and second peak increased compared to the ones of control sample *100OPC* and *85OPC–15LP*. Accordingly, the cumulative heat per mass of OPC of the *70OPC–30FA* and the *50OPC–50FA* was lower than the one of control *100OPC* up to 35 hr and 39 hr, respectively, then they were higher than the control (Fig. 3.23b). The cause of delayed acceleration and amplification of the heat flow when 30% FA and 50% FA was introduced into OPC can be attributed the slightly larger particle size of FA compared to OPC and LP, and retarded contribution of the filler effect, nucleation site and pozzolanic reaction. As the clinker was diluted, the cumulative heat per binder gm was much lower for the *70OPC–30FA* and *50OPC–50FA* than *100OPC* (Figure 3.23c). The cumulative heat of *70OPC–30FA* and *50OPC–50FA* per binder gm at 24 hr was about 68% and 38% of the cumulative heat of control *100OPC*.

The induction period was shortened, and the main peak and second peak were accelerated once LP was added into ternary mixtures. Figure 3.23a shows that the peaks of *55OPC–30FA–15LP* was shifted to left and sharpened with respect to the ones of *70OPC–30FA*, and the peaks of *45OPC–40FA–15LP* was shifted to left with respect to the ones of *50OPC–50FA*, whereas the amplification of peaks were similar for *45OPC–40FA–15LP* and *50OPC–50FA*. Hence, the cumulative heat per gm of OPC of *55OPC–30FA–15LP* and *45OPC–40FA–15LP* was less than the one of control *100OPC* up to 26 hr and 29 hr, respectively, then they exceeded the cumulative heat of the control mixture (Fig. 3.23b). These suggest that addition of LP in ternary mixtures with FA contributed the alleviation of retardation of reaction in binary mixtures containing FA. Even though the peaks amplification of *55OPC–30FA–15LP* and *45OPC–40FA–15LP* was similar, they were slightly retarded as the FA content was increased from 30% to 40%. Yet, the cumulative heat per OPC gm of *45OPC–40FA–15LP* was higher than the one of *55OPC–30FA–15LP* after 53 h. Thus, it can be concluded that as the substitution of FA increases from 30% to 40% in ternary mixtures, the retardation of hydration reaction was compensated over time (in 2 to3 days) with the presence of LP in the blended cement. It is also notable that the cumulative heat per binder gm of *45OPC–40FA–15LP* was higher than the one of *50OPC–50FA* up to 28 hr, even though the replacement ratio of *45OPC–40FA–15LP* was more than *50OPC–50FA*. Given this evidence, it can be concluded that the effect of clinker dilution can be reduced by the addition of LP in ternary mixtures containing FA.

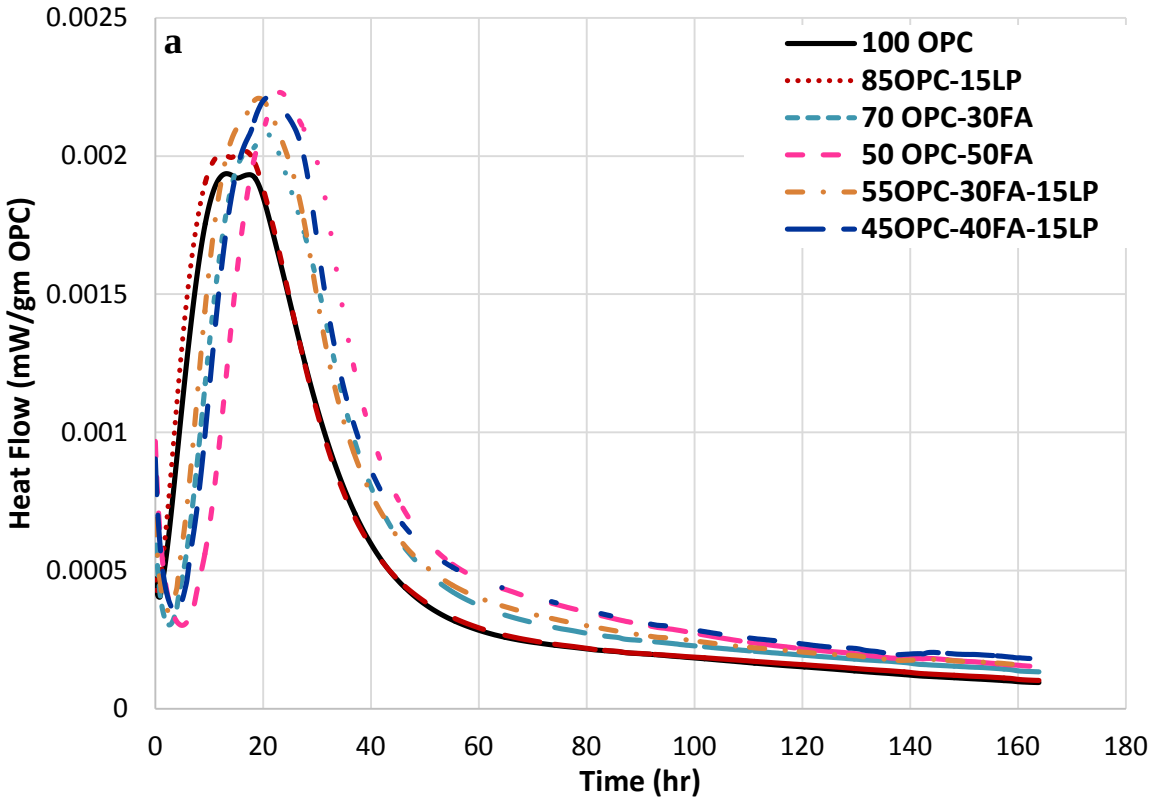
a
0.0025
0.002
0.0015
0.001
0.0005
0
Heat Flow (mW/gm OPC)
0
20
40
60
80
100
120
140
160
180
Time (hr)
100 OPC
85OPC-15LP
70 OPC-30FA
50 OPC-50FA
55OPC-30FA-15LP
45OPC-40FA-15LP

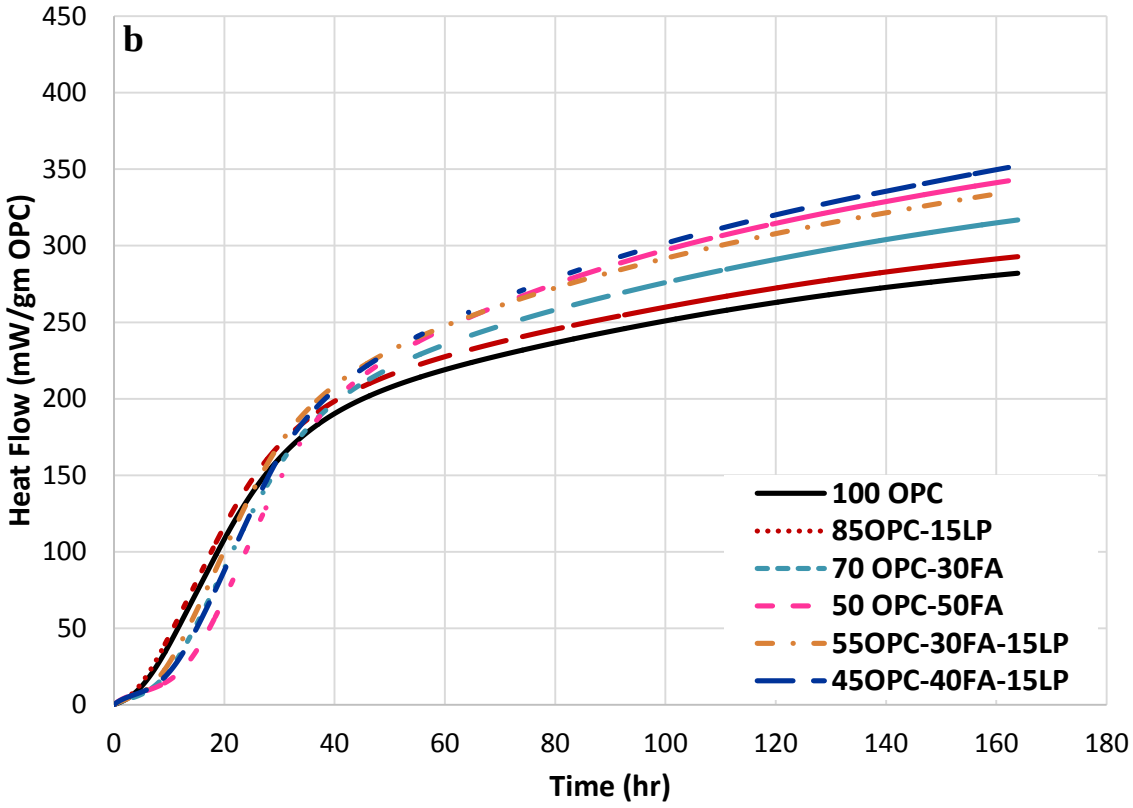
b
450
400
350
300
250
200
150
100
50
0
Heat Flow (mW/gm OPC)
0
20
40
60
80
100
120
140
160
180
Time (hr)
100 OPC
85OPC-15LP
70 OPC-30FA
50 OPC-50FA
55OPC-30FA-15LP
45OPC-40FA-15LP

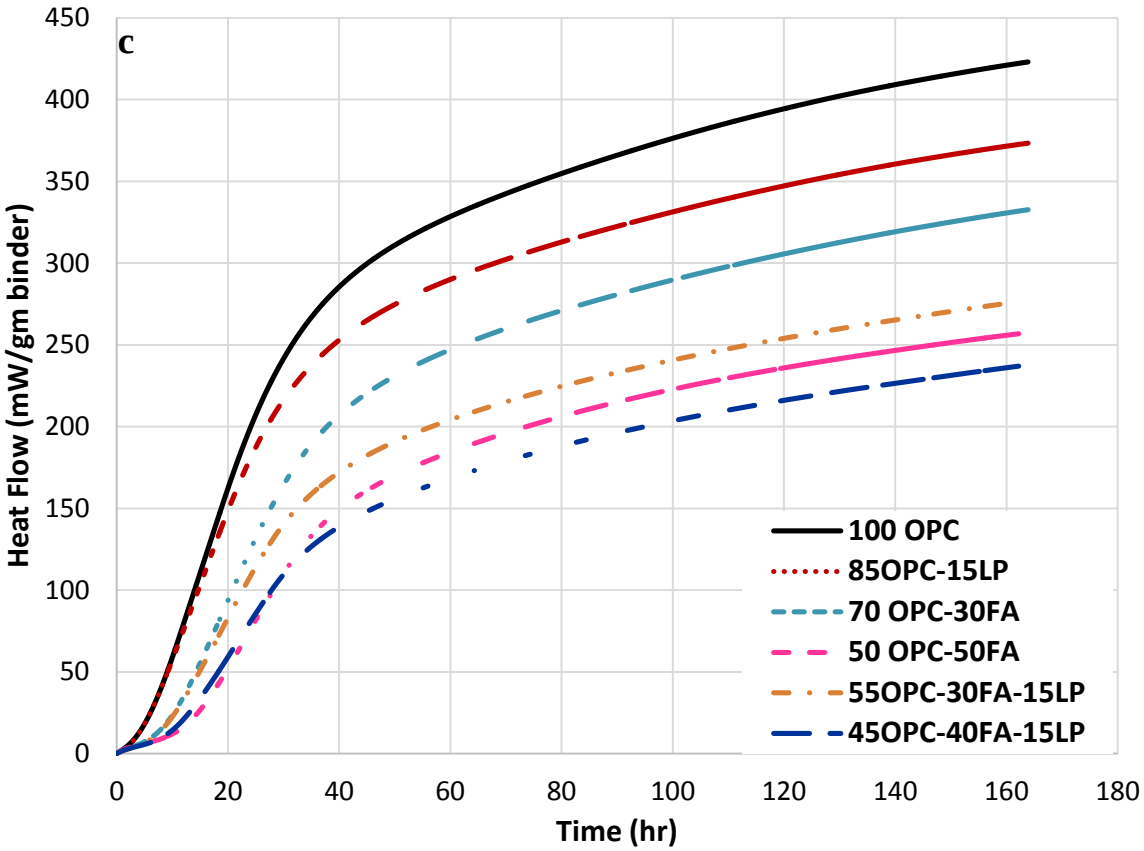

Figure 3.23 Isothermal calorimetry of cement blends containing fly ash and/or limestone powder (a) Heat flow and (b) cumulative heat flow is normalized to the OPC content denoted as (mW/gm OPC) and (c) cumulative heat flow is normalized to the binder content denoted as (mW/gm binder)

3.3.2.1.3 Comparison of isothermal calorimetry between HVNP and HVFA pastes

Figure 3.24 shows that introducing NP or FA into the binary cement mixtures greatly affect the shape of the heat flow curves with regards to induction period, acceleration and amplification of peaks. The induction period, the main peak and second peak of binary containing 30%FA and 50%FA was retarded compare to the ones of NP mixtures incorporated with 30%NP and 50% NP (Fig. 3.24a). Besides, the heights of peaks were shorter for the binary FA mixtures with the only exception that the amplification of second peaks were similar for *70OPC–30NP* and *70OPC–30FA*. However, the retardation of binary FA mixtures was recovered by the time as the cumulative heat per OPC gm of *70OPC–30FA* and *50OPC–50FA* was higher than the one of NP equivalents after 49h and 54h, respectively (Fig. 3.24b). This suggests that even though the particle size of FA is slightly larger than the one of NP providing less surface area for the nucleation and growth of reaction products at first days, the reactivity of FA was accelerated after 2 days.

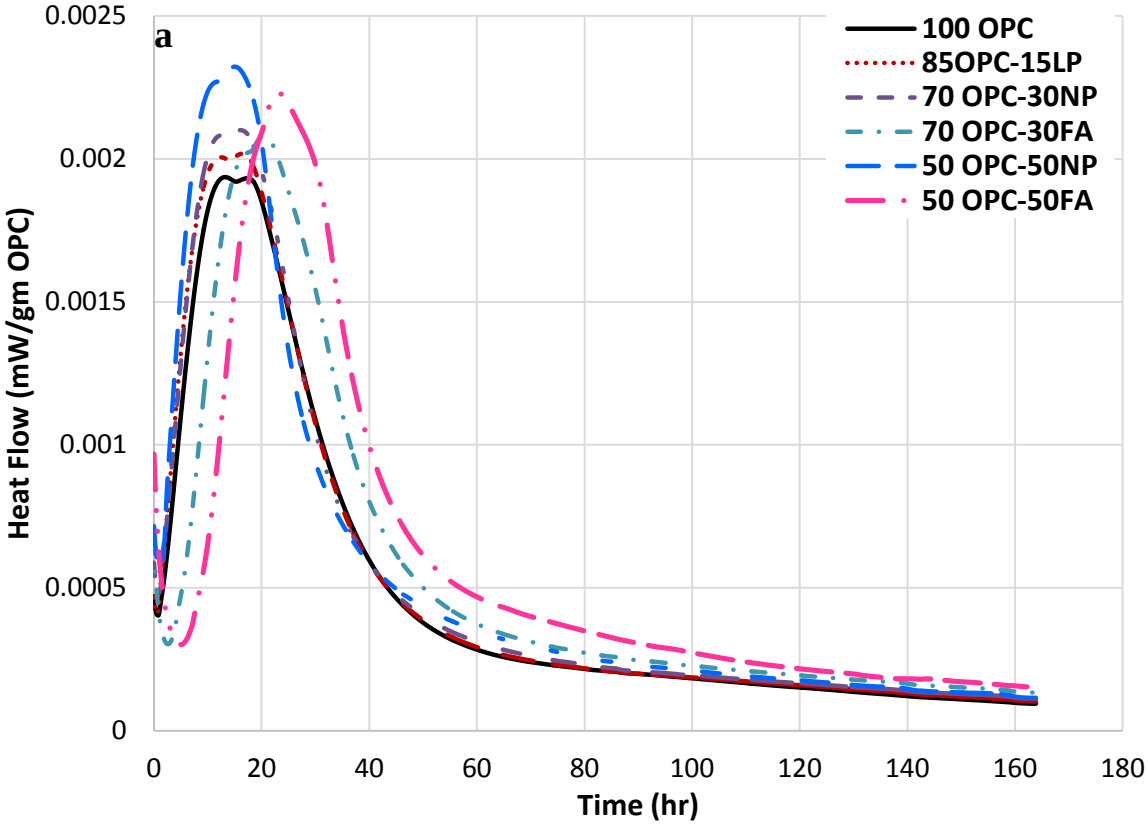
a
Heat Flow (mW/gm OPC)
Time (hr)
0.0025
0.002
0.0015
0.001
0.0005
0
0
20
40
60
80
100
120
140
160
180
100 OPC
85OPC-15LP
70 OPC-30NP
70 OPC-30FA
50 OPC-50NP
50 OPC-50FA

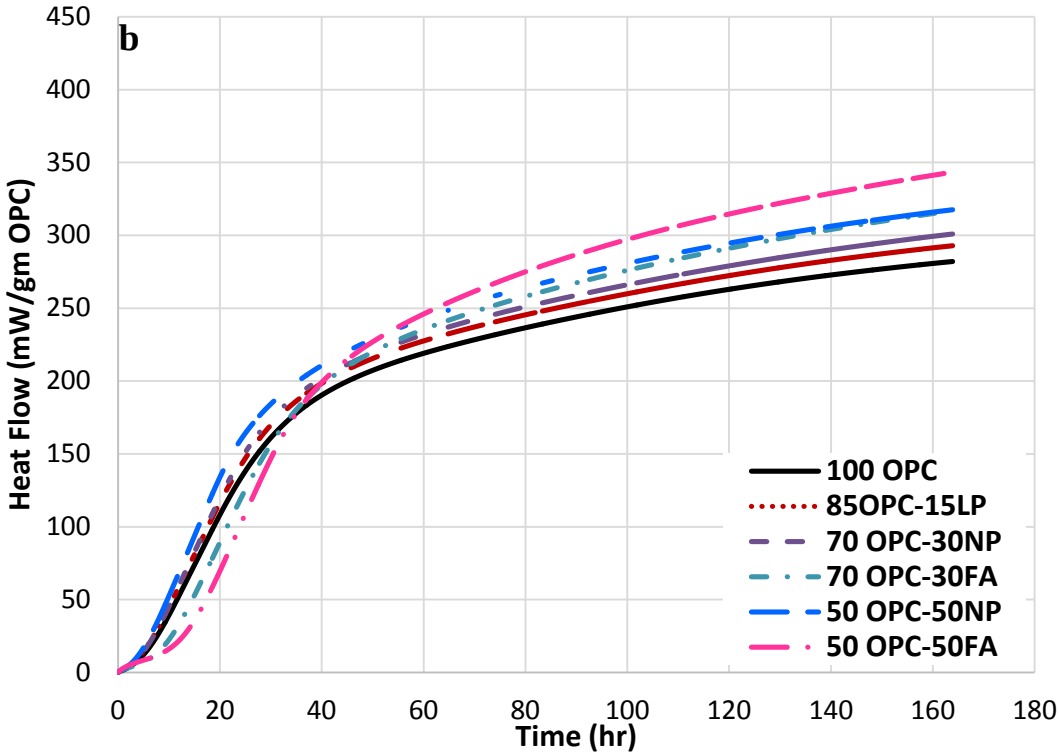
b
Heat Flow (mW/gm OPC)
Time (hr)
450
400
350
300
250
200
150
100
50
0
0
20
40
60
80
100
120
140
160
180
100 OPC
85OPC-15LP
70 OPC-30NP
70 OPC-30FA
50 OPC-50NP
50 OPC-50FA

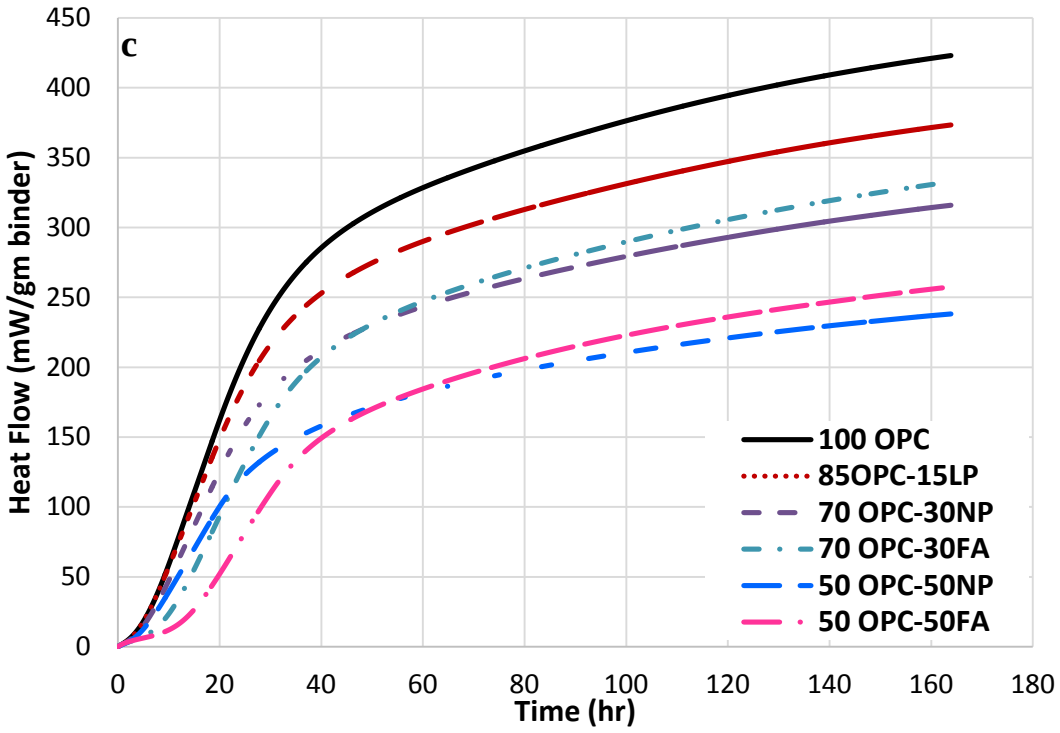

Figure 3.24 Isothermal calorimetry of binary cement blends containing natural pozzolan or fly ash (a) Heat flow and (b) cumulative heat flow is normalized to the OPC content denoted as (mW/gm OPC) and (c) cumulative heat flow is normalized to the binder content denoted as (mW/gm binder)

The effect of 15% LP presence on the heat flow of ternary mixtures containing 30% and 40% of NP or 30% and 40% FA is shown in Fig. 3.25. The addition LP in both NP and FA mixtures accelerated the heat of hydration, while FA mixtures were still delayed compared to NP and control mixtures (Fig. 3.25a). The main peak and second peak of NP ternary mixtures were also more sharpened than the ones of FA (Fig. 3.25a). The main peaks were more prominent in the mixtures containing NP. Yet, the cumulative heat per OPC gm of *55OPC–30FA–15LP* and *45OPC–40FA–15LP* was higher than the one of NP equivalents after 49h and 60h, respectively (Fig. 3.25b). This could be concluded that addition on LP in ternary mixtures containing NP at the first days resulted in higher acceleration of heat flow, whereas it was improved later ages for the ternary mixtures including FA.

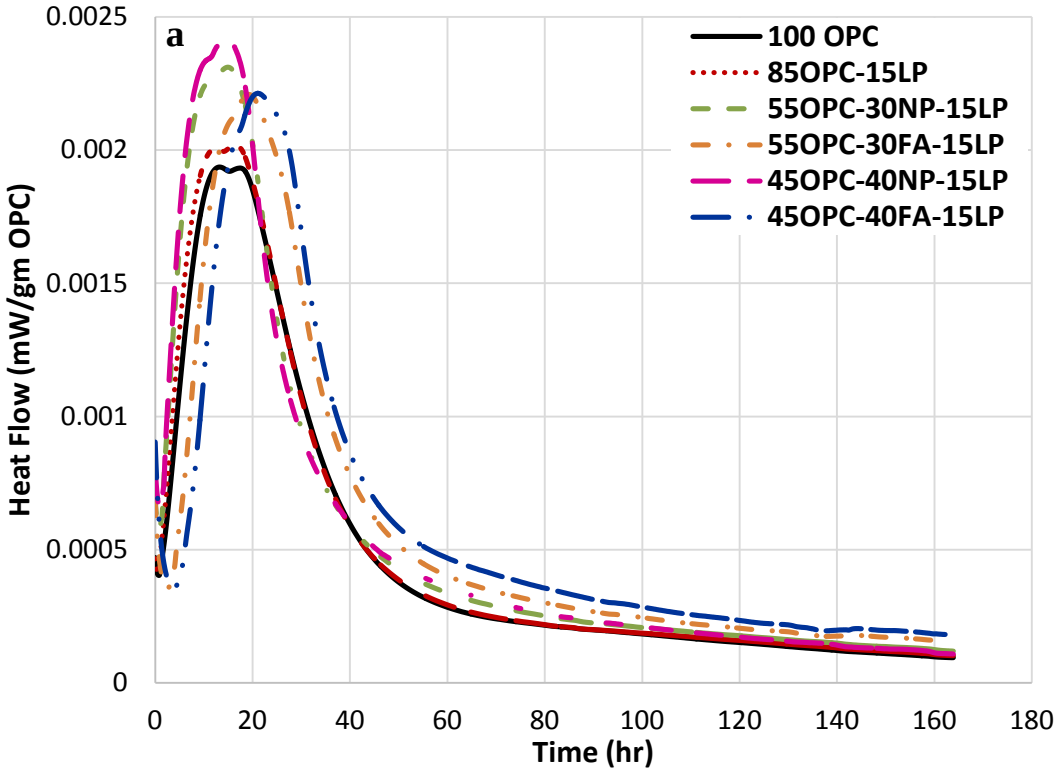

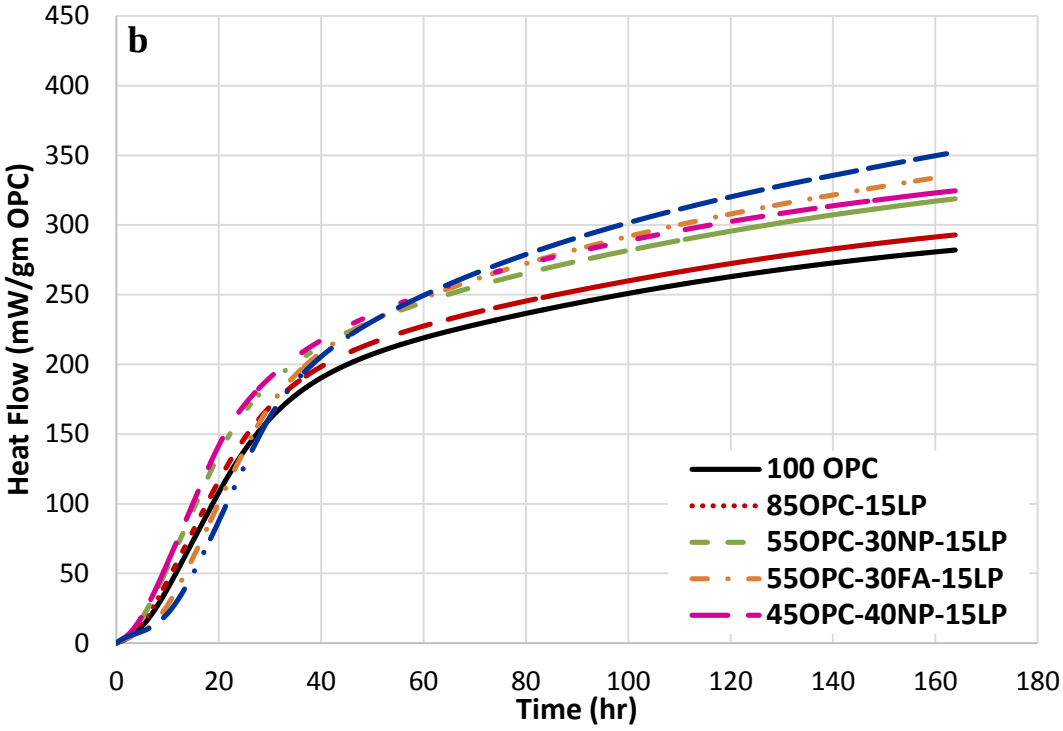

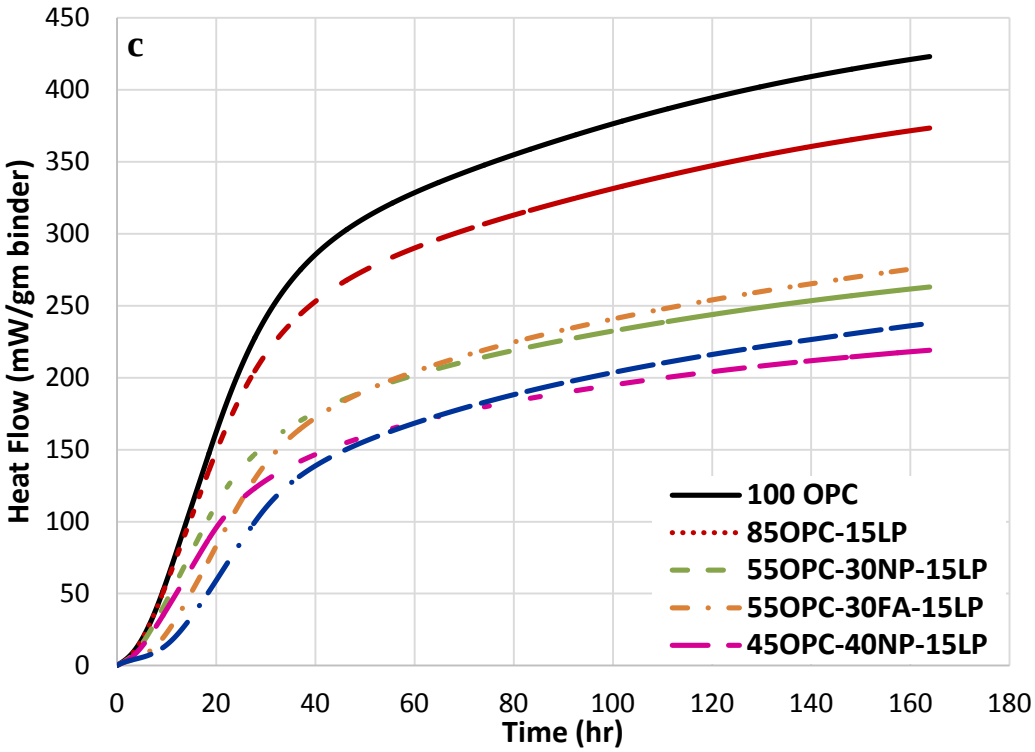

Figure 3.25 Isothermal calorimetry of ternary cement blends containing natural pozzolan and limestone powder or fly ash and limestone powder (a) Heat flow and (b) cumulative heat flow is normalized to the OPC content denoted as (mW/gm OPC) and (c) cumulative heat flow is normalized to the binder content denoted as (mW/gm binder)

3.3.2.2 Thermogravimetric analysis (TGA)

Thermogravimetric analysis was carried out the on the cement pastes at 7, 28, and 91 days to determine the effect of natural pozzolan, fly ash and limestone powder replacement on the contents of bound water (H), that comes from hydrates decomposition and was deduced from the weight loss between 40°C and 550°C, calcium hydroxide (CH) and calcium carbonate (CC). CH and CC was found by the weight loss between 400 °C and 550 °C, and the weight loss between 600 °C and 900 °C, respectively. Figure 3.26 shows the thermogravimetric analysis (TGA) spectra of all blended cements at 7 days (Figure 3.26a), 28 days (Figure 3.26b), and 91 days (Figure 3.26c) of hydration.

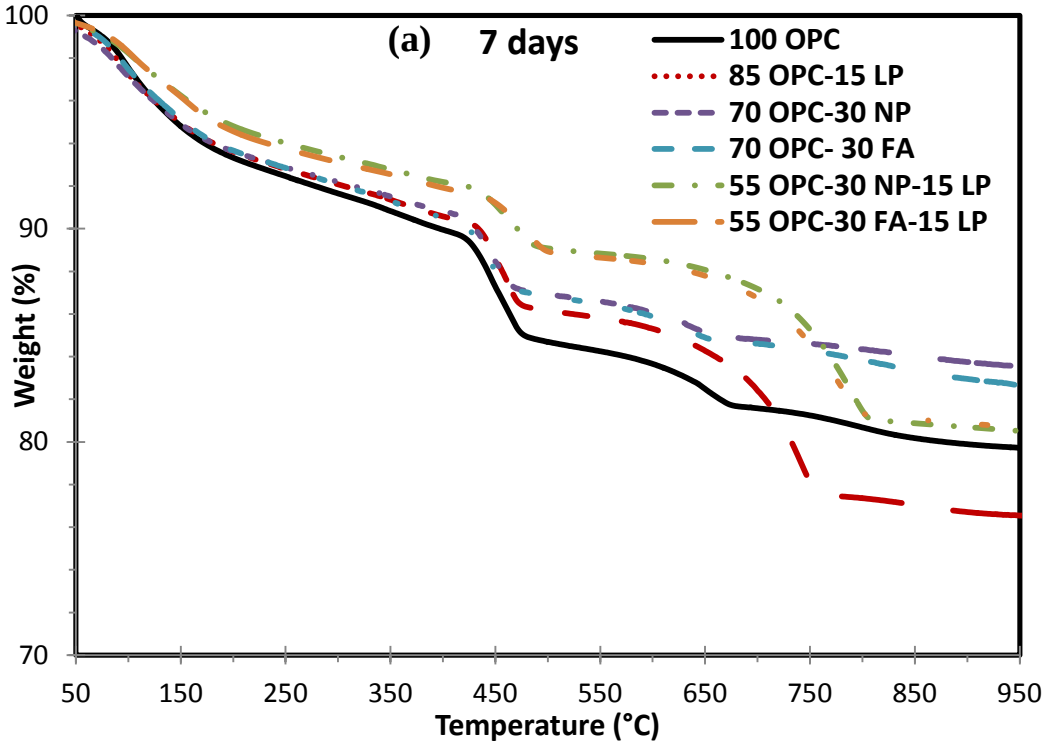

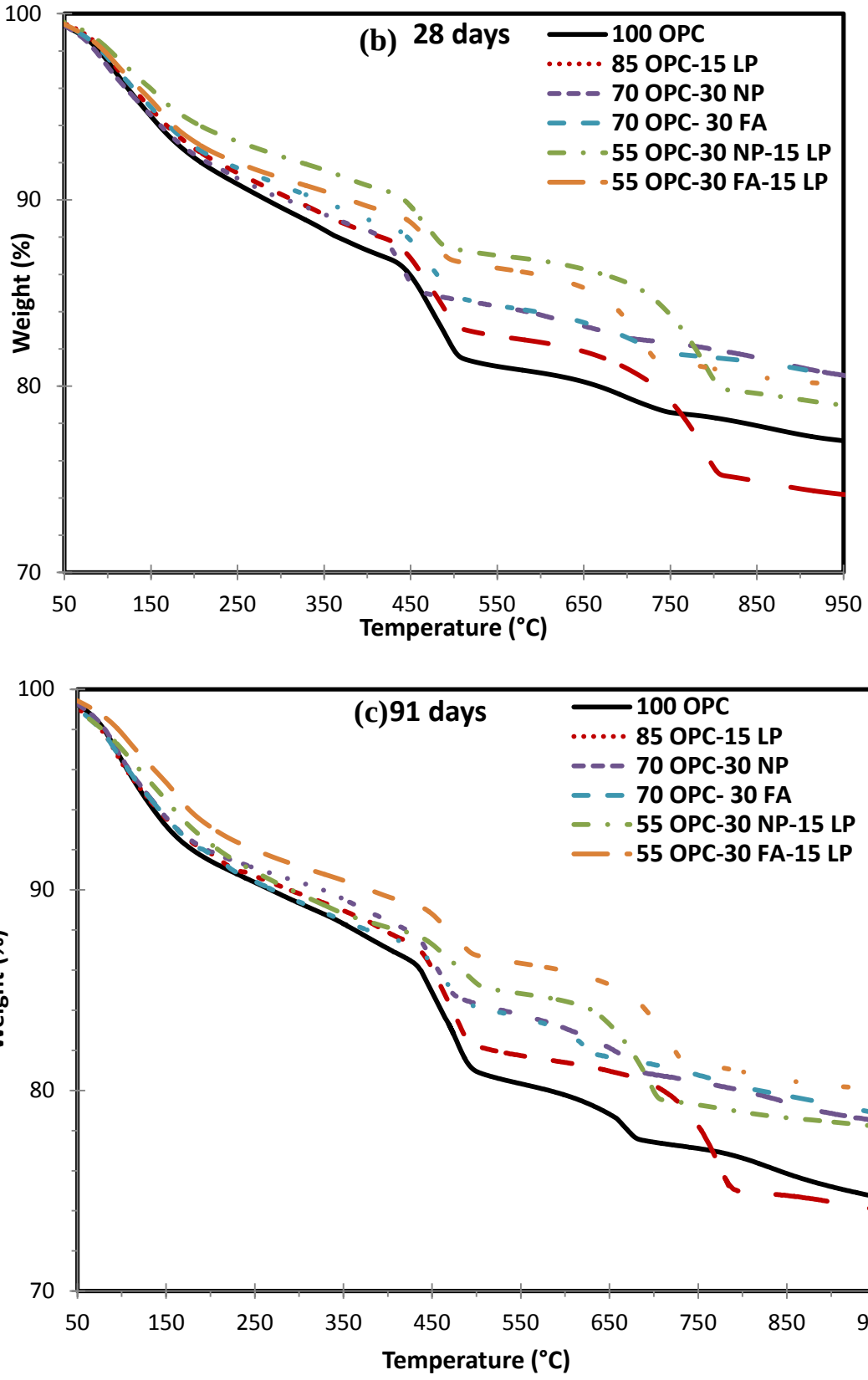

Figure 3.26 TGA data of blended cements at (a) 7days, (b) 28 days (c) 91 days of hydration

Figure 3.27 and Table 3.10 shows that *100OPC* had the highest amount of bound water and lowest amount normalized bound water compared to the blended cement pastes at all tested ages. This can be attributed to the filler effect that the replacement of OPC with LP, NP, or FA increased the amount of hydration products per OPC which can be seen in the section of 3.3.1 (XRD analysis) and 3.3.2.1 (IC analysis). This enhancement, however, did not compensate for the dilution effect in the binary and ternary cement composites, since the total hydrate water of 100 OPC was higher than the all blended cement composites (Table 3.10).

Due to the filler effect, replacing 15% of OPC with limestone powder (LP) resulted in increased amount of bound water per OPC (Figure 3.27b), while it decreased the amount of bound water per binder relative to *100OPC*.

The 30% OPC replacement with NP or FA in binary mixtures raised the content of normalized H compare to *100OPC* and *85OPC–15LP* indicating the enhancement in the amount of reaction products. This improvement is due to the increased effective water to OPC ratio, and the extra surface area for hydration products to precipitate on by replacing OPC with finely ground natural pozzolan or fly ash [150]. The bound water content per binder of binary mixtures was decreased compared to *100OPC* showing that the filler effect did not make up for the replacement of the OPC with natural pozzolan or fly ash which is in agreement with the results of other studies [62, 112, 150]. The result also show that *70OPC–30FA* had slightly higher amount of bound water than the one of *70OPC–30NP* at 7 days, yet they had similar amount of hydrate water at later ages indicating the improved reactivity of fly ash compared to natural pozzolan at early ages.

The ternary blended cement containing 30% NP or 30% FA along with 15% LP had greater amount hydrate water relative to the binary blended cement containing 30% NP or 30% FA, respectively. This suggests that incorporation of LP with NP or FA did not interfere with the hydration reaction, instead filler effect of NP or FA was further increased with LP. *55OPC–30FA–15LP* had higher amount of hydrate water than the equivalent one with NP instead of FA up 91 days of curing. This result suggests an extra increase in the amount of hydration products of ternary cement pastes containing FA and LP compared to the one with NP and LP.

Table 3.10 The content of bound water and calcium hydroxide with respect to the content of binder and OPC after 7, 28 and 91 days of hydration

Sample	Age	H (%)	H/OPC (%)	CH (%)	CH/OPC (%)
100OPC	7 days	18.4	18.4	14.0	14.0
100OPC	28 days	22.9	22.9	16.0	16.0
100OPC	91 days	23.9	23.9	18.5	18.5
85OPC–15LP	7 days	16.3	19.1	13.2	15.5
85OPC–15LP	28 days	20.5	24.2	14.8	17.4
85OPC–15LP	91 days	21.6	25.4	16.0	18.9
70OPC–30NP	7 days	14.9	21.3	10.7	15.3
70OPC–30NP	28 days	18.2	26.1	11.1	15.9
70OPC–30NP	91 days	18.9	27.0	10.3	14.7
70OPC–30FA	7 days	15.4	22.0	10.3	14.7
70OPC–30FA	28 days	18.2	25.9	10.3	14.7
70OPC–30FA	91 days	19.0	27.1	9.5	13.5
55OPC–30NP–15LP	7 days	12.3	22.3	9.0	16.4
55OPC–30NP–15LP	28 days	14.7	26.6	8.6	15.7
55OPC–30NP–15LP	91 days	15.1	27.5	8.2	14.9
55OPC–30FA–15LP	7 days	12.6	22.9	8.6	15.7
55OPC–30FA–15LP	28 days	15.3	27.9	8.2	14.9
55OPC–30FA–15LP	91 days	15.4	28.0	7.4	13.5

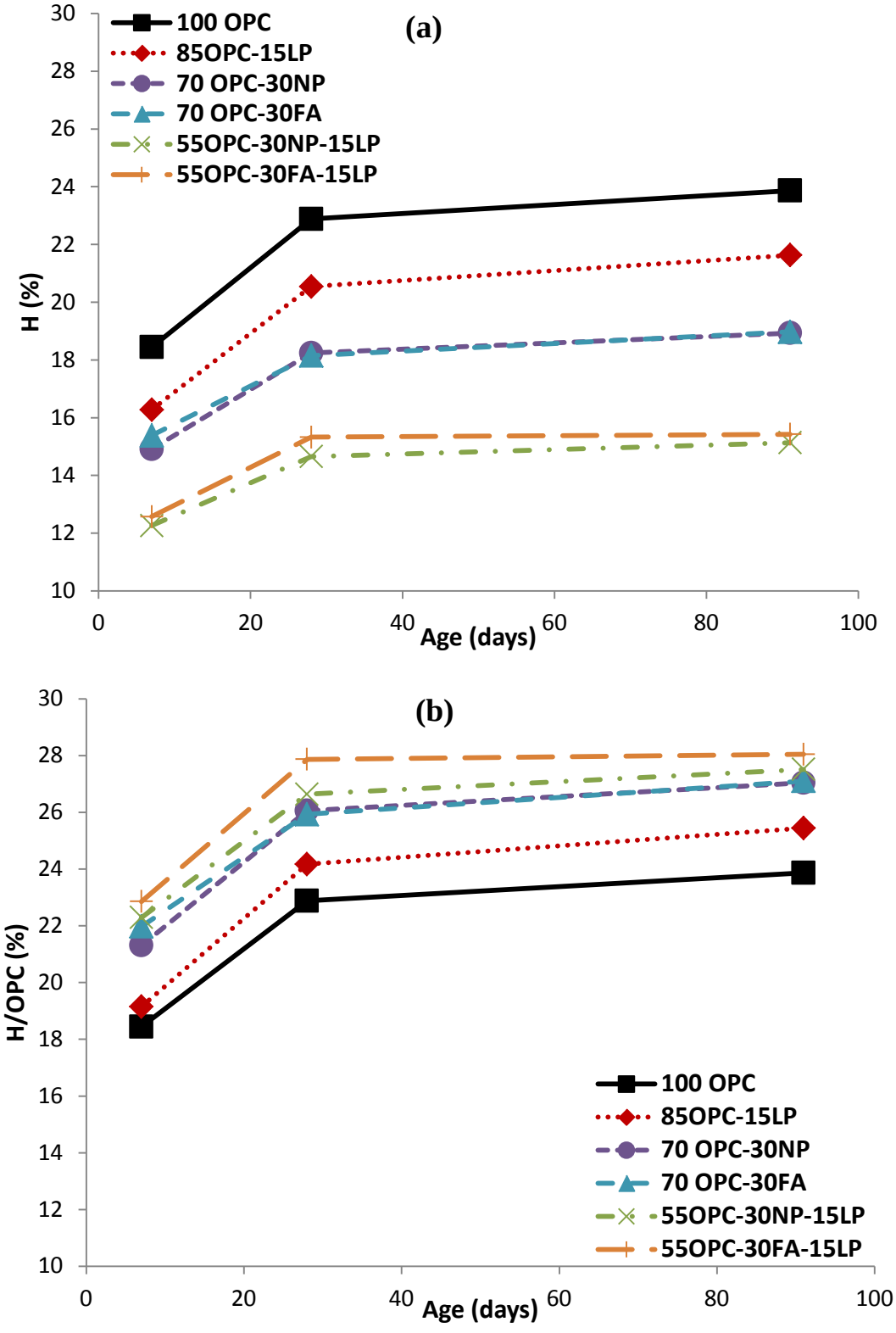

Figure 3.27 The bound water contents (H) a) per binder b) per OPC after 7, 28 and 91 days of hydration

Figure 3.28 shows that the amount of calcium hydroxide (CH) of cement composites containing 100% OPC and 85wt.%OPC–15wt.%LP increased with time up to 91 days of hydration. However, replacing 30% of OPC with NP or FA resulted in slightly increase in the amount of CH at 28 days of curing and decrease CH at 91 days of curing. The observed reduction in CH indicates that pozzolanic activity of NP and FA with time. However, a further OPC reduction of 15% through limestone powder incorporating with 30% NP or 30% FA resulted in reduced CH at 28 days of hydration. This can be attributed to both accelerated pozzolanic reaction of NP/FA and formation of hydration products that consume CH such as hemicarboaluminate hydrate [150, 163].

The normalized calcium hydroxide content of all binary and ternary blended cements containing LP, NP and FA was greater than the one of *100OPC* at 7 days of hydration due to the increased nucleation site and the more space for the reaction of OPC, namely due to the filler effect of mineral admixtures. In addition the normalized CH of *85OPC–15LP* was higher than the one of *100OPC* at all tested ages. However, the CH per OPC of binary cements incorporated with 30% NP or 30% FA was similar the one of *100OPC* at 28 days of curing and the lower at 91 days of hydration. This suggests that the reduction of CH in the binary cement composites containing 30% replacement is due to the pozzolanic reaction of NP or FA. Expectedly, the further replacement with 15% LP along with 30% NP or 30% FA in the cement composites resulted in the lower normalized CH relative to *100OPC* at 28 days and later ages. It is interesting to see that even though the paste containing ternary blended cements had higher amount of normalized CH than the one containing binary blended cements at 7 days of hydration, they had similar amount of CH per OPC at later ages. It indicates that the ternary blended cements consumed more CH than the binary blended cements. These observations highlight the possible synergetic effect between LP and NP or FA on the pore refinement of cement paste [62, 112, 163].

The cement composites incorporating with NP had the higher amount of CH per OPC relative the one with FA at all tested ages. Besides the reduction of CH in cement composite containing FA was more prominent than the one with NP.

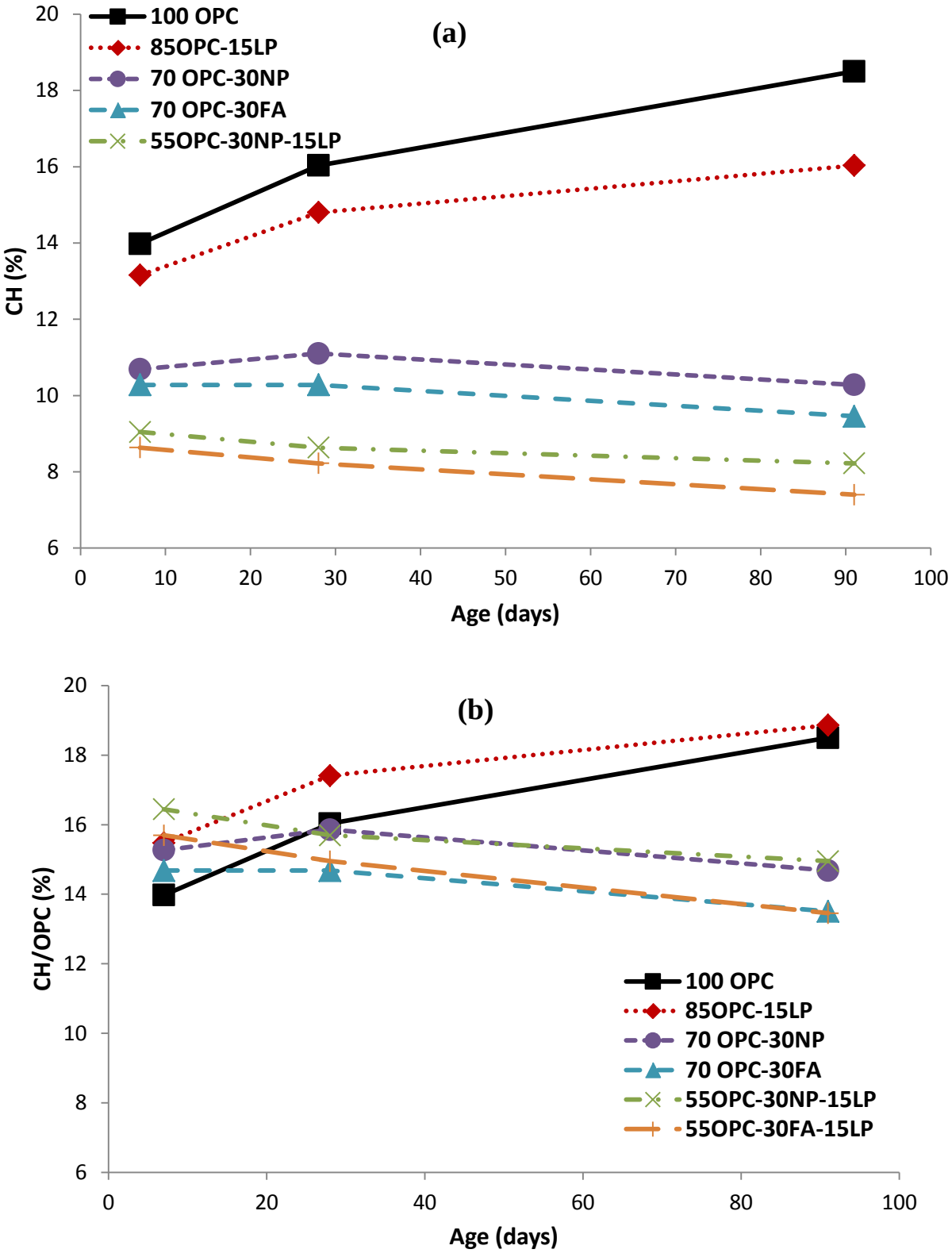

Figure 3.28 The calcium hydroxide contents (CH) (a) per binder (b) per OPC after 7, 28 and 91 days of hydration

Thermal analysis reveals the presence of calcite in all samples (Figure 3.29). The samples that did not contain limestone powder in the blended cements had less than 3% of calcite by weight, indicating the existence of negligible carbonation at all tested ages. The calcite content decreased with time in the cement composites incorporated with limestone powder. The reduction in the calcite content suggests that calcite from limestone was consumed with the reaction of aluminates resulted in the formation of calcium-carboaluminates [42, 43] which prevents the formation of monosulfate [164]. The amount of residual calcite in the cement composites containing natural pozzolan or fly ash was less than the one containing only OPC and LP. This can be attributed to the accelerated reaction of calcite with aluminate phases from natural pozzolan and fly ash. The residual mass fraction of calcite in the ternary cement pastes containing natural pozzolan and fly ash was 61% and 57%, respectively. It was calculated by dividing the mass fraction of calcite at the hydration of 7 days by the one at the hydration of 91 days. This indicates that fly ash containing mixtures consumed the greater amount of calcite relative to the one containing natural pozzolan.

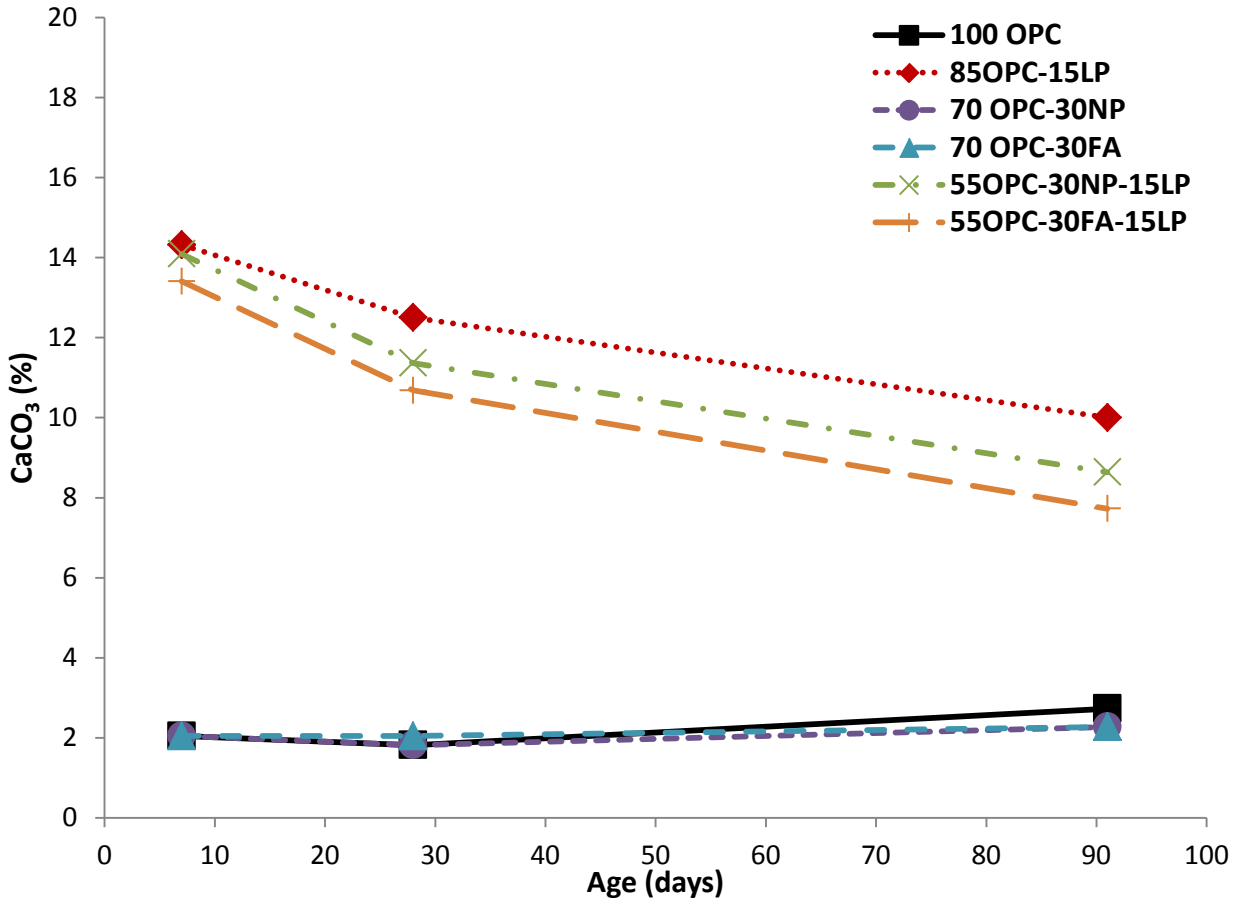

Figure 3.29 The calcium carbonate contents after 7, 28 and 91 days of hydration

3.3.3 Scanning Electron Microscope (SEM)

The dense opaque cementitious matrix of the *70OPC–30NP* concrete mix at one year hydration (Figure 2.4i) results from amorphous cementitious hydrates that surround partially-reacted NP particles (Figure 2.4d). Lava rock particles of NP generally remain dark and intact, suggesting that their fibro-palagonite ground mass (Figure 2.4f) has less pozzolanic reactivity with OPC than the gel-palagonite. The cementitious matrix of the *50OPC–50NP* mix contains a qualitatively greater proportion of unreacted gel- and fibro-palagonite particles than the *70OPC–30NP* mix, suggesting that the overall proportion of NP might be too high to produce optimal reaction with OPC and bonding, even after one year hydration. The *50OPC–50NP* mixture has lower compressive strength, higher water absorption, and greater chloride penetration compared with the *70OPC–30NP* mix.

Surface coatings of fluoroapatite, or calcium fluorophosphate ($Ca_5(PO_4)_3F$), in vesicles of the gel-palagonite particles (Figure 2) could possibly have had a positive influence on binding. Experimental tests of C_3S and C_3A hydration processes indicate that a phosphorous (P_2O_5) and fluorine (F^-) soaking solution reduced early exothermic heat release, and in small concentrations produced an interconnected and compact microstructure in C_3A cementitious hydrates, and a uniform and fine-grained microstructure in C_3S hydrates [165]. Secondary fluoroapatite is common in basaltic cinder deposits [88, 89], and easily identified with petrographic analysis in thin section even when not detectable through X-ray diffraction analyses.

Figure 3.30 gives examples of how cementitious hydrate compositions vary with proximity to the relicts of gel-palagonite in the *70OPC–30NP* concrete at the micrometer scale. The OPC bulk composition has calcium in much greater abundance than the basaltic ash, 62.9 vs. 8.9 wt.% CaO, respectively; the NP bulk composition has MgO, Na_2O, K_2O, TiO_2, and FeO_2 in far greated abundance than OPC (Table 2.2, Figure 3.31). Ratios of these cation abundances relative to aluminum and silicon measured in SEM-EDS analyses are plotted in atomic ratio scatter diagrams to provide qualitative illustrations of the incorporation of the chemical species of gel-palagonite in the cementitious binding phase. For example, the coarse silt-sized ash particle of Figure 3.30a has gel-palagonite groundmass and reaction rim with moderate Na+Mg+K+Ti+Fe/(Al+Si)=0.4 and low Ca/(Al+Si)=0.2, while the cementitious hydrates in the interfacial transition zone have higher Na+Mg+K+Ti+Fe/(Al+Si)=0.6–0.7, and moderate Ca/(Al+Si)=0.4–0.6. These compositions seem to reflect close interaction of the neighboring gel-palagonite with OPC pore solutions and incorporation of the dissolved species in alkali-rich cementitious hydrates. In contrast, cementitious hydrates 6–12 μm distant from the gel-palagonite have variable Na+Mg+K+Ti+Fe/(Al+Si)=0.25–0.40 and higher Ca/(Al+Si)=0.70–0.90, suggesting closer interaction with calcium-rich OPC pore solutions. Plagioclase feldspar in the same particle also reacts with OPC, to form hydrates with lower Na+Mg+K+Ti+Fe/(Al+Si)=0.20–0.25 and Ca/(Al+Si)=0.25–0.40 (Figure 3.30b). The poorly crystalline calcium-aluminum-silicate hydrate (C-A-S-H) in the cementitious matrix 2–5 μm distant has moderate Na+Mg+K+Ti+Fe/(Al+Si)=0.25–0.35, and higher Ca/(Al+Si)=0.70–0.85, which seems to reflect closer interaction with calcium-rich OPC pore solutions. Fibrous clusters in open pores (Figure 3.30c) have higher Na+Mg+K+Ti+Fe/(Al+Si)=0.6, and Ca/(Al+Si)=2.15–3.7, compared with C-A-S-H in the nearby cementitious matrix. These unusual compositions

may reflect relict cement grains that may have partially hydrated in alkaline pore fluids with high Na, Mg, Ti, and Fe derived from NP.

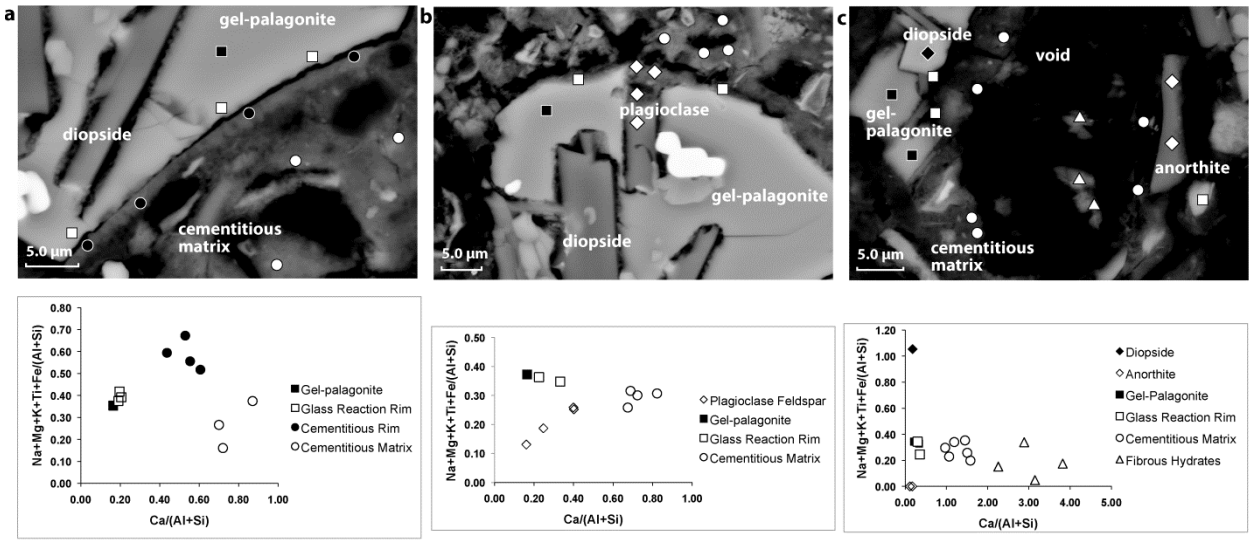

Figure 3.30 Reactive components of the basaltic ash and associated cementitious hydrates. Scanning electronic microscope, back-scattered electron images of basaltic ash-OPC reaction products, 5 µm scale bar.

Pozzolanic reaction is predominantly an attack on the SiO_2 or Al_2O_3–SiO_2 framework of a reactive material by OH- ions, so that silicate and other anions detach from the framework, and either remain in place or pass into solution [29, 166]. The early-formed, *in situ* product is likely to have K+ and Na+ as the predominant cations. Al^{+3} substitutes for Si^{+4} in tetrahedral sites, so C-A-S-H with low Ca/Si can absorb more Na^+ and K^+ in interlayer sites due to a valence compensation mechanism as well as increased silanol binding capacity [167]. The alkali-enriched cementitious products in the transition zone of Figure 3.30a thus provide an indication that the palagonitic glass is decomposing and releasing cations through pozzolanic reaction with OPC to form alkali-rich C-A-S-H. Farther from the pozzolanic glass, C-A-S-H in the cementitious matrix shows a range of compositions, for example, Ca/(Al+Si)=0.70-0.90 adjacent to pozzolanic glass (Figure 3.30a, b), and Ca/(Al+Si)=1.0–1.5 adjacent to a relict pore (Figure 3.30c).

Figure 3.31a summarizes the heterogeneous compositions of the Jabal Kadaha NP components and binding cementitious products in the *70OPC–30NP* and *50OPC–50NP* concretes at one year hydration. Unreacted volcanic ash components have Ca/Si<0.5, and Na+Mg+K+Ti+Fe cation concentrations that reflect gel-palagonite, fibro-palagonite, and diopside and plagioclase crystal compositions (Figure 3.31a). The compositions of gel-palagonite reaction rims and interfacial transition zones vary from about Na+Mg+K+Ti+Fe/(Al+Si)=0.2–0.7 and Ca/Si=0.2–0.8. This may reflect heterogeneous depletion of the gel-palagonite and local alkali enrichment in cementitious hydrates associated with pozzolanic reaction. The plot of Si/Ca and Al/Mg atomic ratios (Figure 3.31b) shows that there are no measurements of cementitious hydrate compositions that fall in the range of hydrotalcite compositions, Al/Mg=0.23–0.52, common in slag cement pastes [59]. Rather, the compositions seem to correspond to C-A-S-H with Al/Mg=1–5, Si/Ca=0.6–1.5 and Al/Ca=0.1–0.4 (Figures 3.31b, c), roughly similar to aluminous C-S-H

associated with slag cements [59]. Previous research has shown that adding aluminosilicate pozzolan to OPC lowers the mean Ca/Si ratio of C-S-H gel substantially below its typical value, about 1.7 [167]. Indeed, C-A-S-H in the cementitious matrix of the *50OPC–50NP* concrete mainly has lower Ca/(Al+Si)=0.6–1.0 than the *70OPC–30NP* concrete, with Ca/(Al+Si)=0.8–1.9 (Figure 3.31a). This suggests that a lower proportion of OPC leads to lower calcium concentrations overall. Alkali-cation concentrations in C-A-S-H range from about 0.2–0.5 (Figure 3.31a); these seem to be a function of proximity to gel-palagonite (Figure 3.30). C-A-S-H associated with the diverse reactive components of scoriacous volcanic ash in the monuments of ancient Rome and glassy pumiceous ash in ancient Roman seawater concretes, for example, also has a range of compositions [168, 169]. Laboratory experiments [167], have shown that the presence of Al enhances alkali binding in C-A-S-H, and inhomogeneous alkali sorption likely occurs in small clusters of C-A-S-H with low Ca/Si compositions similar to those observed here.

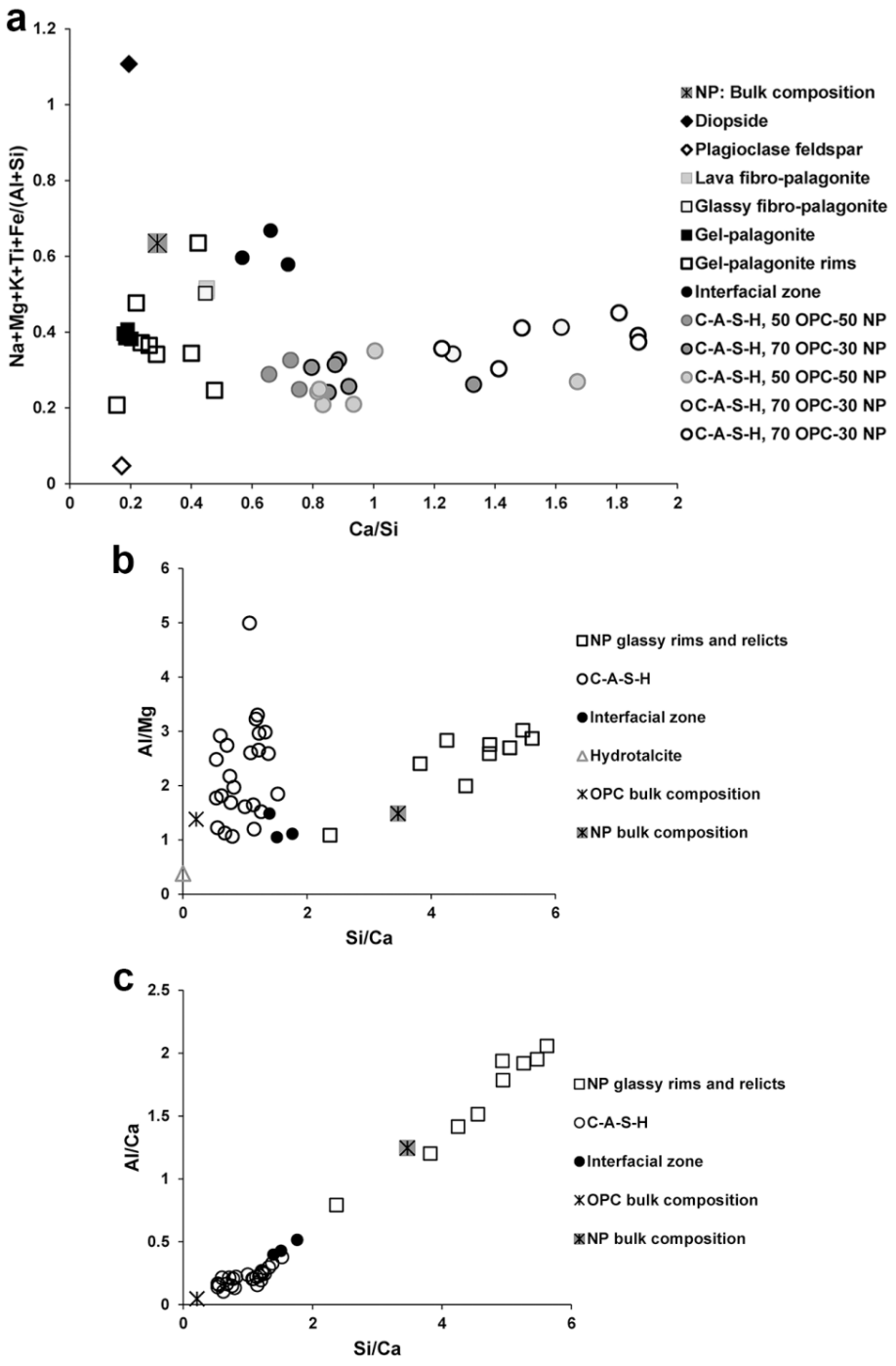

Figure 3.31 Compositional overview of the basaltic pozzolan and associated cementitious hydrates showing examples of (a) cation abundances and Ca/Si of the diverse components of NP, and the C–A–S–H binding phase, (b) Si/Ca and Al/Ca of NP gel-palagonite and the C–A–S–H binding phase, (c) Si/Ca and Al/Mg of NP gel-palagonite and the C–A–S–H binding phase. See Table 2.2 for XRF analyses of NP and OPC, calculated here as elemental percent. All other values are atomic ratios measured from SEM–EDS analyses.

The long-term strength of concretes fabricated with volcanic pozzolans presumably occurs through ongoing reaction of the volcanic ash in the presence of moisture to produce cementitious hydrates, long after OPC is consumed [30, 3]. In moist geologic environments gel-palagonite, the

principal pozzolanic component of Jabal Kadaha NP (Figures 2.1, 3.31), commonly reacts with ground and surface waters to produce natural zeolite mineral cements, which bind loose volcanic ash into a coherent rock called tuff [36]. A well-known example of this is the Tufo Lionato palagonitic tuff building stone of Rome, which developed natural zeolite cements within a mid-Pleistocene, and is the predominant decimeter-sized aggregate of the highly durable composite concretes of imperial age Roman monuments [168, 170]. Although the gel-palagonite of Jabal Kadaha cinder cone did not develop zeolitic alteration products in the arid environment of western Saudi Arabia, it is conceivable that in a humid concrete environment the gel-palagonite pozzolan could eventually produce secondary zeolitic cementitious hydrates. Ancient Roman pozzolanic harbor concretes, for example, developed zeolites in the pores of a pumiceous mortar while submerged in seawater [169]. Basaltic cinder cone fields occur throughout the world and their gel-palagonite component, detected through the petrographic analyses described in this study, could play an important role in enhancing the very long-term chemical and mechanical durability of environmentally-sustainable concretes, while substantially reducing CO_2 emissions associated with kiln-fired OPC.

3.4 Environmental Assessment

Estimated GWP (in CO_2-eq) and criteria air emissions associated with each concrete mixture incorporating with FA are shown in Table 3.11. The concrete containing NP was not included in this study since it was not obtained from the local sources. Calculations are obtained from the GreenConcrete LCA tool based on assumptions presented in Table 2.7 and Table 2.8.

For comparison purposes, typical ordinary Portland cement (OPC) concrete having a 28-day strength of 18, 30, and 60 MPa (low-strength, medium-strength, and high-strength, respectively) causes emissions of about 220, 300 and 440 kg CO_2/m^3, respectively. In comparison, all self-consolidating FA-LPC mixtures have a smaller cement content and therefore lower $CO_{2\text{-eq}}$ emissions than even the low-strength OPC concrete.

These estimates can be compared to typical SCC mixtures obtained from the literature [68, 73, 171, 172]. An example SCC, which used 30% silica fume (SF) and 10% FA, would result in higher CO_2 emissions than typical concrete mixtures. Because of the high volumes of SCMs in the mixture, it has similar estimated $CO_{2\text{-eq}}$ emissions (299 kg CO_2/m^3) compared to medium strength OPC concrete. This is still higher than the FA-LPC SCCs studied herein. Figure 3.32 shows strength versus GWP trends for the mixtures and compares average compressive strength (MPa) of the concrete mixtures over time (days). The red line shows the calculated total GWP for concrete production (kg $CO_{2\text{-eq}}$ / m^3 of concrete) and the blue line shows the contribution to the GWP of the Portland cement used in the mixtures. GWP increases with the quantity of Portland cement used in concrete mixture. Figure 3.33 shows the calculated intensity of CO_2-eq emissions per unit volume of concrete per 365-day compressive strength versus 365-day compressive strength for the concrete mixtures used in the study. The CO_2-eq intensity is considered a good measure of the impact of concrete use [173] because this indicator allows for the consideration of both performance (e.g., compressive strength) and contribution of concrete mixtures to GWP per unit volume and strength. For a given strength, lower CO_2-eq intensities are achieved by Portland cement being replaced with SCMs as observed in Figure 3.33. For example, at about 53 MPa strength, a 85wt.% OPC–15 wt.% limestone powder concrete mixture

produces 9.2 kg CO_2-eq.m^{-3}/MPa, while a 55 wt.%OPC–20 wt.% fly ash – 25 wt.% limestone powder mixture has a lower intensity, 6.1 kg CO_2-eq.m^{-3}/MPa. Therefore, for a given performance measure, with improvements in mixture design as well as selection of materials, it is possible to reduce the CO_2-eq intensity of concrete mixtures.

As shown in Table 3.11, similarly to GWP, criteria air emissions appear to increase with increase in Portland cement use, mostly because of fuel combustion during pyroprocessing. The CO emissions are the only exception, which appear higher for concrete mixtures with higher fly ash content. This is attributable to the natural gas, with a comparably higher CO emission factor, used for drying the fly ash.

Table 3.11 Material GWP, and criteria air pollutants

OPC–FA–LPC	CO_2-eq (kg /m^3)	CO (kg /m^3)	NO_X (kg /m^3)	PMtotal (kg /m^3)	SO_2 (kg /m^3)
100–0–0	5.69E+02	1.35E-01	2.99E+00	3.64E-01	1.35E+00
85–0–15	4.87E+02	1.26E-01	2.61E+00	3.09E-01	1.15E+00
75–0–25	4.34E+02	1.20E-01	2.36E+00	2.73E-01	1.03E+00
70–30–0	4.12E+02	1.49E-01	2.27E+00	2.62E-01	9.74E-01
50–50–0	3.11E+02	1.57E-01	1.82E+00	1.97E-01	7.31E-01
55–30–15	3.33E+02	1.39E-01	1.91E+00	2.09E-01	7.84E-01
45–40–15	2.82E+02	1.43E-01	1.68E+00	1.77E-01	6.63E-01
35–50–15	2.32E+02	1.47E-01	1.45E+00	1.44E-01	5.44E-01
25–60–15	1.83E+02	1.52E-01	1.23E+00	1.12E-01	4.27E-01
55–20–25	3.32E+02	1.29E-01	1.90E+00	2.07E-01	7.83E-01
45–30–25	2.81E+02	1.33E-01	1.67E+00	1.74E-01	6.61E-01
35–40–25	2.31E+02	1.38E-01	1.44E+00	1.42E-01	5.42E-01
25–50–25	1.82E+02	1.43E-01	1.22E+00	1.10E-01	4.26E-01

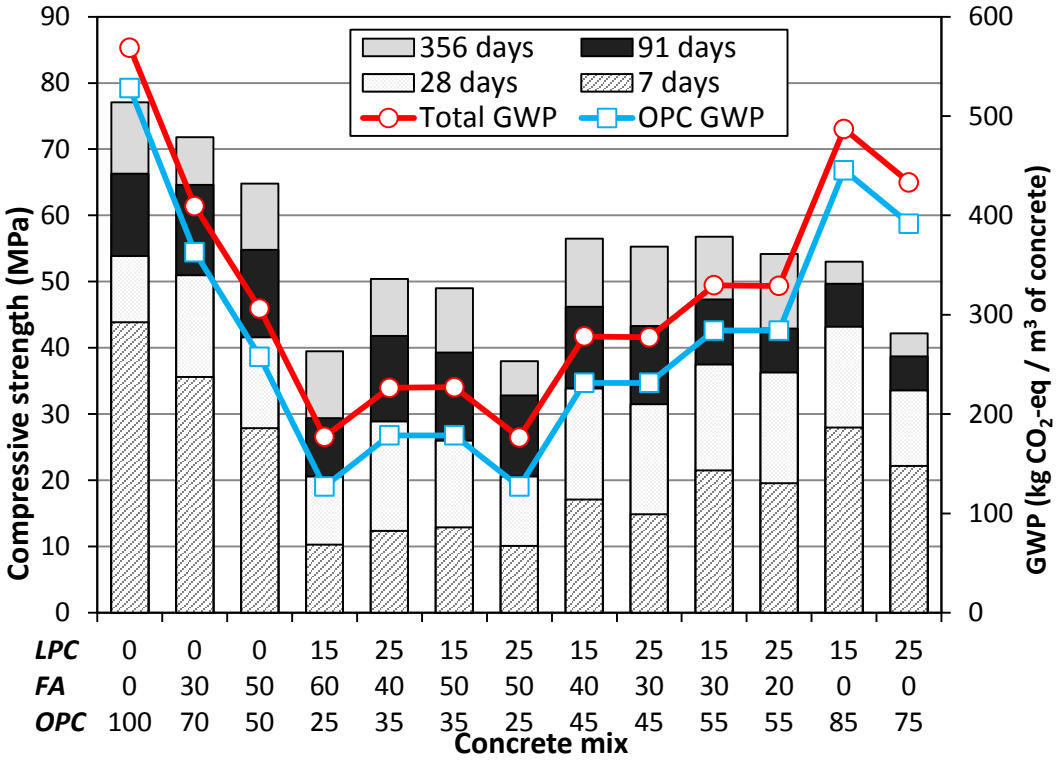

Figure 3.32 Comparison of average compressive strength (MPa) of the concrete mixtures over time (days). Red line shows the calculated total GWP for concrete production (kg CO2-eq / m3 of concrete). Blue line shows the contribution of the Portland cement used in the mixtures to the GWP.

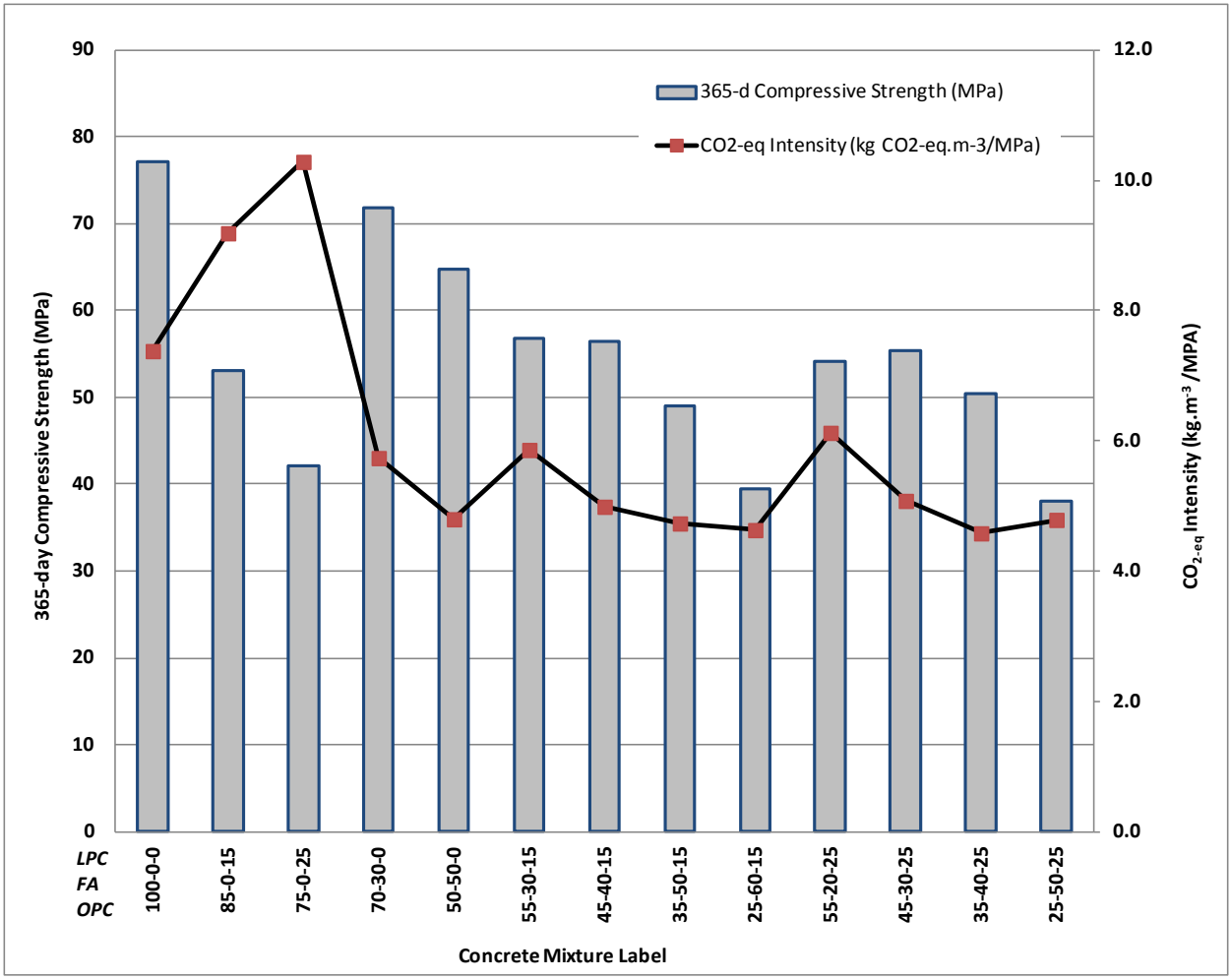

Figure 3.33 Comparison of 365-day compressive strength (MPa) of the studied concrete mixtures and $CO_{2\text{-eq}}$ intensity values

GWP by major concrete ingredients are investigated in further details through Figures 3.34 to 3.37. In Figure 3.34, total GWP for each of the concrete mixtures involve direct and supply-chain emissions from all the quarrying, production, and transportation processes taking place within the system boundary. With a total of about 570 kg of CO_2-eq, the concrete mixture with 100wt.% Portland cement (which is responsible for about 93% of the total) has the largest of GWP (see Figure 9 and Figure 10). With the decreasing amount of Portland cement and increasing amount of SCMs, e.g. for the *25OPC–60FA–15LPC* mixture, GWP from Portland cement can be as low as 69% of the total concrete production. Transportation of materials to the concrete batching plant is the second highest source of emissions, changing between 4% and 18% of the total depending on the amount of materials conveyed and transportation distance and mode (Figure 3.36). When we further examine the sources of the major GHG emissions from other non-cementitious ingredients, their mass contribution remains almost constant for all mixtures, about 4 kg for fine aggregates (1-2%), 4-5 kg for superplasticizers (1-2%), 3 kg for coarse aggregates (1%), and 1.5 kg for concrete mixing and batching activities (0.3-1%), as shown in Figure 3.36. Finally, Figure 3.37 summarizes the GWP from limestone production and fly ash preparation, which can be as high as 3% of the total for the mixture with highest cement replacement content, e.g., *25OPC–60FA–15LPC*. GWP from fly ash is found to be larger by a

factor of 5-10 for the same weight of limestone powder used in the mixture. This difference can be explained by the higher amount of fuel utilized per unit mass of fly ash during the drying process as part of treatment prior to mixing in the concrete [174].

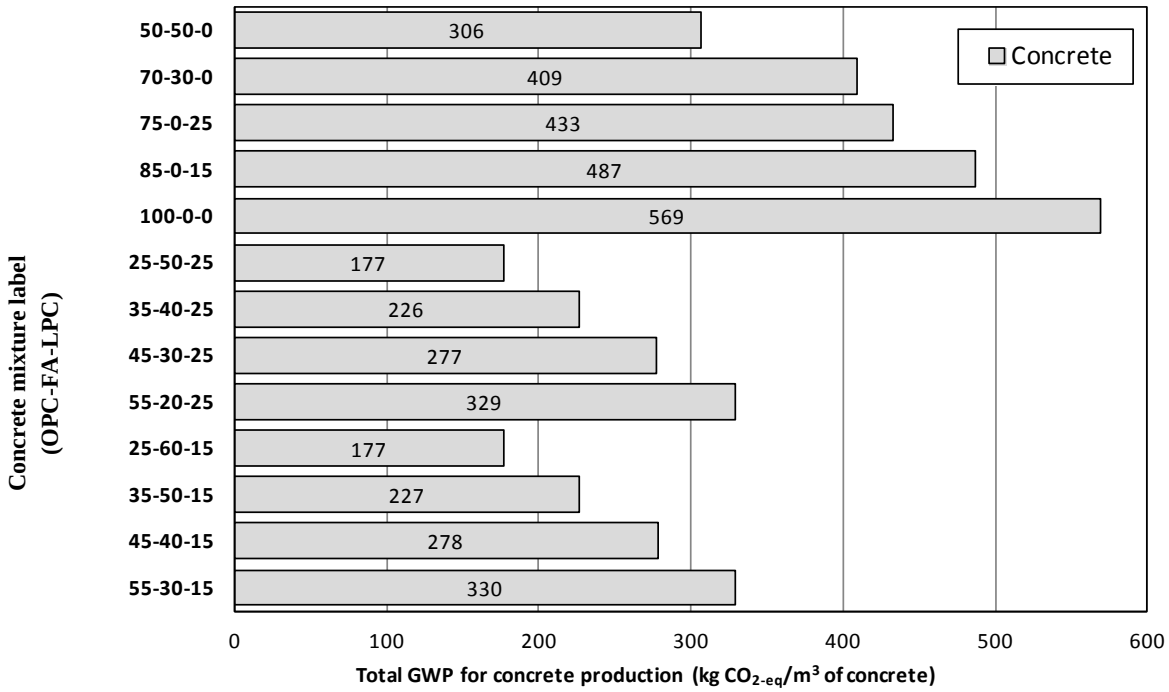

Figure 3.34 Comparison of total GWP for the studied concrete mixtures (kg CO_2-eq / m^3 of concrete)

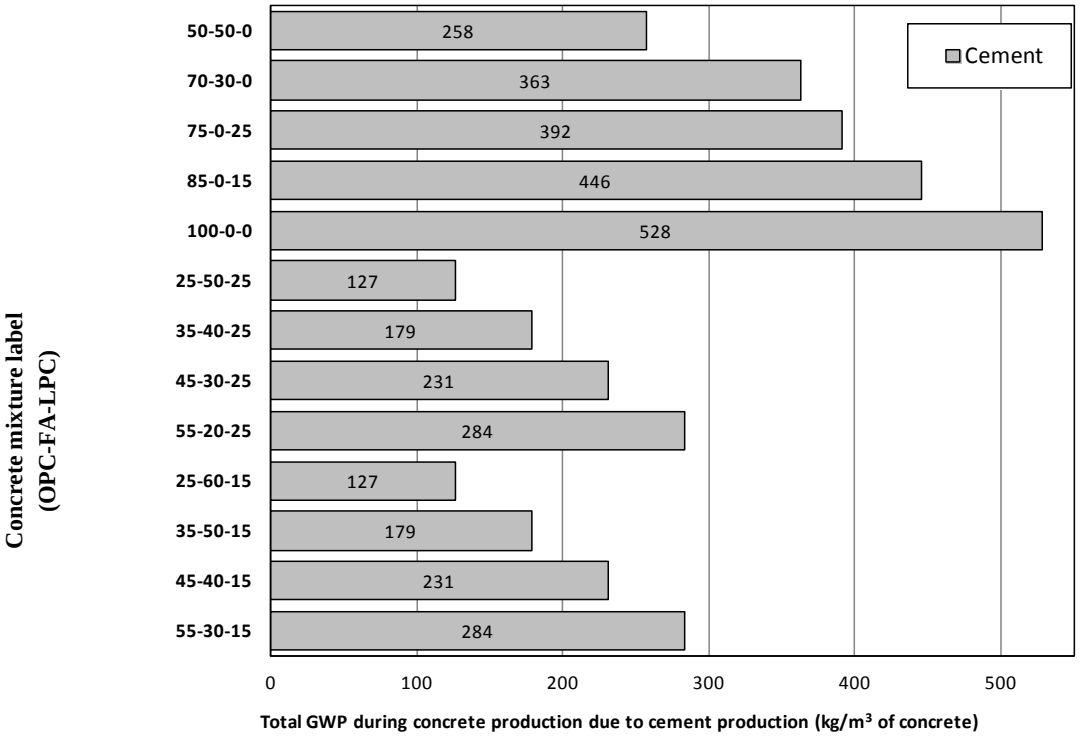

Figure 3.35 Comparison of GWP associated with cement production only (kg CO_2-eq / m^3 of concrete)

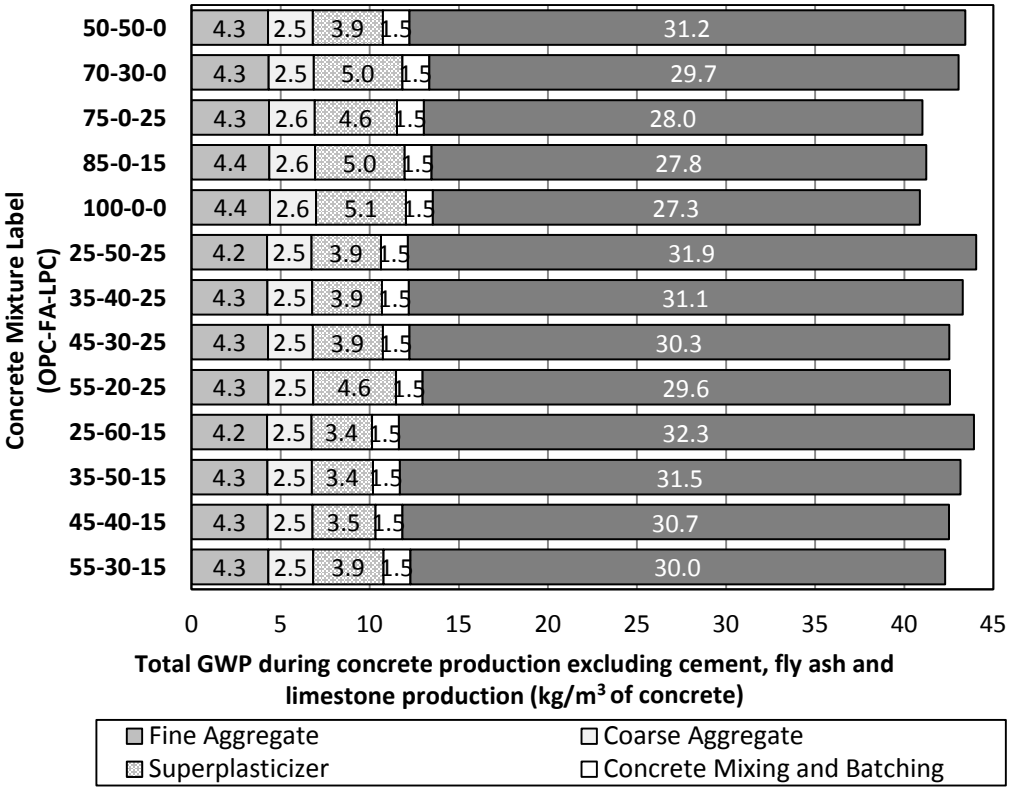

Figure 3.36 Total GWP associated with concrete production, excluding cement, fly ash and limestone production (kg CO_2-eq / m^3 of concrete)

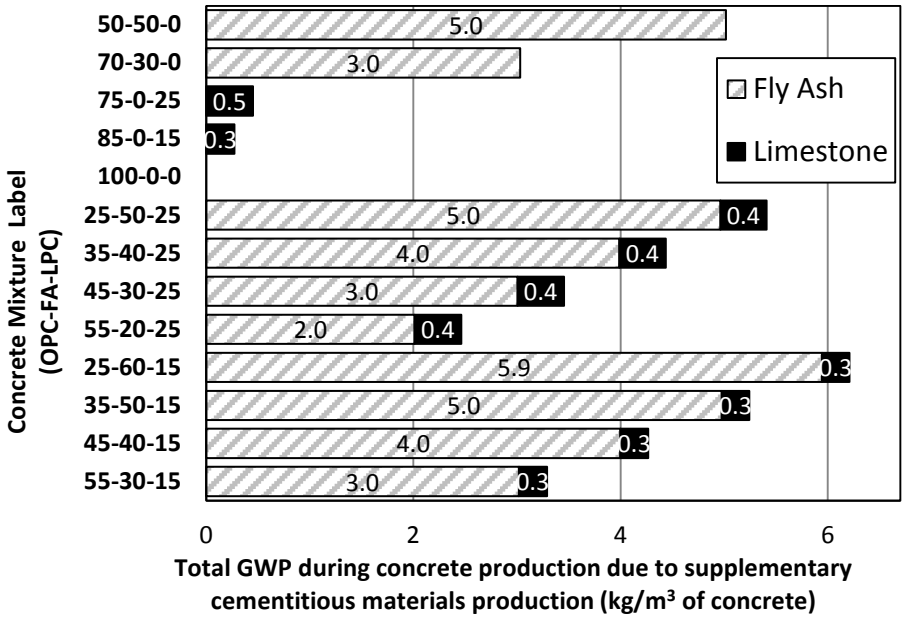

Figure 3.37 Total GWP associated with fly ash preparation and limestone production processes (kg CO2-eq / m3 of concrete)

4 Conclusion and future work

4.1 Conclusion

This study focuses on developing and characterization of SCC mixtures utilizing basaltic ash pozzolan (NP) or Class F-fly ash (FA) with limestone powder (LPC and LP). As an extension of this study, life-cycle assessment (LCA) was employed on the selected concrete mixtures for the detailed analysis and quantification of emissions and global warming potential (GWP) from the concrete production. The following observations can be made, from the obtained results for NP or FA incorporating mixtures:

Finely-ground natural basaltic ash pozzolan with or without finely-ground LPC provides an effective high volume substitute for up to 50% by weight OPC in experimental concretes with good workability, which satisfy self-compacting concrete criteria without costly viscosity-modifying admixtures. Petrographic and scanning electron microscopy studies of the finely–ground basaltic ash and *70OPC–30NP* and *50OPC–50NP* concretes indicate that resinous, yellow-brown gel-palagonite is the predominant pozzolanic component. Cementitious hydrates in the interfacial zone along the rims of gel-palagonite particles have Ca/(Al+Si)=0.4–0.6 and Na+Mg+K+Ti+Fe/(Al+Si)=0.6–0.7, which reflect the lower calcium and higher alkali concentrations of the reacting basaltic glass relative to OPC. The composition of C-A-S-H in the binding cementitious matrix vary from Ca/(Al+Si)=0.70–1.9, which seem to reflect relative proximity to partially reacted gel-palagonite particles and the proportion of NP in the cement mixture. A *70OPC–30NP* binary blend produced 28 day and later strengths of 54–73 MPa, similar to the *100OPC* control; the *50OPC–50NP* blend shows far lower strengths, 34–57 MPa, perhaps because the cementitious matrix contains a greater proportion of anhydrous phases, including unreacted NP grains. At 28 days, this mixture showed higher strength than the *45OPC–40NP–15LPC* ternary mixture, suggesting that the ternary system requires more time to develop cohesion in the hydrated cement paste than the binary system; both mixtures had similar strengths at strengths at 90 days and one year, 43 MPa and 57 MPa, respectively. The performance of the *50OPC–50NP* mixture with basaltic ash pozzolan is quite similar to concretes blended with 50 wt.% natural zeolite or volcanic tuff replacement of OPC [60], in terms of both early and ultimate strength at 180 days hydration.

The use of 15 wt.% LPC particles with 48 μm median diameter produced lower strength at early and ultimate ages in both the binary and ternary mixtures relative to the pure OPC control. A similar study [40] demonstrated that the replacement of 10 wt.% OPC by LPC with a fine (16 μm median diameter) and a coarse (80 μm median diameter) particle size in binary mixtures with w/c of 0.35 also produced lower strength. In comparison, intergrinding Portland clinker and limestone generates a finer LPC particle size [175]. The resulting binary mortar mixture with 10 and 20 wt.% LPC replacement also had slightly lower strength than that of an OPC control at 7 days and 28 days. This suggests that incorporation of LPC leads to slightly lower strength, overall.

All the binary and ternary blended mixtures produced higher resistance to chloride penetration than the *100OPC* and *85OPC–15LPC* reference mixtures, as has been shown for many blended pozzolanic concretes [135, 136, 176]. This may be related to pore refinement through pozzolanic

cementitious processes and the latent hydraulic properties of NP and LPC [166]. Greater than 55% OPC replacement in the ternary mixtures resulted in higher water absorption. This could be associated with a higher volume of capillary voids, related to the vesicularity and higher water absorption capacity of the basaltic ash, coupled with the dilution effect of LPC and unreacted NP on cementitious processes associated with OPC hydration.

Overall, the *55OPC–30NP–15LPC* blend produces a low-cost and environment-friendly concrete that does not require calcining of NP or LPC with OPC and would reduce CO_2 emissions 48% compared with the *100OPC* control, while providing higher ultimate strength and resistance to chloride penetration, and an aluminous cementitious system associated with basaltic glass-OPC reactions.

It is also concluded that without the use of any viscosity modifying admixtures, self-consolidating concrete mixtures can be produced with cement, high-volume fly ash, limestone powder, high ratio of the aggregate to cementing powders, and a low dose of superplasticisers.

A wide range of early and long term strengths were attainable depending on the selected mixture proportion. The rate of strength gain increased with increasing fly ash content, and it was observed that for 25% limestone powder, the mixture with 20% fly ash exceeded the strength of the control mixture that contains only 25% limestone powder by 28 days. The mixture with 30% fly ash performed similarly but by 91 days. This means that the synergistic effect between limestone powder and fly ash leads to strength gain with increasing curing time. Similar but less pronounced the rate of strength gain was observed either with 15% limestone and fly ash mixtures or zero limestone and fly ash mixtures. Concrete mixtures with 50% or less supplementary cementing materials attained 30 MPa of compressive strength by 28 days, and all concrete mixtures attained 30 MPa by 91 days.

The binary and ternary mixtures with fly ash or fly ash and limestone powder were resulted in higher resistance to chloride penetration compared to *100OPC*, *85OPC–15LPC*, and *75OPC–25LPC* control mixtures. The binary mixtures and ternary mixtures with 25% LPC produced lower water absorption capacity than the reference mixtures of *100OPC* and *75OPC–25LPC*, respectively. However, the greater than 45% fly ash and LPC addition in the ternary mixtures that contains 15% LPC demonstrated higher water absorption than *85OPC–15LPC* control mixture.

It is worth to note that an additional benefit of using large amount of supplementary cementitious materials in the reduction of heat of hydration [153] is not tested in this study. The reduction of heat of hydration could be resulted in higher strength and durability performance for concrete with high-cement content and concrete members with large size (i.e., foundations, piers, and dams).

In the binary mixtures, the increased amount of NP/FA used as OPC replacement resulted in either decreased superplasticizer content or T_{50} times suggesting that both NP and FA might increase the flowability of concrete mixtures.

The *70OPC–30NP* blend resulted in 12%, 6%, 2% higher strength than the *70OPC–30FA* mixture at the age of seven-, 28- and 91-days, respectively. The *50OPC–50NP*, however, showed 18% and 12% lower strength than the *50OPC–50FA* at 28- and 91-days, correspondingly.

Among the ternary mixtures, *55OPC–30NP–15LPC* mixture had higher strength, while *45OPC–40NP–15LPC* and *35OPC–50NP–15LPC* mixtures had lower strength when compared to the corresponding mixtures with FA.

In general, the mixtures with FA or FA–LPC demonstrated higher chloride migration resistance compared to the ones with NP or NP–LPC with the exception of *55OPC–30FA–15LPC* which showed slightly lower resistance to chloride migration at one year.

The water demand of NP blended specimens was higher than the one with FA for desired normal consistency, while setting time of NP was lower than FA. This could be attributed the consistency loss due to higher water absorption capacity of NP particles.

In general all binary and ternary FA samples had higher strength than NP mortar samples up to 1 year. This suggests that the pozzolanic activity of FA is higher than NP which is supported by XRD, IC and TGA analysis.

It is important to note here that LP and FA led to produce the blended mortars with higher compressive strength than the control specimen with 15%LP replacement. This can be associated with the synergistic effect between FA and LP. This hypothesis agreed well with the complimentary XRD, IC, and TGA results of this study.

The substitution of basaltic ash pozzolan or Class F-fly ash by themselves or along with limestone powder in ordinary Portland cement has a substantial impact on the kinetics and products of hydration reaction of binary and ternary mixtures. The addition of limestone powder increased the rate of hydration reaction relative to the control *100OPC* as it was observed in isothermal calorimetry analysis. It was also detected that the hydration products were enhanced due to the further participation of aluminate phases in hydration reaction which is also confirmed with XRD results by the observations of hemi-carboaluminate and mono-carboaluminate. In addition, TGA analysis showed that the amount of hydration products per OPC increased in *85OPC–15LP* relative to the control *100OPC*, indicating the enhancement of hydration reaction possibly due to the filler effect and reaction of LP with aluminate phases. It is important to note that the improvement of hydration reaction was not sufficient to compensate for the dilution effect, since the hydration products per binder of *85OPC–15LP* was less than *100OPC*. Even though the presence of FA in binary and ternary mixtures retarded the acceleration of hydration reaction compared to the one of NP in the beginning of reaction, the reactivity of FA increased after 2 days and exceeded the cumulative heat of NP equivalents (Fig. 3.24b). This result is supported by TGA analysis in Fig.3.27 for the binary and ternary mixtures showing that the samples containing FA had greater amount of hydrate water relative to the one with NP. Addition of limestone powder in the ternary cement of *55OPC–30NP–15LP* and *55OPC–30FA–15LP* resulted in stabilization of the transformation of ettringite to monosulfate and introduction carboaluminates into the hydration product. This result can be associated with higher resistance to chloride migration of the ternary mixtures (*55OPC–30NP/FA–15LP* and *45OPC–40NP/FA–15LP*) to the equivalent binary mixtures (*50OPC–50NP/FA*).

The TGA results show the degree of reaction of NP and FA. In both NP and FA containing samples that had binary and ternary mixtures, calcium hydroxide was consumed due to the pozzolanic reaction. The degree of pozzolanic reaction was greater for the FA–containing binary and ternary mixtures than the one of NP. This result complies with XRD analyses and the strength development of the mortar samples in Fig.3.18 where the FA containing samples produced higher strength than the NP containing samples overtime.

GHG emissions and the analyzed criteria air pollutants were in all cases similar to or lower than emissions from typical ordinary Portland cement concrete. The only exception was CO emissions, which were estimated to be slightly higher for mixtures with higher fly ash content due to the use of natural gas in drying the fly ash prior to use in concrete. Regarding GHG emissions from other non-cementitious ingredients, their mass contribution remains almost constant for all mixtures. The GWP from fly ash is found to be 5-10 times greater for the same weight of limestone powder used in the mixture. This difference can be explained by the higher amount of fuel utilized per unit mass of fly ash handled during the drying process as part of treatment prior to mixing into the concrete.

4.2 Future work

Based on the results of this dissertation, following studies are recommended;

The present research studied qualitative XRD analyses on the binary and ternary mixtures containing basaltic ash pozzolan, Class F-fly ash and limestone powder. It is worth to perform Rietveld refinement on the results to quantify the phases of hydration products.

To investigate porosity and tortuosity of the cement paste and mortar samples, non-destructive test techniques should be used e.g. micro-computed and nano-computed tomography.

The pozzolanic activity of FA is greater than NP which is supported by XRD and TGA analysis. However, further investigation is recommended by SEM technique on the FA containing sample to have better insight of this phenomenon.

To improve the reactivity of NP, FA and LP, SCMs can be treated by calcination, acid treatment, cation exchange and further grinding.

Lastly, to compare the GHG emissions and GWP of concrete containing NP to the one of containing FA, LCA method should be employed on the production of NP containing concrete where both material locally available.

References

[1] WBCSD-CSI, Recycling Concrete, in: H. Klee (Ed.), Geneva, Switzerland, 2009, pp. 1-42.
[2] USGS, Cement - Mineral Commodity Summaries, in: Cement Statistics and Information - Annual Publications, U.S. Department of the Interior, U.S. Geological Survey, 2011.
[3] P.K. Mehta, P.J.M. Monteiro, Concrete: Microstructure, Properties, and Materials, 4th Edition ed., McGraw-Hill, USA, 2014.
[4] P.K. Mehta, Reducing the Environmental Impact of Concrete, Concrete International, 23 (2001) 61-66.
[5] W.B.C.f.S.D. (WBCSD-CSI), Cement Industry Energy and CO_2 Performance "Getting the Numbers Right", in, Washington DC, 2009.
[6] IEA-WBCSD, Cement Technology Roadmap 2009 - Carbon emissions reductions up to 2050, in, 2009.
[7] M.L. Marceau, M.A. Nisbet, M.G. VanGeem, Life Cycle Inventory of Portland Cement Manufacture, in, Portland Cement Association [PCA], Skokie, IL, 2006.
[8] C.G.C.M.U.G.D. Institute), Economic input–output life cycle assessment (EIO-LCA), US 1997 industry benchmark model, in, 2008.
[9] C.D. Tomkins, Redefining What's Possible for Clean Energy by 2020, in, Gigaton Throwdown, San Francisco, 2009.
[10] P.K. Mehta, Global Concrete Industry Sustainability: Tools for Moving Forward to Cut Carbon Emissions, Concrete International, (2009) 45-48.
[11] P.K. Mehta, Sustainable Cements and Concrete for the Climate Change Era – A Review, in: P.C. Zachar, T R Naik, E Ganjian (Ed.) Second International Conference on Sustainable Construction Materials and Technologies, Coventry University and The University of Wisconsin Milwaukee Centre for By-products Utilization, Italy, 2010.
[12] H.G.v. Oss, Slag—Iron and Steel, in: 2011 Minerals Yearbook, U.S. Geological Survey, Washington DC, 2013.
[13] ASTM, C125-15 Standard Terminology Relating to Concrete and Concrete Aggregates, in, 2015.
[14] ASTM, C618-12a Standard Specification for Coal Fly Ash and Raw or Calcined Natural Pozzolan for Use in Concrete, in, 2013.
[15] R. Taylor, Characterization of C-S-H in early and late age systems containing admixtures in: School of Civil Engineering, The University of Leeds, 2010.
[16] R.J. Lauf, Microstructure of coal fly ash particles, Ceramic Bulletin, 61 (1982) 487-490.
[17] P.K. Kolay, D.N. Singh, Physical, chemical, mineralogical, and thermal properties of cenospheres from an ash lagoon, Cement & Concrete Research, 31 (2001) 539-542.
[18] Vanessa Rheinheimer, Yunpeng Wu, Tao Wu, Rae Taylor, Kemal Celik, Junyan Wang, Min-Hong Zhang, Peter Wriggers, P.J.M. Monteiro, Multi-scale Study of High Strength Low Thermal Conductivity Cementitious Materials with Cenospheres, in, Department of Civil and Environmental Engineering, University of California, Berkeley, 2015.
[19] P.K. Mehta, Pozzolanic and Cementitious Byproducts as Mineral Admixtures for Concrete - A Critical Review, Special Publication, 79 (1983).
[20] Y. Halse, H.U. Jensen, P.L. Prett, Development of Microstructure and other properties in flyash OPC systems, Cement & Concrete Research, 14 (1984) 491.

[21] J.C. Hower, R.F. Rathbone, J.D. Robertson, G. Peterson, A.S. Trimble, Petrology, mineralogy and chemistryof magnetically-separated size fly ash, Fuel, 78 (1999) 197-203.
[22] S. Gomes, M. Francois, M. Abdelmoula, P. Refait, C. Pellisier, O. Evrard, Characterization of magntite in silico-aluminous fly-ashby SEM, TEM, XRD, magnetic susceptibility, and Mössbauer spectroscopy., Cement and Concrete Research, 29 (1999) 1705-1711.
[23] H. Uchikawa, Effect of blending compenents on hydration and structure formation, in: 8th ICCC, Rio de Janeriro, Brasil, 1986, pp. 249-280.
[24] R. Helmuth, Fly Ash in Cement and Concrete, Portland Cement Association, Skokie, Illinois, 1987.
[25] S. Goni, M.P. Lorenzo, A. Guerrero, M.S. Hernandez, Calcium hydroxide saturation factors in the pore soultion of hydrate Portland cement fly ash pastes, Journal of American Ceramic Society, 79 (1996) 1041-1046.
[26] R. Kovács, Effect of the hydration products on the properties of fly-ash cements, Cement and Concrete Research, 5 (1975) 73-82.
[27] X. Fu, Z. Wang, W. Tao, C. Yang, W. Hou, Y. Dong, X. Wu, Studies on blended cement with a large amount of fly ash, Cement and Concrete Research, 32 (2002) 1153-1159.
[28] A.V. Girao, Morphology and nanostructure C-S-H in white Portland cement-fly ash hydrated at 85°C Advances in Applied Ceramics, 106 (2007) 283-293.
[29] F. Massazza, Pozzolana and pozzolanic cements, in: P.C. Hewlett (Ed.) Lea's Chemistry of Cement and Concrete, Elsevier Ltd., London, 1998, pp. 471-632.
[30] G. Habert, N. Choupay, J. Montel, D. Guillaume, G. Escadeillas, Effects of the secondary minerals of the natural pozzolans on their pozzolanic activity, Cem Concr Res, 38 (2008) 963-975.
[31] R. Snelling, G. Mertens, J. Elsen, Supplementary Cementitious Materials, Reviews in Mineralogy and Geochemistry, 74 (2012) 211-278.
[32] M. Jackson, D. Deocampo, F. Marra, B. Scheetz, Mid-Pleistocene pozzolanic volcanic ash in ancient Roman concretes, Geoarchaeology, 25 (2010) 36-74.
[33] A.A. Sabtan, W.M. Shehata, Evaluation of engineering properties of scoria in central Harrat Rahat, Saudi Arabia, Bulletin of Engineering Geology and the Environment, 59 (2000) 219-225.
[34] M.J. Roobol, J.J. Pint, M.A. Al-Shanti, A.J. Al-Juaid, S.A. Al-Amoudi, S. Pint, Preliminary Survey for Lava-Tube Caves on Harrat Kishb, Kingdom of Saudi Arabia, in, Saudi Geological Survey, Jeddah, Kingdom of Saudi Arabia, 2002, pp. 1-46.
[35] M.R. Moufti, A.A. Sabtan, O.R. El-Mahdy, W.M. Shehata, Assessment of the industrial utilization of scoria materials in central Harrat Rahat, Saudi Arabia, Engineering Geology, 57 (2000) 155-162.
[36] M.I. Khan, A.M. Alhozaimy, Properties of natural pozzolan and its potential utilization in environmental friendly concrete, Canadian Journal of Civil Engineering, 38 (2011) 71-78.
[37] P.D. Tennis, M.D.A. Thomas, W.J. Weiss, State-of-the-Art Report on Use of Limestone in Cements at Levels of up to 15%, in, Portland Cement Association, 2011.
[38] T. Matschei, B. Lothenbach, F.P. Glasser, The role of calcium carbonate in cement hydration, Cem Concr Res, 37 (2007) 551-558.
[39] A.-M. Poppe, G. De Schutter, Cement hydration in the presence of high filler contents, Cem Concr Res, 35 (2005) 2290-2299.
[40] D.P. Bentz, E.F. Irassar, B.E. Bucher, W.J. Weiss, Limestone Fillers Conserve Cement Part 2: Durability issues and the effects of limestone fineness on mixtures, Concr Int, December (2009) 35-39.

[41] R.D. Hooton, M. Nokken, T. M.D.A., Portland-Limestone Cement: State-of-the-Art Report and Gap Analysis for CSA A 3000, in, University of Toronto, Ontairo, 2007.
[42] A. Ipavec, R. Gabrovšek, T. Vuk, V. Kaučič, J. Maček, A. Meden, Carboaluminate Phases Formation During the Hydration of Calcite-Containing Portland Cement, Journal of the American Ceramic Society, 94 (2011) 1238-1242.
[43] B. Lothenbach, G. Le Saout, E. Gallucci, K. Scrivener, Influence of Limestone on the Hydration of Portland Cements, Cem Concr Res, 38 (2008) 848-860.
[44] V. Bonavetti, H. Donza, V. Rahhal, E. Irassar, Influence of initial curing on the properties of concrete containing limestone blended cement, Cement and Concrete Research, 30 (2000) 703-708.
[45] P. Hawkins, P. Tennis, R. Detwiler, The Use of Limestone in Portland Cement- A State-of-the-Art Review, in, Portland Cement Association, Skokie, Illinois, USA, 2003.
[46] G. Kakali, S. Tsivilis, E. Aggeli, M. Bati, Hydration products of C3A, C3S and Portland cement in the presence of CaCO3, Cem Concr Res, 30 (2000) 1073-1077.
[47] J. Péra, S. Husson, B. Guilhot, Influence of finely ground limestone on cement hydration, Cem Concr Compos, 21 (1999) 99-105.
[48] V. Bonavetti, H. Donza, G. Menéndez, O. Cabrera, E.F. Irassar, Limestone filler cement in low w/c concrete: A rational use of energy, Cem Concr Res, 33 (2003) 865-871.
[49] B. Lothenbach, G. Le Saout, E. Gallucci, K. Scrivener, Influence of limestone on the hydration of Portland cements, Cement and Concrete Research, 38 (2008) 848-860.
[50] D.P. Bentz, E.F. Irassar, B.E. Bucher, J. Weiss, Limestone Fillers Conserve Cement Part 1: An analysis based on Powers' model, Concr Int, (2009).
[51] Y. Benachour, C.A. Davy, F. Skoczylas, H. Houari, Effect of a high calcite filler addition upon microstructural, mechanical, shrinkage and transport properties of a mortar, Cem Concr Res, 38 (2008) 727-736.
[52] R. Dhir, M. Limbachiya, M. McCarthy, A. Chaipanich, Evaluation of Portland limestone cements for use in concrete construction, Materials and Structures, 40 (2007) 459-473.
[53] V.M. Malhotra, High-Performance High-Volume Fly Ash Concrete, Concrete International, 24 (2002) 30-34.
[54] P.K. Mehta, D. Manmohan, Sustainable High-Performance Concrete Structures, Concrete International, 28 (2006) 37-42.
[55] V.M. Malhotra, P.K. Mehta, High-Performance, High-Volume Fly Ash Concrete for Building Durable and Sustainable Structures 4th edition ed., Supplementary Cementing Materials for Sustainable Development, 2012.
[56] P.K. Mehta, Sustainable Concrete Industry in the Era of Unpredictable Wheather Extremes and Exponentially Rising Cement Production, in: V.M. Malhotra (Ed.) Thirteenth International Conference on Recent Advances in Concrete Technology and Sustainability Issues, Committee for Organization of International Conferences, Ottowa, Canada, 2015.
[57] L. Gurney, D. Bentz, T. Sato, W. Weiss, Reducing Set Retardation in High-Volume Fly Ash Mixtures with the Use of Limestone, Transportation Research Record: Journal of the Transportation Research Board, 2290 (2012) 139-146.
[58] D.P. Bentz, T. Sato, I. de la Varga, W.J. Weiss, Fine limestone additions to regulate setting in high volume fly ash mixtures, Cement and Concrete Composites, 34 (2012) 11-17.
[59] K. Celik, C. Meral, A. Petek Gursel, P.K. Mehta, A. Horvath, P.J.M. Monteiro, Mechanical properties, durability, and life-cycle assessment of self-consolidating concrete mixtures made

with blended portland cements containing fly ash and limestone powder, Cement and Concrete Composites, 56 (2015) 59-72.
[60] B. Uzal, L. Turanli, P.K. Mehta, High-Volume Natural Pozzolan Concrete for Structural Applications, ACI Mater J, 104 (2007) 535–538.
[61] P. Pipilikaki, M. Katsioti, Study of the hydration process of quaternary blended cements and durability of the produced mortars and concretes, Constr Build Mater, 23 (2009) 2246-2250.
[62] K. De Weerdt, K.O. Kjellsen, E. Sellevold, H. Justnes, Synergy between fly ash and limestone powder in ternary cements, Cem Concr Compos, 33 (2011) 30-38.
[63] S.D. Hwang, K.H. Khayat, O. Bonneau, Performance-Based Specifications of Self-Consolidating Concrete Used in Structural Applications, ACI Mater J, 103 (2006) 121-129.
[64] K.H. Khayat, Workability, Testing, and Performance of Self-Consolidating Concrete, Materials Journal, 96 (1999) 346-353.
[65] H. Okamura, M. Ouchi, Self-Compacting Concrete, Journal of Advanced Concrete Technology, 1 (2003) 5-15.
[66] I. Afshoon, Y. Sharifi, Ground copper slag as a supplementary cementing material and its influence on the fresh properties of self-consolidating concrete, The IES Journal Part A: Civil & Structural Engineering, 7 (2014) 229-242.
[67] B. Safi, A. Benmounah, M. Saidi, D. Aboutaleb, Effect of Calcined Silt on the Rheological Behavior of Cement Pastes of the Self Compacting Concrete SCC, European Journal of Scientific Research, 40 (2010) 287-296.
[68] A.W. Saak, H.M. Jennings, S.P. Shah, New Methodology For Designing Self-Compacting Concrete, ACI Materials Journal, 98 (2001) 429-439.
[69] Y.A. Van K. Bui, P.S. Surendra, Rheological Model for Self-Consolidating Concrete, Materials Journal, 99 (2002).
[70] D. Feys, K.H. Khayat, A. Perez-Schell, R. Khatib, Development of a tribometer to characterize lubrication layer properties of self-consolidating concrete, Cement and Concrete Composites, 54 (2014) 40-52.
[71] B. Esmaeilkhanian, K. Khayat, A. Yahia, D. Feys, Effects of mix design parameters and rheological properties on dynamic stability of self-consolidating concrete, Cement and Concrete Composites, 54 (2014) 21-28.
[72] K.M. K. H. Khayat, and A. Trudel, In Situ Mechanical Properties of Wall Elements Cast Using Self-consolidating Concrete, Materials Journal, 94 (1997) 492-500.
[73] M. Ouchi, S. Nakamura, T. Osterson, S. Hallberg, M. Lwin, Applications of Self-Compacting Concrete in Japan, Europe and the United States, in: International Symposium on High Performance Concrete, Orlando, FL, 2003, pp. 20.
[74] A.W.J. Saak, H.M.; Shah,S.P., A, A generalized approach for the determination of yield stress by slump and slump flow, Cement and Concrete Research, 34 (2004) 363-371.
[75] G. Le Saoût, V. Kocaba, K. Scrivener, Application of the Rietveld method to the analysis of anhydrous cement, Cement and Concrete Research, 41 (2011) 133-148.
[76] C.W. Hargis, J. Moon, B. Lothenbach, F. Winnefeld, H.-R. Wenk, P.J.M. Monteiro, Calcium Sulfoaluminate Sodalite (Ca4Al6O12SO4) Crystal Structure Evaluation and Bulk Modulus Determination, Journal of the American Ceramic Society, (2013) n/a-n/a.
[77] A.P. Gursel, A. Horvath, GreenConcrete LCA Tool, in, University of California, Berkeley, Berkeley, CA, 2012.
[78] G. Rebitzer, T. Ekvall, R. Frischknecht, D. Hunkeler, G. Norris, T. Rydberg, W.P. Schmidt, S. Suh, B.P. Weidema, D.W. Pennington, Life cycle assessment: Part 1: Framework, goal and

scope definition, inventory analysis, and applications, Environment International, 30 (2004) 701-720.
[79] K. Celik, M.D. Jackson, M. Mancio, C. Meral, A.H. Emwas, P.K. Mehta, P.J.M. Monteiro, High-volume natural volcanic pozzolan and limestone powder as partial replacements for portland cement in self-compacting and sustainable concrete, Cement and Concrete Composites, 45 (2014) 136-147.
[80] ASTM, C778 – 12 Standard Specification for Standard Sand, in, 2012.
[81] Pallister J.S., M. W.A., Jonsson S., Lu Z., Zahran H.M., Hadidy S. E., Aburukbah A., Stewart I. C. F., Lundgren P.R., White R. A., Moufti M.R.H., Broad accommodation of rift-related extension recorded by dyke intrusion in Saudi Arabia, Nature Geosci, 3 (2010) 705-712.
[82] C. Meral, C.J. Benmore, P.J.M. Monteiro, The study of disorder and nanocrystallinity in C–S–H, supplementary cementitious materials and geopolymers using pair distribution function analysis, Cement and Concrete Research, 41 (2011) 696-710.
[83] S.A. Bilgrami, Serpentinite-limestone contact at Taleri Mohammad Jan, Zhob Valley, , West Pakistan, The American Mineralogist, 45 (1960) 1008-1019.
[84] D.N. Lumsden, Discrepancy between thin-section and X-ray estimates of dolomite in limestone, Journal of Sedimentary Research, 49 (1979) 429-435.
[85] G. Durn, F. Ottner, D. Slovenec, Mineralogical and geochemical indicators of the polygenetic nature of terra rossa in Istria, Croatia, Geoderma, 91 (1999) 125-150.
[86] H.-A. Wenk, A.G. Bulakh, Minerals, their constitution and origin, Cambridge University Press, Cambridge, 2009.
[87] N. Stroncik, H.-U. Schmincke, Palagonite - a review, International Journal of Earth Sciences, 91 (2002) 680-697.
[88] S.R. Gíslason, Á. Snorrason, H.K. Kristmannsdóttir, Á.E. Sveinbjörnsdóttir, P. Torsander, J. Ólafsson, S. Castet, B. Dupré, Effects of volcanic eruptions on the CO2 content of the atmosphere and the oceans: the 1996 eruption and flood within the Vatnajökull Glacier, Iceland, Chemical Geology, 190 (2002) 181-205.
[89] R.A. Exley, J.V. Smith, The role of apatite in mantle enrichment processes and in the petrogenesis of some alkali basalt suites, Geochimica et Cosmochimica Acta, 46 (1982) 1375-1384.
[90] ASTM, C192/C192M – 07 Standard Practice for Making and Curing Concrete Test Specimens in the Laboratory1, in: Safety Precautions, Manual of Aggregate and Concrete Testing, Annual Book of ASTM Standards, ASTM, 2007, pp. 1-8.
[91] ASTM, C1611/C1611M – 09b Standard Test Method for Slump Flow of Self-Consolidating Concrete, in, ASTM, 2009, pp. 1-6.
[92] S.E.P. Group, The European Guidelines for Self Compacting Concrete, in, 2005.
[93] E.P. Koehler, D.W. Fowler, Inspection manual for self-consolidating concrete in precast members, in, Center for Transportation Research The University of Texas at Austin, 2007.
[94] ASTM, C39/C39M – 10 Standard Test Method for Compressive Strength of Cylindrical Concrete Specimens, in, ASTM, 2010, pp. 1-7.
[95] ASTM, C1231/C1231M-12 Standard Practice for Use of Unbonded Caps in Determination of Compressive Strength of Hardened Concrete Cylinders, in, ASTM, 2012, pp. 1-5.
[96] ASTM, C617/C617M-12 Standard Practice for Capping Cylindrical Concrete Specimens, in, 2012, pp. 1-6.
[97] S.A. Issa, M.S. Islam, M.A. Issa, A.A. Yousif, M.A. Issa, Specimen and Aggregate Size Effect on Concrete Compressive Strength, Cem Concr Aggr, 22 (2000) 103-115.

[98] M. Tokyay, Ozdemir, M., Specimen shape and size effect on the compressive strength of higher strength concrete, Cem Concr Res, 27 (1997) 1281-1289.
[99] NORDTEST, NT BUILD 492: Concrete, mortar and cement-based repair materials: chloride migration coefficient from non-steady-state migration experiments, in, Nordtest, Finland, 1999, pp. 1-8.
[100] ASTM, C948 – 81 Standard Test Method for Dry and Wet Bulk Density, Water Absorption, and Apparent Porosity of Thin Sections of Glass-Fiber Reinforced Concrete, in, 2009, pp. 1-2.
[101] RILEM, RILEM TC 116-PCD: Permeability of concrete as a criterion of its durability Materials and Structures, 32 (1999) 174-179.
[102] J.J. Kollek, The determination of the permeability of concrete to oxygen by the Cembureau method- a recommendation, Materials and Structures, 22 (1989) 225-230.
[103] ASTM, C305_Standard Practice for Mechanical Mixing of Hydraulic Cement Pastes and Mortars of Plastic Consistency, in, 2012.
[104] ASTM, C187-11 Standard Test Method for Amount of Water Required for Normal Consistency of Hydraulic Cement Paste, in, 2011.
[105] ASTM, C191 – 08: Standard Test Methods for Time of Setting of Hydraulic Cement by Vicat Needle, in, 2008.
[106] ASTM, C109_Standard Test Method for Compressive Strength of Hydraulic Cement Mortars (Using 2-in. or [50-mm] Cube Specimens), in, 2011.
[107] V.S. Ramachandran, J.J. Beaudoin, Handbook of Analytical Techniques in Concrete Science and Technology Noyes Publictions, New Jersey, New York, 2001.
[108] M. Boháč, M. Palou, R. Novotný, J. Másilko, D. Všianský, T. Staněk, Investigation on early hydration of ternary Portland cement-blast-furnace slag–metakaolin blends, Construction and Building Materials, 64 (2014) 333-341.
[109] J.I. Escalante-García, J.H. Sharp, The microstructure and mechanical properties of blended cements hydrated at various temperatures, Cement and Concrete Research, 31 (2001) 695-702.
[110] H.M. Dyson, Early hydration in binary and ternary blended cement systems in: Civil Engineering, University of Leeds, Leeds, 2005.
[111] X. Wu, D.M. Roy, C.A. Langton, Early stage hydration of slag-cement, Cement and Concrete Research, 13 (1983) 277-286.
[112] K.D. Weerdt, E. Sellevold, K.O. Kjellsen, H. Justnes, Fly ash–limestone ternary cements: effect of component fineness, Advances in Cement Research, 23 (2011) 203-214.
[113] V. Kocaba, Development and evaluation of methods to follow microstructural development of cementitious systems including slags, in, EPFL, 2009.
[114] V.S. Ramachandran, R.M. Paroli, J.J. Beaudoin, A.H. Delgado, Handbook of Thermal Analysis of Construction materials, Building Materials Series, 2003.
[115] O.M.d.S. Girao, The nanostructure and Degradation of C-S-H in Portland and Blenede Cements, in: School of Civil Engineering, Leeds, Leeds 2007.
[116] I.G. Richardson, Electron Microscopy of Cements, in: J. Bensted, P. Barnes (Eds.) Structure and Performance of Cement, Spon Press, 2002.
[117] P.J. Goodhew, J. Humphreys, R. Beanland, Electron Microscopy and Analysis, Taylor & Francis, London, New York, 2001.
[118] unl.edu, Specimen Interaction, in, 2008.
[119] A. Petek Gursel, E. Masanet, A. Horvath, A. Stadel, Life-cycle inventory analysis of concrete production: A critical review, Cement and Concrete Composites, 51 (2014) 38-48.

[120] ISO, Environmental management - Life Cycle Assessment: Principles and Framework. ISO 14040:2006, in, International Organization for Standardization, Geneva, Switzerland, 2006a.
[121] ISO, Environmental management - Life Cycle Assessment: Requirements and Guidelines. ISO 14044:2006, in, International Organization for Standardization, Geneva, Switzerland, 2006b.
[122] A. Barker, H. Cory, The early hydration of limestone-filled cements., in: R.N. Swamy (Ed.) Blended Cements in Construction, Elsevier Science, London, 1991, pp. 107-124.
[123] S. Hans-Henning, Fundamentals of Corrosion, in: Corrosion Mechanisms in Theory and Practice, Third Edition, CRC Press, 2011, pp. 1-104.
[124] EPA, Life Cycle Assessment: Principles and Practice, in, U.S. Environmental Protection Agency - National Risk Management Research Laboratory, Office of Research and Development, Cincinnati, Ohio, 2006.
[125] IPCC, IPCC Guidelines for National Greenhouse Gas Inventories, in, Intergovernmental Panel on Climate Change - National Greenhouse Gas Inventories Programme Technical Support Unit Geneva, Switzerland, 2006.
[126] IPCC, Climate Change 2007: The Physical Science Basis, in: C.U. Press (Ed.) Contribution of Working Group I to the Fourth Assessment Report of the Intergovernmental Panel on Climate Change, World Meteorological Organization (WMO) and the United Nations Environment Programme (UNEP), Cambridge, United Kingdom, 2007, pp. 996.
[127] C. Hendrickson, L. Lave, S. Matthews, Environmental Life Cycle Assessment of Goods and Services-An Input-Output Approach, Resources for the Future, Washington, D.C., 2006.
[128] EIA, Electricity Net Generation by State by Type of Producer by Energy Source, Annual Back to 1990 (EIA-906, EIA-920, and EIA-923), in, U.S. Energy Information Administration Washington, DC, 2011g.
[129] H.-s. Shi, B.-w. Xu, X.-c. Zhou, Influence of mineral admixtures on compressive strength, gas permeability and carbonation of high performance concrete, Construction and Building Materials, 23 (2009) 1980-1985.
[130] CEA, Canadian Electricity Association - Industry Data, in, 2012.
[131] A. Abbas, M. Carcasses, J.P. Ollivier, The importance of gas permeability in addition to the compressive strength of concrete, Mag Concrete Res, 52 (2000) 1-6.
[132] G. Menéndez, V. Bonavetti, E.F. Irassar, Strength development of ternary blended cement with limestone filler and blast-furnace slag, Cement and Concrete Composites, 25 (2003) 61-67.
[133] N. Diamantonis, I. Marinos, M.S. Katsiotis, A. Sakellariou, A. Papathanasiou, V. Kaloidas, M. Katsioti, Investigations about the influence of fine additives on the viscosity of cement paste for self-compacting concrete, Construction and Building Materials, 24 (2010) 1518-1522.
[134] O.E. Gjørv, Durability design of concrete structures in severe environments, in, Taylor & Francis, New York, 2009.
[135] K.M.A. Hossain, M. Lachemi, Corrosion resistance and chloride diffusivity of volcanic ash blended cement mortar, Cement and Concrete Research, 34 (2004) 695-702.
[136] P. Pipilikaki, M. Katsioti, Study of the hydration process of quaternary blended cements and durability of the produced mortars and concretes, Construction and Building Materials, 23 (2009) 2246-2250.
[137] S. Tsivilis, J. Tsantilas, G. Kakali, E. Chaniotakis, A. Sakellariou, The permeability of Portland limestone cement concrete, Cement and Concrete Research, 33 (2003) 1465-1471.

[138] B. Uzal, L. Turanlı, Blended cements containing high volume of natural zeolites: Properties, hydration and paste microstructure, Cement and Concrete Composites, 34 (2012) 101-109.
[139] J. Castro, R. Spragg, P. Kompare, J. Weiss, Portland Cement Concrete Pavement Permeability Performance, in, Joint Transportation Research Program, Indiana Department of Transportation and Purdue University, West Lafayette, Indiana, 2010.
[140] S. Kolias, C. Georgiou, The effect of paste volume and of water content on the strength and water absorption of concrete, Cement and Concrete Composites, 27 (2005) 211-216.
[141] T. Sugiyama, T.W. Bremner, Y. Tsuji, Determination of chloride diffusion coefficient and gas permeability of concrete and their relationship, Cement and Concrete Research, 26 (1996) 781-790.
[142] K.E. Hassan, J.G. Cabrera, R.S. Maliehe, The effect of mineral admixtures on the properties of high-performance concrete, Cem Concr Compos, 22 (2000) 267-271.
[143] A. Abbas, M. Carcasses, P.P. Ollivier, Gas permeability of concrete in relation to its degree of saturation, Materials and Structures, 32 (1999) 3-8.
[144] T. Sugiyama, T.W. Bremner, T.A. Holm, Effect of Stress on Gas Permeability in Concrete, ACI Mater J, 93 (1996) 443-450.
[145] T. Sugiyama, T.W. Bremner, Y. Tsuji, Determination of chloride diffusion coefficient and gas permeability of concrete and their relationship, Cem Concr Res, 26 (1996) 781-790.
[146] A. Itim, K. Ezziane, E.-H. Kadri, Compressive strength and shrinkage of mortar containing various amounts of mineral additions, Construction and Building Materials, 25 (2011) 3603-3609.
[147] C. Atiş, High-Volume Fly Ash Concrete with High Strength and Low Drying Shrinkage, Journal of Materials in Civil Engineering, 15 (2003) 153-156.
[148] K.E. Hassan, J.G. Cabrera, R.S. Maliehe, The effect of mineral admixtures on the properties of high-performance concrete, Cement & Concrete Composites, 22 (2000) 267-271.
[149] A. Abbas, M. Carcasses, J.P. Ollivier, The importance of gas permeability in addition to the compressive strength of concrete, Magazine of Concrete Research, 52 (2000) 1-6.
[150] K. De Weerdt, M.B. Haha, G. Le Saout, K.O. Kjellsen, H. Justnes, B. Lothenbach, Hydration mechanisms of ternary Portland cements containing limestone powder and fly ash, Cement and Concrete Research, 41 (2011) 279-291.
[151] M. Zajac, A. Rossberg, G. Le Saout, B. Lothenbach, Influence of limestone and anhydrite on the hydration of Portland cements, Cement and Concrete Composites, 46 (2014) 99-108.
[152] B. Lothenbach, Thermodynamics and hydration of blended cements, in: Symposium on Concrete Modelling (CONMOD 2010), Lausanne, Switzerland, 2010, pp. 10/CP.
[153] B. Lothenbach, K. Scrivener, R.D. Hooton, Supplementary cementitious materials, Cement and Concrete Research, 41 (2011) 1244-1256.
[154] M. Codina, C. Cau-dit-Coumes, P. Le Bescop, J. Verdier, J.P. Ollivier, Design and characterization of low-heat and low-alkalinity cements, Cement and Concrete Research, 38 (2008) 437-448.
[155] J.I. Escalante-Garcia, J.H. Sharp, The chemical composition and microstructure of hydration products in blended cements, Cement and Concrete Composites, 26 (2004) 967-976.
[156] T.D. Dyer, R.K. Dhir, Hydration reactions of cement combinations containing vitrified incinerator fly ash, Cement and Concrete Research, 34 (2004) 849-856.
[157] K.A. Snyder, P.E. Stutzman, J. Philip, D. Esh, Hydrated phases in blended cementitious systems for nuclear infrastructure, in: V. L'Hostis, R. Gens, C. Gallé (Eds.) NUCPERF 2009 -

Long Term Performance of Cementitious Barriers and Reinforced Concrete in Nuclear Power Plants and Waste Management, RILEM Publications SARL, France, 2009, pp. 91-98.
[158] K. Luke, E. Lachowski, Internal Composition of 20-Year-Old Fly Ash and Slag-Blended Ordinary Portland Cement Pastes, Journal of the American Ceramic Society, 91 (2008) 4084-4092.
[159] G. Baert, Physico-Chemical Interactions in Portland Cement - (HighVolume) Fly Ash Binders, in: Faculty of Engineering and Architecture, Ghent University, 2009.
[160] J.D. Rachel, P.K. Mehta, Chemical and Physical Effects of Silica Fume on the Mechanical Behavior of Concrete, Materials Journal, 86.
[161] D.B. Jussara Tanesi, and Ahmad Ardani, Enhancing High Volume Fly Ash Concretes Using Fine Limestone Powder, (2013).
[162] A.-M. Poppe, G. De Schutter, Cement hydration in the presence of high filler contents, Cement and Concrete Research, 35 (2005) 2290-2299.
[163] K. Vance, M. Aguayo, T. Oey, G. Sant, N. Neithalath, Hydration and strength development in ternary portland cement blends containing limestone and fly ash or metakaolin, Cement and Concrete Composites, 39 (2013) 93-103.
[164] F. Deschner, F. Winnefeld, B. Lothenbach, S. Seufert, P. Schwesig, S. Dittrich, F. Goetz-Neunhoeffer, J. Neubauer, Hydration of Portland cement with high replacement by siliceous fly ash, Cement and Concrete Research, 42 (2012) 1389-1400.
[165] C. Guo, J. Zhu, W. Zhou, Z. Sun, W. Chen, Effect of phosphorus and fluorine on hydration process of tricalcium silicate and tricalcium aluminate, Journal of Wuhan University of Technology--Materials Science Edition, 27 (2012) 333-336.
[166] H.F.W. Taylor, Cement Chemistry, Taylor and Francis, London, 2004.
[167] S.-Y. Hong, F.P. Glasser, Alkali sorption by C-S-H and C-A-S-H gels: Part II. Role of alumina, Cement and Concrete Research, 32 (2002) 1101-1111.
[168] M.D. Jackson, J.M. Logan, B.E. Scheetz, D.M. Deocampo, C.G. Cawood, F. Marra, M. Vitti, L. Ungaro, Assessment of material characteristics of ancient concretes, Grande Aula, Markets of Trajan, Rome, Journal of Archaeological Science, 36 (2009) 2481-2492.
[169] M.D. Jackson, G. Vola, D. Všianský, J.P. Oleson, B.E. Scheetz, C. Brandon, R.L. Hohlfelder, Cement Microstructures and Durability in Ancient Roman Seawater Concretes Historic Mortars, in: J. Válek, J.J. Hughes, C.J.W.P. Groot (Eds.), Springer Netherlands, 2012, pp. 49-76.
[170] M.D. Jackson, F. Marra, R.L. Hay, C. Cawood, E.M. Winkler, The judicious selection and preservation of tuff and travertine building stone in ancient Rome, Archaeometry, 47 (2005) 485-510.
[171] DOE, Transportation Data Book, in, Oak Ridge National Laboratory-Vehicle Technologies Program Office of Energy Efficiency and Renewable Energy U.S. Department of Energy (USDOE), Oak Ridge, Tennessee, 2011.
[172] DOE, Buildings Energy Data Book. Chapter:1 Buildings Sector. 1.1 Buildings Sector Energy Consumption. 1.1.1 U.S. Residential and Commercial Buildings Total Primary Energy Consumption, in, U.S. Department of Energy [DOE] - Energy Efficiency and Renewable Energy., 2011.
[173] B.L. Damineli, F.M. Kemeid, P.S. Aguiar, V.M. John, Measuring the eco-efficiency of cement use, Cement and Concrete Composites, 32 (2010) 555-562.

[174] C. Chen, G. Habert, Y. Bouzidi, A. Jullien, A. Ventura, LCA allocation procedure used as an incitative method for waste recycling: An application to mineral additions in concrete, Resources, Conservation and Recycling, 54 (2010b) 1231-1240.
[175] E.F.I. Dale P. Bentz, Brooks E. Bucher, and W. Jason Weiss, Limestone Fillers Conserve Cement Part 1: An analysis based on Powers' model, Concr Int, (2009).
[176] M. Ghrici, S. Kenai, M. Saidmansour, Mechanical properties and durability of mortar and concrete containing natural pozzolana and limestone blended cements, Cem Concr Compos, 29 (2007) 542-549.